THE UNIVERSITY
of EDINBURGH

Computational Fatigue Assessment of Mooring chains accounting for Residual Stresses

Imanol Martínez Pérez

THE UNIVERSITY *of* EDINBURGH

Thesis summited in fulfilment of the requirements for the degree of Doctor of Philosophy to the University of Edinburgh-2018

Declaration

I declare that this thesis has been composed solely by myself and that it has not been submitted, either in whole or in part, in any previous application for a degree. Except where otherwise acknowledged, the work presented is entirely my own.

Imanol Martínez Pérez

November 2018

Abstract

Mooring chains are used to keep dynamically floating structures on a fixed geographical position within a specified tolerance. Chains for permanent moorings have been traditionally used by the Oil and Gas industry for Floating Production Storage and Offloading (FPSO) and have recently found application in the Offshore Renewable Energy Industry, as for example in mooring floating wind turbines. For both industries, the failure of the mooring can give rise to large accidents with devastating economic losses as well as drastic environmental consequences. During the last decade, the increasing number of mooring incidents has rise to concern among Oil and Gas companies. In most of these incidents, chain links were the root cause, and fatigue the main damage mechanism.

This research aims to investigate the fatigue of mooring chains from a global approach. That is, to follow the life cycle of a mooring chain, which is mainly composed of two stages: manufacturing, and service life. The fatigue of mooring chains has been studied using the Dang Van fatigue criterion. Dang Van fatigue criterion and critical plane methods are a set of fatigue criteria that have proven to be accurate, and account for complex phenomena (for example non-proportionality of the loading, mean load effects, among others); however, they have a complex mathematical formulation which involves solving optimization problems, and therefore such methods carry substantial computational overhead if they are applied to an industrial component with complex geometry. The research of this thesis is divided in three main parts.

In the first part, different numerical methods are reviewed for solving the optimization problems faced when applying critical plane methods and Dang Van fatigue criterion. The best performing method for applying the Dang Van fatigue criterion is identified.

In the second part, the residual stress field after the manufacturing of a chain is predicted by means of Finite Element Analysis (FEA). Relevant manufacturing steps are modelled. A qualitative validation using data from the literature is presented.

Finally, using the numerical method identified in the first part for applying Dang Van fatigue criterion, and the residual stress prediction derived in the second part, the computational fatigue assessment of mooring chains is performed. Two different loading modes have been studied, tension and twisting. The first one is the nominal loading mode; however current standards do not account for the effect of the mean load. The influence of mean load is assessed, and a simplified fatigue assessment method implementing Dang Van fatigue criterion is proposed. The accuracy of the proposed method is proven by comparing the predictions with full scale fatigue testing carried out in sea water at TWI Ltd as part of a Joint Industry Program (JIP). The second loading mode (twisting) is not fully accounted for in the standards; the fatigue analysis predicts cracks at locations that do not correspond with fatigue breakage locations under tension loading or Out-of-Plane Bending (OPB). The predicted fatigue crack initiation locations match very well with cracks found in chains recovered from the field after more than 15 years in service.

Acknowledgement

During my PhD, at every presentation I have given, either in conferences or in seminars, the second-to-last slide had the following quote ”*Standing at the shoulders of giants*” from one of the most brilliant British scientist, Isaac Newton. I like this quote for its humility and its simplicity. Now that I am writing the last words of my thesis, I think that this quote should change position and be at the first pages of my thesis.

I must thank my two academic supervisors, Professor Vengatesan Venugopal and Professor Alistair Borthwick, their guidance and advice have been of great help. They have played a key role in my PhD.

It is fair to continue with the person that started everything. I still can remember as if it was yesterday when I received a call from the UK (I was living in Paris at that time) telling me that my profile matched quite well with the candidate he was looking for. I was surprised because the person at the other end of the line had a strong French accent. I must admit that my English was not very good at that time, and I had to ask him to send me an email. Of course, I am talking of Philippe Bastid. He has been a great support and has played a key role during my PhD. Moreover, I would like to thank TWI Ltd for sponsoring my PhD, I am very grateful for the opportunity. Yanhui Zhang, Markus Warwick and other PhD students with whom I have shared many hours of hard work, deserve special mention. Nicholas O’Meara and Simon Smith must be acknowledged as well.

Andrei Constantinescu and Eric Charkaluk from Ecole Polytechnique (Palaiseau, France) must be thanked for their invaluable involvement. They gave me the opportunity to spend three months at the Ecole Polytechnique learning multiaxial fatigue criteria and numerical methods.

Their help and support have gone well beyond the period I spent in Paris, being key for the fourth and sixth chapter of my thesis.

One of the reasons I chose to do my PhD at TWI was that during the interview, Markus Warwick, described me the industrial orientation of the research. All along my PhD I had the chance of having a great industrial mentor, Philip Smedley (BP). During our regular meeting he has given me an accurate and clear perspective of the industrial dimension of my research and he has proposed me research directions of interest to industry. Moreover, he has motivated me showing me the industrial relevance of my academic research. Øystein Gabrielsen (Equinor, former Statoil) has been a great support too. He has encouraged me and has showed interest in my work from the early stages of my PhD. Our discussions have been very encouraging and productive. Furthermore, I am grateful that he has allowed me to publish a picture of recovered links in my thesis.

I appreciate the technical discussions and guidance during the write up stage of my thesis of Håkon Ottar Nordhagem and Paul Qvale, both of them from SINTEF.

I would like to extend my gratitude to Vicinay Cadenas for giving me the opportunity to visit their manufacturing facility in Sestao (Spain). It enabled me to align my modeling assumptions with the actual manufacturing process of chain links. I also must acknowledge the help and willingness to answer all my questions related to mooring chain steel of Jose Antonio Ezquerro (Sidenor Special Steels).

I would like to end acknowledging my Parents, the two only persons that have supported me well before I knew what a mooring chain was.

Contents

List of Figures

List of Tables

Nomenclature

a	Material Parameter
b	Material Parameter
$C_a(\boldsymbol{n}^*)$	Shear stress amplitude on the critical plane
E	Young Modulus
f_0	Fatigue limit in repeated bending
$\sqrt{J_{2,a}}$	Alternating shear in the octahedral plane
$\mathbf{n}$	Normal vector to a particular plane
N	Number of cycles to failure
N_f	Number of cycles to failure
$N_{max}(\boldsymbol{n}^*)$	Maximum normal stress on the critical plane
P_m	Mean hydrostatic stress
$\mathbf{s}^*$:	Center of the smallest hypersphere that circumscribes the path of the stress deviator
t_{-1}	Fatigue limit in alternating torsion
σ_a	Stress Amplitude

$\Delta\sigma$	Stress Range
σ_f'	Fatigue Strength Coefficient
$\tilde{\sigma}$	Stress tensor at mesoscopic level in the elastic shakedown scale
$\sigma(t)$	Stress tensor at the macroscopic level
$\sigma_h(t)$	Hydrostatic stress.
σ_e	Fatigue strength for N cycles under zero mean stress.
σ_u	Ultimate tensile strength.
$\boldsymbol{\sigma}(M,t)$	Stress tensor at a generic point *M*
$\sigma^Y_{0.2\%}$	Yield Stress
σ^U	Ultimate tensile strength
$\tau(t)$	Maximum mesoscopic shear stress in the elastic shakedown state
τ_a	Shear Stress Amplitude
θ and φ	Euler angles with respect to the Cartesian coordinate system
ε_f	Elongation to failure
ν	Poisson ratio

Chapter 1: Introduction

1.1 Background

The marine environment has been an important source of energy and food for humans. The first energy related industrial activity in the marine environment was developed by the oil and gas sector at the beginning of the 20th century. The first offshore wells were drilled along the Gulf coast of Texas and Louisiana. Many other offshore wells, distributed all over the world have followed, some attaining water depths of up to 3000 m. More recently, aligned with the need of reducing the dependency of fossil fuels and seeking sources of clean energy, humankind has turned its interest to seas and oceans as a source of renewable energy. The technologies that will harvest energy from oceans include, offshore wind turbines, wave energy converters, and tidal energy devices. Inherent to these activities in the marine environment, is the need for mooring floating structures, either on a temporary or permanent basis.

The main purpose of a mooring system is the station-keeping of floating structures within a specified motion tolerance. Such structures can be permanently moored (for example production units such as FPSOs (Floating, Production, Storage and Offloading) or floating offshore wind turbines) or temporary (drilling rigs or vessels). Mooring systems have been traditionally used by the oil and gas industry, although recently they have found application in the offshore renewable industry, for example in floating wind turbines. In both industries, the failure of the mooring system can result in severe economic losses as well as drastic environmental consequences (such as oil spills).

Environmental loads, such as wind, waves, tides or currents, offset the position of a floating structure. The purpose of the mooring system is to restore its nominal position. To do so, the

mooring system has to produce a restoring force equal to the environmental load so that the floating structure regains its nominal position. There are two main types of mooring systems: Taut and Catenary (see Figure 1.1). Both types of mooring systems withstand environmental loads through different mechanisms. In a catenary system, the mooring line has freedom to move in the vertical direction. This displacement of the mooring line onto the seabed produces the restoring force, although there can be some line stretch. In the case of a taut system, the lower part of the mooring line does not have freedom to move vertically; consequently, the restoring force relies on the elastic response of the mooring line. An additional type of mooring is semi-taut; this is a combination of taut and catenary mooring systems.

Catenary systems require longer mooring lines than taut systems; they are more frequently used in shallow water than taut mooring systems. The tension in catenary systems is significantly lower than in taut systems; consequently, catenary systems have longer fatigue lives than taut systems. Taut systems are frequently used for deep water depths. In such cases, the mooring line is usually composed of two chain segments, which are located at both ends of the mooring line, with rope (polyester or wire rope) joining both segments. With this layout, a significant reduction in the weight of the mooring line is achieved, especially for deep moorings.

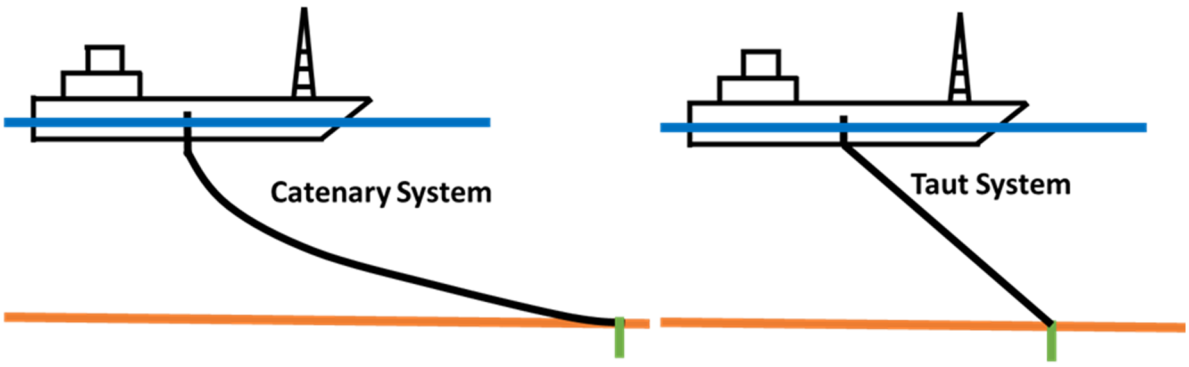

Figure 1.1 Mooring Systems: Catenary and Taut moorings.

1.2 The Context of Research

The rise in the number of mooring incidents is a concern to the oil and gas Industry. Between 2001 and 2011 twenty-one mooring incidents were recorded [1]. Figure 1.2 presents the trend in the number of mooring line failures or replacements during the period from 1997 to 2013. This graph illustrates the conclusions from a survey conducted among Deepstar Joint Industry Project (JIP) members (comprising major oil and gas Companies).

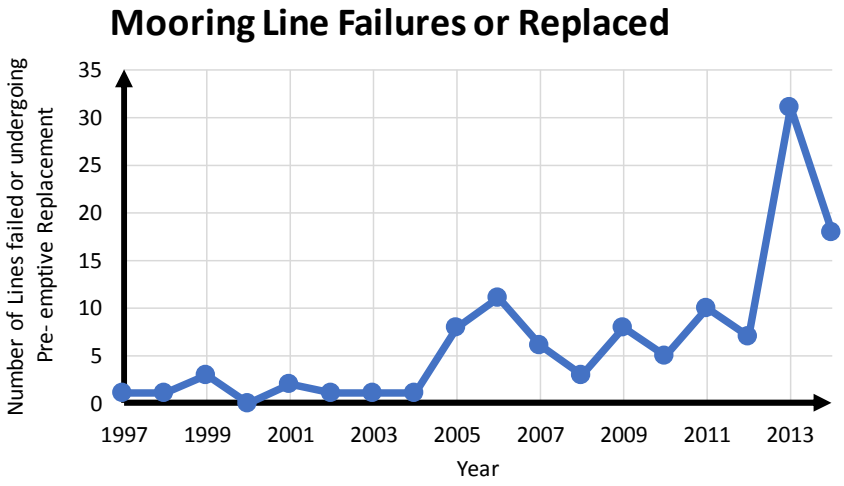

Figure 1.2 Number of individual mooring legs failed or pre-emptively replaced/repaired by year. [Data from [2]]

There is clearly a sharply increasing trend in the number of mooring failures or replacements. Yet mooring lines are a critical component whose structural integrity should be investigated. It is worth reminding that the total cost of replacing all the mooring lines of a FPSO is quantified in terms of millions of dollars. Aging of existing mooring lines is an important factor that can partially explained the trend, more factors are presented in Figure 1.5. A mooring line is composed of different elements, chain links, wire rope, connecters, etc. An important question is which of these components is the most critical, in other words, what is “the weakest link”? In addressing this question, Figure 1.3 reveals that mooring chains are the major cause of breaks or incidents. A break was recorded after the breakage of two or more lines, or when the riser was damaged. Alternatively, an incident was considered for single line breakage. The graphs

show that statistically when an incident or a breakage occurs, there is a strong possibility that the cause relates to chain links. Other components, such as wire or polyester rope, are less likely to be involved (or damaged).

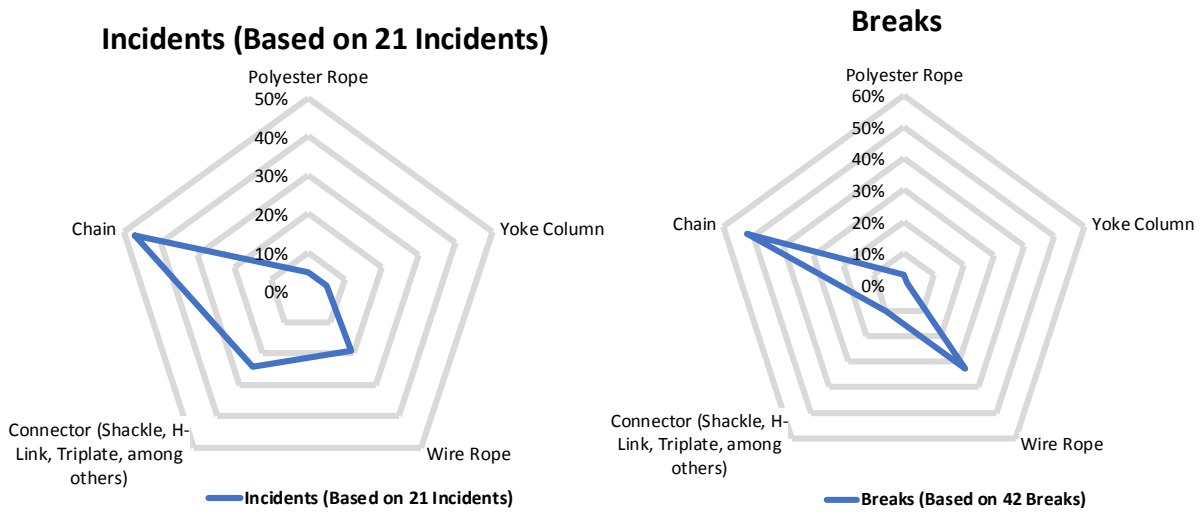

Figure 1.3 Distribution of component types based on 21 incidents (Left Chart) or 42 Breaks (Right Chart)[Data from [1]]

In a mooring chain, not all the links are subjected to the same damage mechanisms. Links near the fairlead are subjected to high tension and are likely to be exposed to Out-of-Plane Bending (OPB). This damage mechanism is described in detail in Section 2.1.2. Although corrosion affects all the submerged links, it is more critical for links located in the splash zone [3] (the splash zone is delimited from 4 m above water level to 5 m underneath mean water level [3]). Links located at the bottom of the mooring line are more susceptible to wear and abrasion, especially if they are in contact with the seabed. Figure 1.4 summarizes the main degradation mechanisms of a mooring chain.

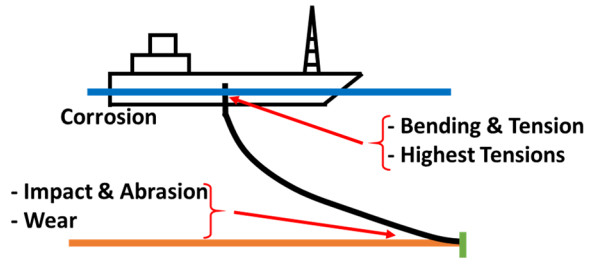

Figure 1.4 Mooring degradation mechanisms[Source [4]]

All the degradation mechanisms presented in Figure 1.4 have a negative effect in the fatigue performance of mooring chains. As has been recorded by different organizations, fatigue failure of chain links is one of the main causes of failure of mooring lines. For example, according to Kvitrud [5], between 2011 and 2013, the 15 failures of mooring line elements that occurred in the Norwegian North Sea were due to the following reasons:

Table 1.1 Causes of 15 mooring failures [Source Kvitrud [5]]

	Failure mechanism		
Mooring line component	**Fatigue**	**Overload**	**Mechanical Damage**
Chains	4	3	
Fibre ropes			3
Steel Wires		2	1
Kenter link	1		
Sum	5	5	4

Table 1.1 confirms that the most critical component in a mooring line is the chain links. Furthermore, the main root cause of failure is fatigue followed closely by overload. Supporting this fact, Fontaine et al. [2] presented results of a survey conducted among members of the Deepstar JIP. According to Fontaine et al, the main root of chain failure was fatigue, followed by installation. Figure 1.5 shows their main findings regarding prevalent failure modes.

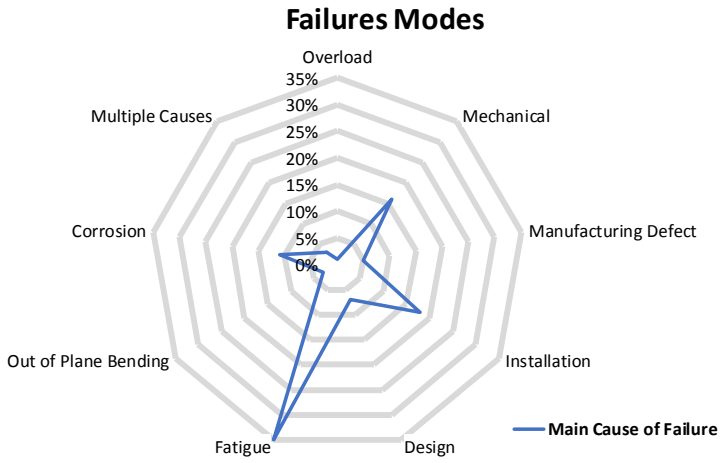

Figure 1.5 Root causes of chain links failures (Data from [2])

Corrosion affects the fatigue performance of mooring chains. In the previous graph, corrosion was recorded as a cause of failure when it caused a significant reduction of the cross section.

All the data presented in this section, gathered by different researchers and organizations, confirm that fatigue of mooring chain links is the main cause of failure or pre-emptive replacement of mooring lines. Consequently, effort should be orientated towards mitigating the fatigue of mooring chains through a better understanding of the influence of different factors, such as corrosion, mean load or residual stresses. Aligned with this objective, fatigue prediction models should be improved. These models should account quantitatively for complex phenomena affecting the fatigue lifetime of mooring chains, such as residual stresses, corrosion, multiaxiality of the stress tensor, and mean load effects.

1.3 Research Objectives

This research aims to investigate the fatigue of mooring chains from a global approach. That is, to follow the life cycle of a mooring chain, which is mainly composed of two stages, manufacturing and service life. The fatigue of mooring chains has been studied using the Dang Van fatigue criterion (the reason for this choice is discussed in Chapter 6). Dang Van fatigue criterion and critical plane methods are a group of fatigue criteria that have proven to be accurate and account for complex phenomena [6] (for example non proportionality of the loading, mean load effects, among others); however, they have a complex mathematical formulation which involves solving optimization problems, and therefore it leads to substantial computational cost if applied to an industrial component with complex geometry. Part of this research has been carried out in an industrial environment at TWI Ltd. This research has aimed to cover the gap between academia and industry.

As noted before, critical plane methods and Dang Van fatigue criterion are not straightforward to implement, and in the case of industrial components, they usually require the use Finite Element Analysis (FEA) for deriving the stabilized multiaxial stress tensor due to service loading. Aiming to bring together a rigorous scientific approach and tools suitable for practitioners, this research proposes a simplified fatigue assessment method of mooring chains under tension using the Dang Van criterion. This simplified method has been successfully implemented in an Excel Spreadsheet. It takes as input, service loading conditions (defined by mean load and load amplitude) and derives the estimated fatigue lifetime accounting for residual stresses from all relevant stages of the manufacturing process. Moreover, the method has been validated against experimental data.

The research work presented here has been based on finding answers to the following questions:

1) Is it possible to apply critical plane methods to an industrial component in reduced computational time using a standard desktop computer? (Methods and solutions are in Chapter 4)
2) Several manufacturing steps comprise the manufacturing process of a mooring chain, and each of them generates residual stresses. Which of the manufacturing steps has more influence in the final residual stress field and therefore should be studied to predict the final residual stress field? (Methods and solutions are presented in Chapter 5)
3) Depending on the loading mode, how do residual stresses influence the fatigue performance of mooring chains? (Chapter 5)
4) Current mooring chain standards (API-RP-2SK [7] and DNV-OS-E301 [3]) do not address the question of the influence of mean load on the fatigue performance of mooring chains. Does mean load have an effect on the fatigue lifetime of mooring chains? (Methods and solutions are described in Chapter 6)

5) Is the Dang Van fatigue criterion accurate and effective for studying the fatigue of mooring chains under tension loading? If so, what are the limitations of this criteria? (Methods and solutions are discussed in Chapter 6)
6) Is it possible to formulate a simplified fatigue assessment method that implements the Dang Van fatigue criterion without compromising the accuracy of the results? (Methods and solutions are illustrated in Chapter 6)
7) Current mooring chain standards (API-RP-2SK [7] and DNV-OS-E301 [3]), do not address in detail the effect of twist in the fatigue performance, they only recommend to limit the value of the twist angle to 5 degrees. If the chain is working in twisted conditions, is there a possibility of initiation of fatigue cracks, even for twist angles lower than 5 degrees? Once initiated, will these cracks propagate until final failure? (Methods and solutions are discussed in Chapter 7)

1.4 Outline

The thesis is divided as follows:

Chapter 1 provides an introduction of the thesis, research context and list of objectives. Chapter 2 reviews the fatigue of mooring chains, focusing on the different fatigue loadings and phenomena affecting fatigue, for example corrosion and wear. It also reviews some of the Joint Industry Programs (JIP) that have been formed for gaining knowledge and understanding of fatigue of mooring chains. Chapter 3 presents a literature review of metal fatigue, giving more attention to high cycle fatigue and critical plane methods. Chapter 4 provides the necessary mathematical tools for applying critical plane methods in reduced computational time. Chapter 5 describes the manufacturing process for mooring chains. It presents different models for predicting the residual stress field after manufacturing. Chapter 6 studies the fatigue of mooring

chains under tension loading, accounting for the previously computed residual stress distribution and applying the Dang Van fatigue criterion. This chapter also addresses the question of the influence of the mean load in the fatigue lifetime. A simplified fatigue assessment methodology implementing the Dang Van fatigue criterion is proposed. This method has been implemented in an Excel spreadsheet and enables application of the Dang Van fatigue criterion with loading conditions as the only input (mean load and load amplitude). Predictions derived by this method are compared against experimental data produced at TWI Ltd. Chapter 7 studies the fatigue behavior of mooring chains under torsion loading using the Dang Van fatigue criterion. Chapter 8 summarizes the conclusions of the work presented in this PhD and provides directions for future work.

1.5 Published papers

Martinez Perez I, Bastid P, Venugopal V. Prediction of Residual Stresses in Mooring Chains and its Impact on Fatigue Life. ASME. International Conference on Offshore Mechanics and Arctic Engineering. doi:10.1115/OMAE2017-61720.

Martinez Perez, I., Bastid, P., Constantinescu, A., and Venugopal, V., 2018, Multiaxial Fatigue Assessment of Mooring Chain Links under Tension Loading: Influence of the Mean Load and Simplified Assessment, ASME. International Conference on Offshore Mechanics and Arctic Engineering. doi:10.1115/OMAE2018-77552.

Martinez Perez, I., Constantinescu, A., Zhang, Z., Bastid, P. and Venugopal, Computational Fatigue Assessment of Mooring Chains under Tension loading (Under Review)

Martinez Perez, I., Constantinescu, A., Bastid, P. and Venugopal, Revisiting Numerical methods for fast fatigue post processing (Under Review)

Chapter 2: Literature Review of the Fatigue of Mooring Chains

In the previous chapter, fatigue of mooring chains has been identified as the main cause of failure or replacement of mooring lines. Therefore, this PhD thesis is focused on understanding and improving fatigue assessment methods. This chapter presents a literature review of fatigue of mooring chains. The chapter commences by describing the main loading modes of mooring chains that can lead to fatigue failure, followed by a review of different phenomena that play an important role in fatigue damage, residual stresses, corrosion, and wear.

2.1 Fatigue Loading Modes of Mooring Chains

Mooring chains can be subjected to different loading modes, all of them capable of causing fatigue failure. Chain links are intended to work under tension loading; however, anomalous loading modes such as Out of-Plane Bending (OPB) and twisting can appear.

2.1.1 Tension Loading

The nominal loading mode of mooring chains is tension. In fact, until recently, this was the only mode considered by standards (DNV-OS-E301 [8] and API-RP-2SK [9]). Both standards provide S-N curves for predicting the fatigue lifetime of mooring chains. Both neglect the influence of the mean load, although recently it has been pointed that its effect should be included [10]. Most research concerning the fatigue of chains under tension loading has focused on deriving S-N curves [11]–[13]. An historical review of S-N curves of chain links can be found in [11]. No multiaxial fatigue criterion has been proposed for predicting the fatigue lifetime of mooring chains under tension loading.

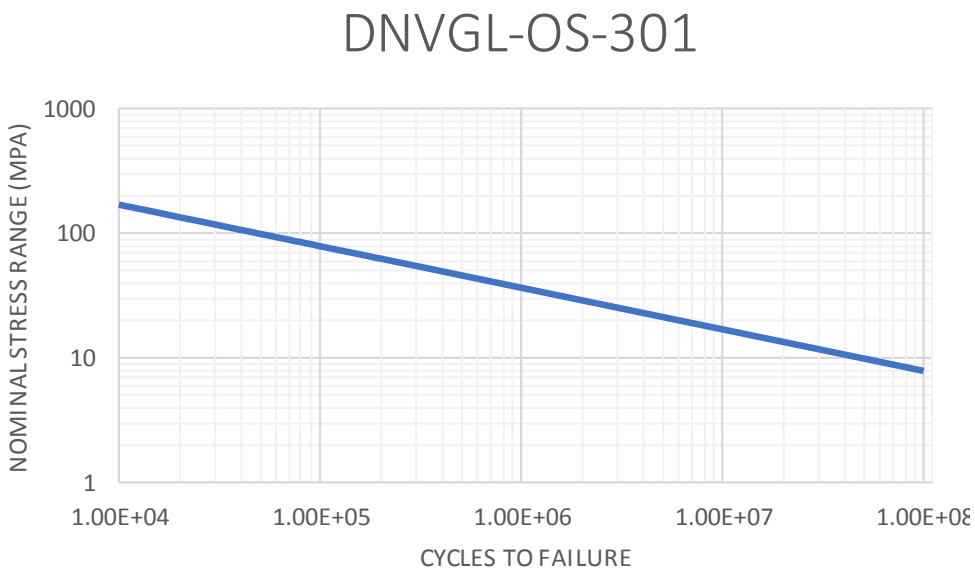

Figure 2.1 Design S-N curve for open links provided by DNVGL-OS-301

2.1.2 Out-of-Plane Bending (OPB)

Until the *Girassol* incident, it was considered that pure tension was the main loading mode of mooring chain links. However, chains can have undesirable loading modes such as OPB, which was responsible for the sudden failure of several chain links in the chainhawse of the *Girassol* buoy. The mooring chain was designed for 20 years of service, nevertheless, it failed after only a year and a half. Although the mooring system had been designed according to industry standards, it failed due to unknown loading mode, OPB [14]. This incident launched a Joint Industry Project (JIP) gathering 28 different companies with the objectives of understanding the mechanism of OPB and establishing recommendations for fatigue life design [15].

The combination of OPB and tension can lead to a fatigue failure. This mode of failure is especially critical at the chain termination (chain-stopper/fairlead) that connects the mooring line with the floating structure. Just to give an order of magnitude of the damaging effect of OPB, Bolt et al. [12] concluded, after performing fatigue testing, that the fatigue life of links located in the fairlead region (susceptible to OPB) might be reduced by a factor of five

compared to the fatigue lifetime of links located in other sections of the mooring line. Moreover, according to a guidance note published by Bureau Veritas [16], the angular variation between two links is negligible and the assumption of pure tension loading is correct for chain links located in the catenary, away from the termination.

Traditionally chain links were considered to be perfectly hinged together by a rolling or sliding mechanism at the contact region between each link [17]. In other words, it was considered that the bending stiffness of the chain could always be neglected. Out-of-plane bending appears when the hinge mechanism between chain links is partially blocked. Proof loading causes important yielding, especially at the contact zone. As a result, the rolling mechanism between chain links is restricted. The stress associated with OPB is proportional to the deviation angle and to the square root of the pretension of the mooring line [14].

The main strategy for minimizing OPB is to improve the articulation of the fairlead or chainhawse [15]. For example, Jean et al. [14] proposed to implement double articulations and low lever arms between the first chain link and articulation axes for reducing the bending moment, consequently reducing the bending stresses and improving the fatigue performance. Lassen et al. [17] proposed similar recommendations and suggested reducing the pretension of the mooring line whenever possible.

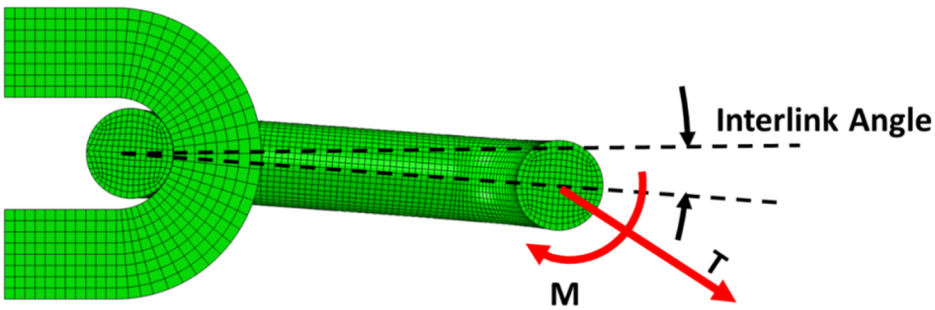

Figure 2.2 Chain links in bending mode

As already noted, a JIP was formed in order to have a better understanding of the OPB mechanism. Different aspects were investigated; special attention was given to determine the interlink contact stiffness, assessing the stress state at different locations, sensitivity studies, and extensive fatigue testing. The main results of the JIP were a set of S-N curves for chains under OPB, a multiaxial safety factor for accounting for OPB and set of recommendations for mitigating the OPB chain fatigue mechanism (multiaxial fatigue). The Dang Van fatigue criterion was used for deriving the multiaxial safety factor. The main conclusions were published in different papers [15] [18].

Once the JIP ended, Bureau Veritas published a guidance note [16] providing methodologies, requirements and recommendations for the fatigue evaluation of top chain (links located near the connection with the floating structure) under combined tension, in-plane bending, and out-of-plane bending loadings.

2.1.3 Chain twisting

Apart from OPB, another anomalous loading is twist, which is equivalent to torsion. A mooring chain can twist due to torque generated in the surrounding elements, or be installed in a twisted condition (it is very difficult to completely avoid twisting during deployment [19]). In fact, a six strand rope generates torque under tension, this can lead to transmission of twist to other mooring elements, either permanently or dynamically [20]. Of the two sources of twisting mentioned earlier, the most common arises from installation. Until now, no major fatigue failure due to twist has been recorded. Research on the twist of mooring chains has been concentrated in two directions, one focusing on the static problem and the other on the effect of twist on the fatigue lifetime.

The static problem encompasses how to determine the effect of twisting in the static strength and the torsional response of the chain links. The effect of twist on the strength of a chain

subjected to impact load was studied by [21] who used numerical models (Finite Element Method) and experimental data for validation. Small chains were studied (14 mm), similar to those used in a chain hoist. Hobbs and Ridge [22] published experimental results. They measured torque as a function of the tension load, remaining the twist angle constant. The tests were performed on a 20.5 mm stud-link chain. Their work pointed out the strong non-linearity of the induced torque with the twist angle. The same authors proposed a frictionless theory for predicting the resultant torque at the links as a non-dimensionalized function of the twist angle [20]. This theory is valid for both stud-less and stud-link chains, regardless of size. Hobbs and Ridge presented another paper comparing their theoretical model with experimental work. They used 20.5 mm stud-link, 41 mm stud-less and 56 mm stud-link chains. In the tests where the load was constant, the resulting torque was found to be higher than predicted by the theoretical model. Hobbs and Ridge attributed this difference to frictional effects and geometrical imperfections in individual chain links. However, in the test where twist remained constant, the measured torques were nearer to the predictions. It is important to keep in mind that the chains used in their experimental work were not proof loaded (no initial plastic deformation in the contact zone). A similar paper was published by the same authors [23]. They presented the afore-mentioned frictionless theory for predicting the resultant torque along with experimental data and the results of a numerical model (Finite Element Method). Constant load and constant twist experiments were performed with 41 mm stud-less chain links and 56 mm stud-link chain. The Finite Element results (taking into account friction) showed a very good correlation with the experimental work, especially for the stud-less chain, confirming the validity of Finite Element models for evaluating the torsional stiffness of a chain under twisted conditions.

Concerning the second research direction, fatigue behavior of mooring chains working under twisted conditions, all the previous work has been done experimentally. Ridge et al. [19]

published results for the static strength and fatigue life of chains in twisted conditions. They tested a 16 mm stud-less chain (similar proportions but smaller than actual chains used in mooring applications, approximately 20% the size of currently used chains). The chains were proof loaded before testing, with a proof load value around 32.5% of the measured breaking strength. The breaking load tests showed an insignificant decrease of the breaking strength for twisted chains (twist angle varying from 0 to 24 degrees), and a similar conclusion was reached from the fatigue life test. The authors acknowledge the limitations of the results obtained due to the smaller size of the chain tested compared to the size of chains used in mooring floating structures.

Finally, Bolt et al. [12] presented results from fatigue tests (tension-tension and tension bending, both performed in air) for larger chains (54,76 and 100 mm), and concluded that twist has a detrimental effect on fatigue performance(based on tension bending tests). They did not find a scale effect between the fatigue performance of 4" and 3" chains.

2.2 Residual Stresses

Residual stress influences the fatigue performance of an industrial component by modifying the value of the mean stress. Consequently, fatigue assessment should account for the residual stress distribution. Fabrication of mooring chains involves a number of manufacturing steps for each link that generate residual stresses. These steps include hot bending of the link's wire, welding, and heat treatment (composed of quenching, tempering and water cooling). In each of these steps, residual stresses are generated due to non-homogenous strains and/or thermal gradients. Furthermore, mooring chains have to undergo a mandatory proof load to check their strength and fitness for service. The proof load is specified to be about 70% of the minimum breaking load (MBL) of the links DNV-OS-302 [8], depending on the material grade and link's size. Because of the magnitude of the applied load, extensive yielding takes place in the link,

resulting in additional residual stresses. Different researchers have presented computational models for predicting residual stresses after proof loading [24]–[28]. All make the assumption that the chain was free of residual stresses prior to proof loading; in other words, they neglected heat treatment as a source of residual stresses. However, it is widely known that quenching and tempering of steel bars leave behind an important residual stress field [29].

2.3 Corrosion

Corrosion is intrinsic to the fatigue of mooring chains since almost the entire chain is submerged in sea water. It is well known that corrosion reduces the fatigue lifetime of metallic components. There are different forms of corrosion, the most relevant to mooring chains are:

- General corrosion: The surface is attacked by a chemical reaction. Generally, it spreads evenly around all the surface.
- Pitting corrosion: Localized corrosion that results in small holes in the surface.
- Intergranular corrosion: This consists of a damage near the grain boundaries of a metal.
- Hydrogen Damage: Hydrogen causes embrittlement of metals, especially high strength steels and titanium alloys. The question of hydrogen damage in mooring chains is an aspect that is being currently investigated.

Corrosion in seawater is mainly influenced by water temperature, dissolved oxygen, water velocity, and pollution [30]. Corrosion Fatigue is the combined effect of cyclic loading and corrosion, that is, the interaction between chemical reactions and strain. Indeed, cyclic stress and corrosion have a mutual influence. Corrosion affects deformation whereas plastic strain alters the electrochemical reactions [31]. Perez Mora [32] compared the corrosion rates of two steel samples (R5 grade) submerged in sea water. One of the samples was subjected to cyclic loading. This sample had a higher corrosion rate than that without cyclic loading. This coupling between corrosion and cyclic loading is responsible for an important deterioration in fatigue

performance. Current Standards (for example DNV-OS-E301 [3]) consider a loss of section thickness for structural elements for every year in service. For a mooring chain, depending on the location, this loss varies between 0.2 mm and 0.8 mm per year; this reduction accounts for the combined effect of corrosion and wear.

Fatigue properties should be derived accounting for corrosion. There are two main approaches, one is to pre-corrode specimens (for example following the standard EN ISO 9227) and the other is to test specimens under sea water flow. The main drawback of testing specimens under sea water flow is that the results depend on the testing frequency, because the effect of corrosion depends on the time spent in a corrosive environment. Perez Mora et al. [32] [33] and Palin-Luc et al. [34] presented fatigue properties of mooring chain steel obtained using pre-corroded specimens tested in air and in flowing seawater. Both performed tests in the very high cycle fatigue regime (VHCF) at high frequencies (20 kHz) and concluded that most of the fatigue life was spent on crack initiation. In the very high cycle, they observed that fatigue cracks started at the surface (similar to the high cycle fatigue regime) but also underneath the surface. Once the fatigue properties of steel accounting for corrosion are known, they can be used for the implementation of a fatigue criterion. Arredondo et al. [35] performed fatigue testing of R4 and R5 specimens in both air and seawater at 0.5 and 10 Hz. The tests were carried out at room temperature of about 20 °C and 27 °C.

From a fracture mechanics approach, the effect of corrosion can be assessed by studying the effect of cyclic stress on the initiation and growth of fatigue cracks under corrosive conditions. Standard BS7910 [36] estimates that at a temperature of 20 °C, the fatigue crack growth threshold (ΔK_0) is 63 N/mm$^{3/2}$. Consequently, if the stress intensity factor (K) is smaller than the fatigue crack growth threshold, a crack will not propagate in a seawater environment.

Finally, it worth mentioning that the SCHORSHIP JIP was launched with the aim of characterizing the corrosion of steel chain and wire operating in warm water. Fontaine et al. [37] and Rosen et al. [38] published the main results of this JIP. The FEARS (Finite Element Analysis of Residual Strength of Severely Corroded/Worn Chain) JIP followed to provide a validated methodology for performing FEA (Finite Element Analysis) of highly degraded (wear and corrosion) chain links in order to assess the remaining strength and remaining fatigue life [39],[40].

More recently, a special effort has been put into determining the remaining life of corroded chains by means of fatigue testing of recovered chains [10]. Surprisingly, these tests have showed that in certain cases the remaining fatigue life of recovered chains was higher than the nominal fatigue lifetime according to current standards.

2.4 Wear

Chain wear is more critical at terminations (hawse pipe, fairleads) and at the sea floor touchdown area (also known as the "trash zone") [4]. UK HSE Safety Notice 3/2005 [41] warned UK Continental Shelf FPSO and FSU operators about the risk of excessive wear of the top sections of their mooring chains. This notice was released after several FPSOs experienced premature mooring chain wear. Yaghin and Melchers [42] presented results from several tests in small chains (16 mm) in which they measured the amount of wear in the contact zone (interlink wear) as a function of the number of cycles. Their main finding was that the load to which the chain is subjected has an important non-linear effect on interlink wear. Similarly, Gotoh et al. [43] presented FEA models to predict interlink wear, and compared the predictions with experimental data obtained in dry conditions. Good agreement between predicted and measured values was obtained for the early stages of experiments.

2.5 Chapter Summary

The literature review presented in this chapter has identified a number of gaps on knowledge of fatigue of mooring chains. This PhD aims to cover several of these gaps. In Chapter 5 a residual stress prediction model accounting for heat treatment and proof loading is presented. In this chapter the question as to whether heat treatment should be considered in the residual stress prediction model or whether proof loading is merely sufficient is addressed. The answer depends on the loading mode of the links. As already said, no stress-based fatigue criterion other than S-N curves has been proposed in the literature for performing the fatigue assessment of mooring chains under tension. In Chapter 6 the Dang Van fatigue criterion is proposed for predicting the fatigue lifetime of mooring chains under tension. An advantage of this criterion compared to S-N curves is that it accounts for complex phenomena such as mean loads or the multiaxiality of the stress tensor, whereas S-N curves do not account for it. In this chapter the fatigue predictions obtained applying Dang Van fatigue criterion are compared with results from fatigue tests of chains tested in seawater under tension loading. This chapter ends by discussing the effect of the mean load on the fatigue performance of mooring chains applying the aforementioned fatigue criterion. Finally, in Chapter 7 a computational fatigue assessment of mooring chains under torsion accounting for the predicted residual stress field after heat treatment and proof loading is addressed.

Chapter 3: Background and Theory: Fatigue of Metals

Following Chapter 1 which highlighted that the main cause of failure or pre-emptive replacement of mooring lines is the fatigue of mooring chain links, this chapter presents a brief literature review of the fatigue of metals. Fatigue of metals is a broad topic, and different approaches for its study have been developed. The literature review concentrates in the high cycle fatigue regime. Moreover, special attention has been paid to multiaxial fatigue criteria based on the multiscale approach, especially the Dang Van fatigue criterion. This criterion is implemented in Chapters 6 and 7 for the fatigue assessment of mooring chains. The chapter ends presenting the theoretical background of residual stresses.

3.1 Phenomenological Description of Fatigue

Fatigue denotes the failure of a structural component under cyclic or variable loading. Its scientific history is considered to start with the Versailles train accident in 1842. Numerous accidents across different industries have followed; within a long list of examples we can cite renewable energy [44], the automotive Industry [45], aeronautics [46], the rail industry [47], nuclear energy [48] and oil and gas [49]. In spite of remarkable progress in the computation and prediction of fatigue during recent decades, fatigue still presents a technical problem to industry.

The formal definition of fatigue according to the American Society for Testing and Materials (ASTM) is the following: " The process of localized permanent structural change occurring in a material subjected to conditions that produce fluctuating stresses and strains at some point or points that may culminate in cracks or complete fracture after a sufficient number of

fluctuations" [50]. Some keywords of this definition provide a phenomenological description of fatigue:

Localized: Fatigue is a local damage process that will occur at the most critical location.

Cracks: Fatigue is driven by the formation and propagation of cracks, generally formed at the surface. This is especially common for components working in corrosive environments, for example sea water. The grains at the surface are in contact with sea water, therefore their strength is decreased by corrosion. Forsyth [51] was one of the first researchers to propose to divide the fatigue process into two different stages, nucleation and propagation. In the nucleation stage, fatigue cracks begin as shear cracks on crystallographic slip planes[52]. In the propagation stage, they grow under applied stress propagating through the material until complete failure. This division of the fatigue process is not unique. For example, Schijve [53] divided the fatigue process in four phases: crack nucleation, micro crack nucleation, short crack propagation, macrocrack propagation, and failure. However, the main idea remains unchanged, i.e., fatigue is composed of an initiation and a propagation stage. In order to differentiate between both periods, Schijve [53] considered the initiation period to be completed when microcracks growth no longer depends on the material surface conditions. Some authors, for example, S. De-Guang et al [54], include a third stage, final fracture.

Failure: A distinctive aspect of fatigue is that the load is not big enough to cause static failure, however, failure takes place after a certain number of load cycles. Under certain conditions, it is possible to avoid final failure. In fact, if the stress fluctuation remains under a certain value (endurance limit), the component will have an unlimited fatigue lifetime. The endurance limit is lower than the yield stress. However, in some cases, the existence of the endurance limit is not guaranteed. In fact, Bathias [55] presented experimental data which demonstrated that there

is no fatigue limit for certain alloys, neither aluminum is considered to have a fatigue limit. Another example is steel in seawater environment which does not present a fatigue limit [32].

There are two main approaches for studying fatigue: cumulative damage and fatigue crack propagation. The first accounts for the accumulation of damage due to a fluctuating stress or strain, and the second is based on fracture mechanics an involves studying the propagation of cracks in structural members under cyclic loading. In this work, the cumulative fatigue damage approach has been selected over fracture mechanics. The reasons for this are explained in detail in Chapter 6.

In high cycle fatigue (when cyclic stresses in the material are mainly elastic), stress is commonly used as the damage variable; on the other hand, for low cycle fatigue strain or energy are used as damage variables.

3.2 Cumulative Fatigue Damage

Fatigue tests are commonly performed under constant load amplitude conditions. However, in industrial applications, structures are not subjected to constant loads. Fatigue damage increases with the applied load cycles in a cumulative manner. Palmgren suggested the concept that the fatigue damage accumulates in a linear manner. In 1945 Miner expressed this concept in a mathematical form, and the resulting formula is known as the Palmgren-Miner rule:

$$\sum_{i=1}^{k} \frac{n_i}{N_i} = C \tag{3.1}$$

where n_i is the number of cycles accumulated at stress level S_i ($\Delta\sigma_i$), N_i is the number of cycles to failure at stress level S_i, and C is the fraction of life consumed when exposed to the cycles at different stress levels. Failure is predicted to occur when C reaches a value of 1.

The Palmgren-Miner rule relies on two assumptions. The first is that the entire fatigue lifetime can be obtained as the sum of the individual fatigue lifetimes corresponding to each stress level. The second is that the order of the applied cycles does not influence the total damage. Simplicity is the main feature of Palmgren-Miner formula. Several authors have proposed modifications to the Palmgren-Miner formula to improve its accuracy. For example, Grover [56] proposed to divide the computation of the damage accumulation into two stages: crack nucleation and crack propagation. As a result, the formula for deriving damage accumulation is different depending on the stage in the fatigue lifetime. In another example, Lemaitre and Chaboche [57] presented a cumulative law based on the nonlinear evolution of the damage parameter as a function of the number of cycles and load level. Furthermore, this law accounts for the influence of load cycles whose amplitudes are below the endurance limit when fatigue damage has been initiated. This law shows a good correlation with physical observations. Fatemi et al [58],[59] presented a review of the existing cumulative damage theories available in the literature. Although Palmgren-Miner's formula has several shortcomings, it is still the method most widely applied method and is recommended by industry standards such as [60].

3.2.1 Stress based approach

3.2.1.1 S-N Curves

The stress based approach was the earliest, and is one of the most commonly used in practical applications [61]. Wöhler set the foundations of this approach by carrying out fatigue tests, axial- bending and torsion, on different notched and unnotched specimens. In 1870 Wöhler published his results as plots of stress amplitude versus number of cycles to failure. This is today known as an S-N curve. Furthermore, Wöhler also identified the detrimental effect of a tensile mean stress in the fatigue lifetime [62].

In 1910, Basquin fitted a mathematical expression to Wöhler's data; associating the stress amplitude with the number of cycles to failure as follows:

$$\sigma_a = \frac{E \cdot \Delta\varepsilon_e}{2} = \sigma_f (2N)^b \tag{3.2}$$

where σ_a is the applied stress range (stress amplitude $\Delta\sigma$ or S), $2n$ is the number of cycles to failure, σ_f' is the fatigue strength coefficient and b is the fatigue strength exponent, which usually varies between -0.5 and -0.7.

3.2.1.2 Multiaxial Fatigue-Critical Plane Approach

A multiaxial stress state is common in engineering components. There are several sources of multiaxiality, for example, external loading, geometric discontinuities, residual stresses, among others. Fatigue criteria have been traditionally based on uniaxial stress paths which are easily related with conventional experiments. An important breakthrough has been the development of multiaxial fatigue criteria, which are often based on critical plane methods. These criteria enable accurate fatigue predictions accounting for complex stress paths, which involve residual stresses, mean stresses, non-proportional loadings etc. Within the multiaxial fatigue assessment techniques, critical plane approach is popular, and found to be the most effective [16].

Critical plane methods are based on the concept that at a given location of the structural component, fatigue cracks will start in the most severely loaded planes. These methods study the normal and shear projections of the stress tensor at a given plane, and by means of a reducing function, they derive an equivalent stress amplitude that is compared with the fatigue properties obtained from uniaxial tests performed on specimens. In its most general form, the equivalent stress can be written as follows:

$$\sigma_{a,equ} = f(\boldsymbol{\sigma}(M,t), \boldsymbol{n}, \boldsymbol{C}) \tag{3.3}$$

Where *f* is the reducing function from a multiaxial stress state to a uniaxial stress state, and it is dependent of the stress tensor at a given point M, the plane considered (defined by its normal vector $\boldsymbol{n}$) and $\mathbf{C}$ a set of material parameters. These methods are phenomenological, they are based on the mechanisms that govern fatigue crack initiation. The form of *f* is based on the observation of the mechanisms that nucleate cracks. These methods consider that crack initiation is driven primarily by shear stress amplitude, with normal stress playing a secondary but important role. The equivalent stress amplitude is then compared with fatigue resistance *K* measured from simple uniaxial tests, which are a function of the number of cycles (N_f) to failure and material constants (m):

$$K = f(N_f, m) \tag{3.4}$$

For a given number of cycles (N_f), fatigue failure will take place if:

$$\sigma_{a,equ} = K(N_f, m) \tag{3.5}$$

From a computational point of view, the main challenge arises from the optimal search for the critical plane, and part of this challenge is the computation of the shear stress amplitude. In the case of structural components where the failure location is not well known a priori, computing the fatigue criterion in reduced running time becomes a necessity. Fast numerical methods for tackling this problem are proposed in Chapter 4. The present chapter continues with a brief review of several plane criteria, with special attention paid to the Dang Van fatigue criterion, because is the criterion used for carrying out fatigue assessment of mooring chains in Chapters 6 and 7. More detailed reviews of critical plane methods can be found in [6], [62]–[66].

From a historical perspective, the first attempts to establish models for studying multiaxial fatigue were based on combined torsion and bending tests. Gough [67] performed fatigue tests of several engineering steels subjected to bending and torsion stresses, and he obtained two empirical formulations to fit the experimental results.

Fatigue cracking is mainly triggered by alternating shear, while the normal component plays a secondary role. If the normal component is tensile, it causes the crack to open and accelerates its propagation [68]. On the contrary, if compressive, the normal stress component will delay propagation. Brown and Miller [68] introduced the concept of Case A and Case B cracks. In Case A, shear stress acts on the free surface in a direction parallel to the crack (in plane shear stresses); therefore, cracks propagate along the surface of the specimen. These cracks are shallow and have small aspect ratio. In Case B, cracks propagate inwards from the surface and are due to out-of-plane shear stresses. Tension loading can display both crack growth models, whereas torsion loading and torsion combined with tension always present Case A cracks [6].

Sines [69] used a linear combination of the octahedral shear stress amplitude and the mean hydrostatic stress as the damage variable (Let us recall that the Von Mises failure criteria studies the shear stress in the octahedral plane). The physical importance of the octahedral shear stress is that it expresses the average effects of slippage on different planes and on different directions of all crystals in the aggregate [6]. Sines observed that the mean torsion does not have an effect on fatigue. He included the effect of static tension by adding the mean hydrostatic stress, obtaining the following equation:

$$\sqrt{J_{2,a}} + a \cdot P_m - b \leq 0 \tag{3.6}$$

where: $\sqrt{J_{2,a}}$ is the alternating shear in the octahedral plane, P_m is the mean hydrostatic stress and a and b are material constants that can be obtained from repeated bending and torsion fatigue tests. $a = \frac{t_{-1} - \frac{f_0}{\sqrt{3}}}{\frac{f_0}{3}}$ and $b = t_{-1}$. f_0 and t_{-1} are the fatigue limits in repeated bending and alternating torsion respectively.

Crossland [70] proposed a fatigue criterion similar to Sines, but he replaced the mean hydrostatic stress, by the maximum hydrostatic stress. Crossland criterion is more suited for brittle materials, while Sines criterion for ductile ones. The value of the fatigue limit in repeated bending might be unavailable, therefore Papadopolus [64] proposed to use the Goodman formula instead.

Findley [71] was the first one to propose the concept of critical plane. His model uses the stress projection at a particular plane (critical plane) of the material. The damage criterion proposed by Finley is a linear combination of the alternating shear stress and the normal stress acting on the critical plane.

$$C_a(\mathbf{n}^*) + aN_{max}(\mathbf{n}^*) - b < 0 \tag{3.7}$$

$$\mathbf{n}^* \text{such that } \max_{\mathbf{n}}[C_a(\mathbf{n}) + aN_{max}(\mathbf{n})] \tag{3.8}$$

where,

$a = \frac{\frac{2t_{-1}}{f_{-1}} - 1}{\sqrt{1 - \left(\frac{2t_{-1}}{f_{-1}} - 1\right)^2}}$ and $b = \frac{t_{-1}}{\sqrt{1 - \left(\frac{2t_{-1}}{f_{-1}} - 1\right)^2}}$. f_{-1} and t_{-1} are the fatigue limits in alternating bending and alternating torsion respectively. $C_a(\mathbf{n}^*)$ and $N_{max}(\mathbf{n}^*)$ are the shear stress amplitude and the maximum normal stress on the critical plane.

Sines [69] and Crossland [70] are critical planes methods, although they consider that the critical plane always corresponds with the octahedral plane. Certain criteria such as Findley [71] define the critical plane as the plane where the linear combination of the shear stress amplitude and the normal stress is maximum. Other authors, for example, Matake [72] or McDiarmid [73] [74], define the critical plane as the plane where the shear stress amplitude is maximum.

Finding the critical plane involves solving an optimization problem, more precisely a maximization. The variable to be maximized depends on the criterion used. The Findley criterion is the most popular criterion that defines the critical plane by maximizing a linear

combination of the shear stress amplitude and the normal stress. However, as reported by Papadopulus [64], this criterion predicts incorrectly an effect of the mean torsion in the torsion fatigue limit. Because of this, Papadopoulos [64] omitted Findley's Criterion in his comparative analysis. Papadopoulos [64] presented a review of several critical plane approaches and he compared the predicted results for out-of-phase loadings.

All the critical plane methods presented in this section present two common challenges: to determine the critical plane, and to compute the alternating shear stress acting on the plane.

Multiscale Approach

Fatigue is a local process, and it frequently starts at imperfectly oriented grains with the formation of slip bands that might be followed by the formation of microcracks [75]. Dang Van criterion [76] analyses the stresses at the mesoscopic level (grain scale) [77]. The main idea behind this criterion is that if elastic shakedown (a structural component is considered to have attained an elastic shakedown state if its asymptotic behavior is elastic, note that it might undergo some plastic deformation in the early cycles) is reached at both scales (macroscopic and mesoscopic) fatigue failure will not take place. Engineers work with macroscopic stresses (for example obtained from FEM calculations or analytically). Considering a state of elastic shakedown at the macroscopic scale and based on Lin-Taylor assumptions (the first one: the strain tensors at macroscopic and mesoscopic scales are equal. The second one: the elastic matrix and the crystal are isotropic and have the same properties), Dang Van derived a change of scale expression that enables to derive mesoscopic stresses from macroscopic ones:

$$\tilde{\sigma} = \sigma(t) - \mathbf{s}^* \tag{3.9}$$

where,

$\tilde{\sigma}$ Stress tensor at mesoscopic level in the elastic shakedown scale

$\sigma(t)$ Stress tensor at the macroscopic level

$\mathbf{s}^*$: Represents the local residual stress state and characterizes the local stress fluctuation at the mesoscopic level. Under elastic shakedown, it is time independent and can be computed as the center of the smallest hypersphere that circumscribes the path of the stress deviator.

The mathematical expression for the fatigue criterion is given by:

$$\max_t[\tau(t) + a \cdot \sigma_h(t)] < b \tag{3.10}$$

where,

- $\tau(t)$: Maximum mesoscopic shear stress in the elastic shakedown state.

- $\sigma_h(t)$: Hydrostatic stress.

- a and b are material parameters.

Fatigue failure will not take place if the Eq. (3.10) is satisfied (i.e. the component will have an infinite fatigue lifetime). The condition that must be fulfilled for the application of the Dang Van criterion is that the stabilized macroscopic stress state corresponds with elastic shakedown. The Dang Van criterion was the first to propose a multiscale approach, that is, to use mesoscopic variables (at grain level) instead of macroscopic ones for studying fatigue. Different methods have followed, for example, the Papadopoulos fatigue criterion [76]. Papadopoulos replaced the maximum mesoscopic shear stress by the maximum mean value of the mesoscopic shear stress amplitude over all possible planes and all possible slip directions corresponding to each plane, Papadopoulos denominated this magnitude as resolved shear stress. This criterion is of an integral nature, because an integral must be evaluated when deriving the resolved shear stress. For simple load cases the integral can be computed analytically, although for more complex cases it is solved through numerical methods.

The Dang Van criterion is an endurance criterion (it determines whether fatigue failure will occur, or the component will have infinite fatigue life). Nevertheless, the Dang Van fatigue

criterion can be also be implemented for finite fatigue life [78] and [79]. It has been adopted for predicting fatigue behaviour in different industrial applications, ranging from cardiovascular stents [80] to mooring chains [15]. Several methods can be found in the literature based on the multiscale approach for finite fatigue life. The first was introduced by Morel [81] who used the accumulated mesoscopic plastic strain as the damage variable. This criterion is difficult to implement for complex loading. In order to overcome this difficulty, Jabbado [82] proposed a criterion whose mathematical expression is similar to that of Manson-Coffin but instead of using the plastic strain amplitude Jabbado chose the accumulated mesoscopic plastic strain as a damage variable. This criterion predicted good results for proportional loadings. Maitournam [83] modified Jabaddo's criterion for improving the fatigue life prediction for non-proportional loadings. Another criterion for finite fatigue life worth mentioning, is the Papadopoulos criterion [84].

3.2.2 Strain based approach

In 1955, Manson and Coffin presented an approach based on strain. They were working separately on thermal fatigue aspects, and demonstrated that plastic strain can also be linearized by mean of logarithmic coordinates. This approach is particularly useful for cases where plastic deformation plays a central role (for example creep problems). They based their approach on the Bauschinger effect (the change of the elastic limit by stress cycles [62]). The Manson-Coffin relationship describes the plastic strain resistance as:

$$\Delta\varepsilon_p = \varepsilon_f^{'}(2N)^c \tag{3.11}$$

where ε_f' is the fatigue ductility coefficient and c is the fatigue ductility exponent.

Manson and Coffin proposed that a metal's resistance to cyclic loading can be determined as the superposition of its elastic and plastic resistance. Combining the Basquin equation and plastic strain resistance, the Manson-Coffin relationship can be derived.

$$\frac{\Delta\varepsilon_T}{2} = \varepsilon_a = \frac{\Delta\varepsilon_e}{2} + \frac{\Delta\varepsilon_p}{2} = \frac{\sigma_f^{'}}{E}(2N)^c \tag{3.12}$$

A shortcoming of this equation is that it does not account for mean stresses or the multiaxiality of the stress tensor.

Similar to the Findley criterion based on the normal and the shear stress on the octahedral plane, Brown and Miller [85] proposed a model using cyclic shear strain (that plays a key role on nucleation) and the normal strain (that influences propagation) on the octahedral plane (the plane whose normal vector forms equal angles with the coordinate system). Brown and Miller studied the nucleation and growth of fatigue cracks and were the first to introduce the concept of Case A and Case B cracks. Brown and Miller proposed a different criterion for each type of cracking:

Case A Case B

$$\left(\frac{\Delta\gamma}{g}\right)^j + \left(\frac{\varepsilon_n}{h}\right)^j = 1 \qquad \left(\frac{\Delta\gamma}{2}\right) = constant \tag{3.13}$$

where, g, h and j are material constants. The value of j depends of the material, taking values of about 1 for brittle materials and about 2 for ductile materials

Roessle and Fatemi [86] proposed a strain-life formula based on a correlation study between tensile data and constant amplitude strain controlled fatigue properties. Their formulation does

not need complex experimental calibration, it merely uses the hardness and the module of elasticity as inputs, which are easily measurable.

For fatigue life prediction, one of the advantages of the stress based approach compared to its strain based counterpart is that it is simpler to take into account the effect of mean stress [61]. In order to overcome this shortcoming, Fatemi and Socie proposed a model combining stresses and strains. This model was based on experimental observation of the fatigue crack growth. Fatemi and Socie used the Brown and Miller model but replaced the normal strain term by the normal stress. This change enables the model to account for crack closure effects. Fatemi and Socie's model is a critical plane approach, given by.

$$\frac{\Delta\gamma}{2} \cdot \left(1 + k\frac{\sigma_{n,max}}{\sigma_y}\right) = \frac{\tau^{'}}{G}(2N)^{b\gamma} + \gamma_f^{'}(2N)^{c\gamma} \tag{3.14}$$

where, k is a constant, G is the shear modulus, τ' the shear fatigue strength coefficient, b is the shear fatigue strength exponent and c is the shear fatigue ductility exponent. These values are obtained from an alternating torsion fatigue test, although they can be approximated from an axial fatigue test [6].

3.3 Energy based approach

Energy based approaches use the strain energy as a damage variable. The plastic strain energy can be derived by integrating the area included in a hysteresis loop. The plastic strain energy can be caused by different types of loading, such as thermal cycling, creep, and fatigue [59]. Furthermore, in conjunction with Glinka's rule [87] it is possible to analyze the damage accumulation of notched specimens using the energy approach. Energy-based damage models can also include mean stress and multiaxial loads because multiaxial fatigue parameters based on strain energy are available [88].

Pan et al. [89] proposed a fatigue strain energy density parameter for the critical plane to predict the fatigue life under multiaxial loading. They modified the fatigue life parameter proposed by Glinka [87]. They compared their model predictions with experimental data. Ellyin [90] proposed a model that took as damage variable the total strain energy density per cycle, which can be defined as the sum of the plastic strain energy and the positive elastic strain energy (the elastic strain energy enables the model to account for mean stress effect):

$$\Delta W^{Total} = \Delta W^{Plastic} + \Delta W^{Elastic} \tag{3.15}$$

The final expression is:

$$\frac{\Delta W^{Total}}{\overline{\rho}} - C = k \cdot N^{\alpha} \tag{3.16}$$

where C, k and α are material constants that can be obtained by fitting the criteria to an S-N curve. $\bar{\rho}$ is a multiaxial constraint factor depending of the magnitude of the principal stresses and the Poisson ratio (ν). Using this parameter, the model takes into account the severity of the types of loading. For uniaxial loading $\bar{\rho} = 1$, for torsion or torsion-tension loading $\bar{\rho} = 1 + \nu$ and for biaxial tension loading $\bar{\rho} = 1 - \nu$.

3.4 Effect of Mean Stress on the fatigue life

It is well known that the fatigue of metals is affected by multiple factors, including, surface conditions, corrosion, residual stress, mean stresses, among others. Certain factors affect the fatigue performance across all the fatigue life span, such as corrosion or mean stress. Others, such as surface condition, affect mainly the crack initiation stage [91]. In this section, the effect of mean stresses is assessed.

Mean stresses are the result of the external loading and the initial stress state of the material (residual stresses). Chapter 5 presents a detailed description of residual stresses and a model for predicting residual stresses after the manufacturing process of a mooring chain.

For a uniaxial loading case, the Haigh diagram and Goodman or Gerber mean stress corrections are widely used to account for the effect of mean load [75]. These correction functions are issued from uniaxial fatigue tests. They are presented in the Figure 3.1.

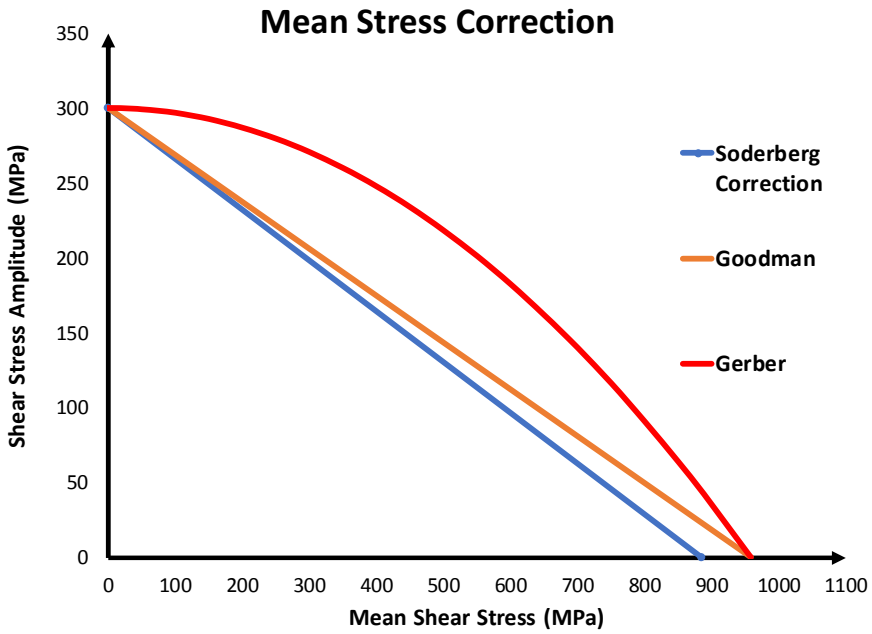

Figure 3.1 Failure criteria for fatigue life prediction with positive mean stress [Source [52]]

The mean stress correction functions are listed bellow as:

Goodman function:

$$\sigma_a = \sigma_e \left[1 - \left(\frac{\sigma_m}{\sigma_u}\right)\right] \tag{3.17}$$

Gerber ellipse:

$$\sigma_a = \sigma_e \left[1 - \left(\frac{\sigma_m}{\sigma_u}\right)^2\right] \tag{3.18}$$

Soderberg function:

$$\sigma_a = \sigma_e \left[1 - \left(\frac{\sigma_m}{\sigma_y}\right)\right] \tag{3.19}$$

where:

σ_e is the Fatigue strength for N cycles under zero mean stress.

σ_a is the Fatigue strength for N cycles under mean stress equal to σ_m.

σ_u is the ultimate tensile strength.

Although the aforementioned mean stress correction functions are the most commonly quoted in academic books, several others exist, such as Morrow, Walker or SWT (Smith Watson and Topper). Dowling [92] presented a review of the existing approaches for estimating mean stress effects on fatigue life. He compared the approaches for different steels. One of the main conclusions is that the Goodman equation is inaccurate by being over conservative because it employs the ultimate tensile stress. Other functions like the Walker equation provided better results; however, they require calibration of material constants, which make it not as straightforward to apply as the Goodman or Gerber equations.

When the stress tensor is not uniaxial and mean stresses from mean load are superimposed with residual stresses, the quantification of the influence of mean stresses is not as straightforward as in the uniaxial case. There is no generally accepted method to quantify the effect of mean stress. The multiaxial criteria presented earlier (Findley, Sines and Dang Van) account for mean stresses by introducing hydrostatic stress in the fatigue damage formulation. Therefore, in principle, these criteria already account for mean load. However, as pointed out by Susmel et al [93], most critical plane methods are based on two assumptions:

1- Mean shear stress does not affect fatigue life as long as its value remains below the yield shear stress of the material.
2- Fatigue strength and static stress are linearly related if the maximum stress during a cycle is below the yield strength.

When these assumptions are not valid, critical plane methods might predict erroneous fatigue lifetimes; therefore, for assessing the influence of the mean load, they should be used acknowledging the limitations of the results (A practical example is presented in Section 6.3.4).

The above statements are not definitive, and some aspects need to be highlighted. Concerning mean shear stress, it is important to point out that some critical plane methods make use of this magnitude. In any case, it is accepted (through mechanical testing) that mean stress effect is very different for pure normal stress and pure shear stress. Regarding the second statement about the linear relation between fatigue strength and static stress, it is not valid for high hardness steels.

3.5 Residual Stresses

Residual stresses comprise the stress field remaining in a structure or component without the action of any external load (mechanical or thermal). The origin of residual stresses is the incompatibility of permanent deformations, which can be of diverse nature, for example macroscopic plastic deformations or microscopic ones due to phase transformation. Depending on the scale at which the incompatible deformations take place, different types of residual stress can be defined:

- Type I: Also known as macro residual stresses because they vary continuously over large distances (order of magnitude of mm). Engineers are mostly concerned by this type of residual stresses because they modify the value of the mean stress, which has an effect on fatigue performance.

- Type II: Micro residual stresses which vary over grain scale (micron range). Also known as intergranular stresses.

- Type III: Residual stresses that vary over atomic scale, around dislocations and crystal interferences.

An example of incompatible strains occurs when non-uniform plastic strains appear under external loading. The condition of compatibility (a simple definition of compatibility is that given two adjacent particles of the same body, under an external load they must deform in such a way that they fit together after deformation [94]) makes the surrounding material deform elastically in order to preserve dimensional continuity, therefore creating residual stresses. Under a non-compatible plastic strain $\boldsymbol{\varepsilon}^P$, an elastic strain field $\boldsymbol{\varepsilon}^{elastic}$ is added in order to make it compatible. Therefore, the final residual strain field will be as follows:

$$\boldsymbol{\varepsilon}^{res} = \boldsymbol{\varepsilon}^{elastic} + \boldsymbol{\varepsilon}^P \tag{3.20}$$

Residual stresses are self-equilibrating; therefore, they must satisfy the following:

$$\mathrm{div}\boldsymbol{\sigma}^R = 0 \text{ over all the entire volume:} \tag{3.21}$$

$$\int_V \nabla \boldsymbol{\sigma}^R \, dV = 0 \tag{3.22}$$

$$\text{over all the surfaces} \quad (\boldsymbol{\sigma}^R \cdot n) = 0 \tag{3.23}$$

where $\boldsymbol{\sigma}^R$ is the residual stress tensor, and *n* the vector normal to the surface. In order to satisfy the equilibrium condition, the residual stress field must be composed of a tensile and compressive part. Finally:

$$\boldsymbol{\sigma}^{res} = \boldsymbol{C} : (\boldsymbol{\varepsilon}^{res} - \boldsymbol{\varepsilon}^P) \tag{3.24}$$

Solving the residual stress tensor involves finding the solution to an elastic problem with an initial plastic strain field $\boldsymbol{\varepsilon}^P$ and without any external loading. Once the residual stress tensor at a particular point *M* is known, the final stress field will be:

$$\boldsymbol{\sigma}(M,t) = \boldsymbol{\sigma}^{res}(M) + \boldsymbol{C} : \boldsymbol{\varepsilon}(M,t) \tag{3.25}$$

Residual stresses are frequently generated during the manufacturing process. Almost every manufacturing operation (heat treatment, rolling, forging, grinding, machining, among others) leaves residual stresses. In some cases, grinding or peening, the main purpose of the operation is to leave compressive residual stresses, which delay crack initiation and to a certain extent crack propagation.

Chapter 4: Fast Numerical Methods for fatigue assessment

This chapter compares different optimization techniques for reducing the computational time of critical plane methods and Dang Van fatigue criterion. From a computational point of view, the main challenge arising is the optimal search for the critical plane; part of this challenge is the computation of the shear stress amplitude. In the case of structural components where the failure location is not well known a priori, computing the fatigue criterion in reduced running time becomes a necessity. Both problems are described in the following sections.

4.1 Introduction

Multiaxial fatigue prediction methods and critical plane methods in particular are known to have a high computational burden and to be time consuming. Note that both, critical locations and the lifetime, have to be determined as part of a computational fatigue assessment. Therefore, for large, complex geometrical structures, the capability of performing fast fatigue analysis is essential. This is especially relevant for industrial applications.

We shall focus next on the heavy computational steps involved in critical plane methods. The two main challenges are:

(P1)- *Finding the smallest enclosing ball (SEB) of a given stress path cycle*, i.e. given a closed stress path, find the minimum enclosing ball defined as the smallest ellipse or ball. This problem appears when computing for example shear stress amplitudes or when constructing the smallest hypersphere in the Dang Van fatigue criterion.

(P2) - *Find the critical plane with respect to a given damage parameter*, i.e. the normal vector of the critical plane which maximizes a given damage indicator, as for example the shear amplitude.

An easy option is to solve the preceding problems by scanning all possible solutions in terms of radius and center of normal facet in the first and second case respectively, but these solutions are computationally time consuming and therefore not of practical interest for industrial applications. Another option is to transform these problems into optimization problems, and to use a standard minimization algorithm to minimize an appropriate cost functional. Optimisation methods can also be time consuming, nevertheless, choosing an advantageous strategy can speed up the process significantly.

The objective is to obtain a sufficiently accurate solution in a reduced computational time. Moreover, the simplicity of the employed method and the availability of the algorithms are equally discussed. The numerical methods used in the present chapter are available in different standard environments (MATLAB[95] , C++[96] or Python [97]), are easy to implement and can be widely applied to other problem types.

Different research papers aiming to reduce the computational cost of multiaxial fatigue analysis based on critical plane methods, can be found in the literature ([98]–[100]). Only one of them employed optimization methods [99]; however they were not implemented efficiently and relied on a particular definition of the critical plane. These contributions are reviewed and discussed in Section 4.3.

This chapter starts with a description of the two main problems that can be computed by means of optimization techniques, (P1) and (P2), in Section 4.2 and Section 4.3 respectively. It is followed by a brief description of the employed numerical methods focused on the Simplex and BFGS method. The fifth section proposes a mathematical formulation of the optimization

problems (P1) and (P2). The chapter continues by comparing the performances of the Simplex and BFGS methods with other standard techniques for solving the (P1) and (P2) problem. The chapter ends by discussing an industrial application, i.e. the fatigue assessment of a mooring chain under Out of Plane Bending (OPB).

4.2 Finding the smallest enclosing ball (SEB) of a given stress path cycle (P1)

This problem is encountered when computing shear stress amplitude or applying the Dang Van fatigue criterion.

4.2.1 Dang Van Fatigue Criterion

The Dang Van fatigue criterion has already been introduced in the previous chapter (see Chapter 3). From a computational point of view, the most expensive operation when applying the Dang Van fatigue criterion is to perform the calculation of the change of scale expression, which enables the computation of mesoscopic stresses from macroscopic ones:

$$\tilde{\sigma} = \sigma(t) - \mathbf{s}^* \tag{4.1}$$

where:

$\tilde{\sigma}$ Stress tensor at mesoscopic level

$\sigma(t)$**:** Stress tensor at the macroscopic level

$\mathbf{s}^*$:Represents the local residual stress state and characterizes the local stress fluctuation at the mesoscopic level. Under elastic shakedown, it is time independent and can be computed as the centre of the smallest hypersphere that circumscribes the path of the stress deviator.

From an implementation point of view, the main challenge is to obtain $\mathbf{s}^*$.It can be calculated through computational geometry [101] although most of the applications in the literature use optimization methods (for example [80], [102]–[104]) or in textbooks [105], and obtain $\mathbf{s}^*$ as:

$$\mathbf{s}^* = \min_{s^*} \max_{t} ||\mathbf{s} - \mathbf{s}^*|| \tag{4.2}$$

Among the optimization techniques that have been used in the literature for solving Eq. (4.2) are the Simplex technique [106], quadratic programming [80] and a modified steepest descent method [102]. It is worth reminding that BFGS (this method is presented in Section 4.4) is a steepest descent method that uses an approximation of the Hessian for improving convergence. The conclusions obtained in this study for obtaining the centre of the smallest hypersphere in 6 dimensions are valid for other criteria that involve the computation of smallest hyperspheres, for example, Bin Li et al. [107] or Deperrois [108].

4.2.2 Shear Stress Amplitude Computation

Consider the plane Δ, which is one of the possible infinite planes passing through a generic point M, and is defined by its normal vector **n.** The cyclic stress vector acting on this plane can be defined as:

$$\boldsymbol{\sigma}_n = \boldsymbol{\sigma}(t, M) \cdot \mathbf{n} \tag{4.3}$$

The stress vector $\boldsymbol{\sigma}_n$ can be decomposed into two vectors, normal (σ) and tangential to the plane (τ):

$$\sigma = \mathbf{n} \cdot \boldsymbol{\sigma}_n = \mathbf{n} \cdot \boldsymbol{\sigma}(t, M) \cdot \mathbf{n} \tag{4.4}$$

$$\boldsymbol{\tau}(t) = \boldsymbol{\sigma}_n - \sigma \cdot \mathbf{n} = \boldsymbol{\sigma}(t, M) \cdot \mathbf{n} - (\mathbf{n} \cdot \boldsymbol{\sigma}(t, M) \cdot \mathbf{n}) \cdot \mathbf{n} \tag{4.5}$$

The direction of the normal stress does not change during the fatigue load cycle, and so finding the amplitude and mean value is straightforward:

$$\sigma_{mean} = \frac{1}{2} \cdot \{\max_t \sigma + \min_t \sigma\} \qquad \sigma_a = \frac{1}{2} \cdot \{\max_t \sigma - \min_t \sigma\} \tag{4.6}$$

The shear stress acting on Δ has two components. In the most general case, the direction and magnitude of shear stress change, although if the loading is proportional the direction remains constant. The tip of the shear stress vector draws a curve in the Δ plane during the fatigue load cycle.

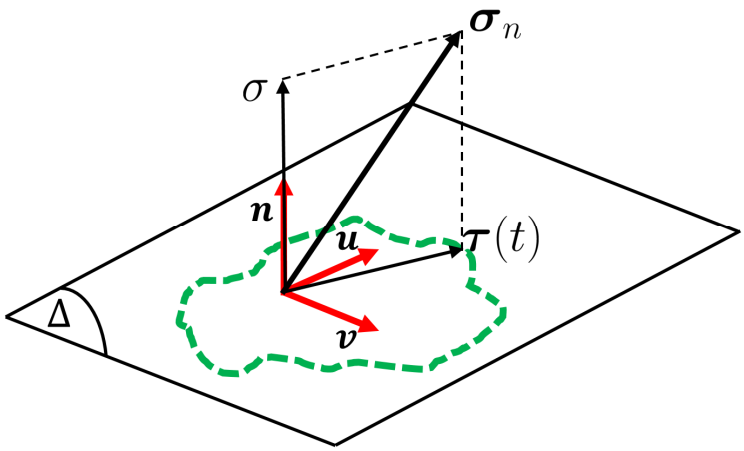

Figure 4.1 Normal and shear projections of the stress path on a generic plane

Different definitions of the shear stress amplitude can be found in the literature: namely the longest chord method [109], the longest projection [110], and minimum circumscribed circle (MCC) [111]. In the case of non-proportional loading, only the MCC definition proposed by Papadopoulos [111] provides a unique definition of the shear stress amplitude. According to this definition, the shear stress amplitude is the radius of the minimum circumscribing circle enclosing the shear stress path, with the centre of the circle representing mean shear stress. This problem is equivalent to finding the SEB of a set of points. Prior to the computation of the radius of the circle, the centre must be known.

Bernasconi [112] [113] presented a review of the different methods available for calculating the shear stress amplitude using the MCC definition (See Figure 4.2). Of the methods presented, the most efficient in terms of running time was the randomized algorithm. The

present chapter continues Bernasconi's work and aims to determine whether other optimization techniques can compute shear stress amplitude more efficiently.

More recently, another definition of shear stress amplitude has been proposed [114] and [115], the minimum circumscribed ellipse (MCE), which accounts better for non-proportional loading. According to this definition, the shear stress amplitude is:

$$\tau_a = \sqrt{R_a^2 + R_b^2} \tag{4.7}$$

where R_a and R_b are the radii of the major and minor semi axes respectively, as displayed in Figure 4.2.

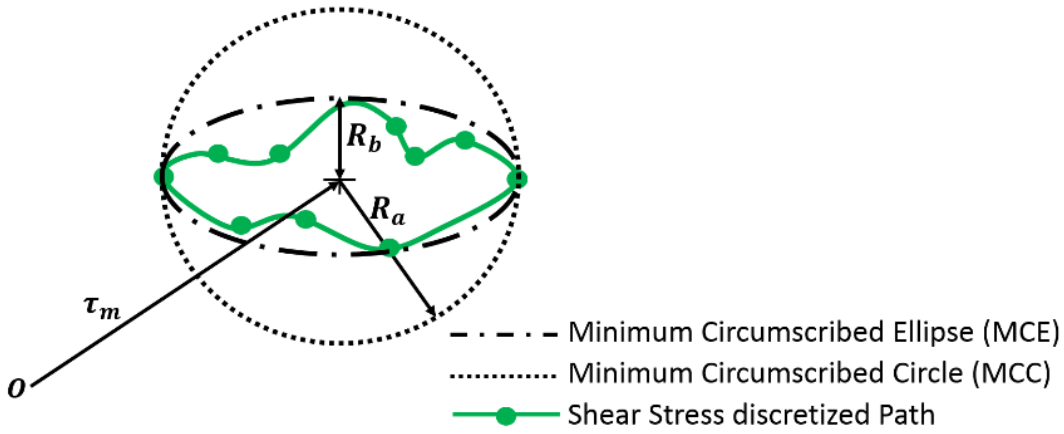

Figure 4.2 Definitions of the shear stress amplitude

Nevertheless, the definition of the mean shear stress remains the same, and needs to be calculated before computation of the shear stress amplitude [107]. Furthermore, this remains the most time consuming operation.

4.3 Finding the critical plane (P2)

Let us assume that the outcome of the mechanical analysis at a generic point M is presented as $\boldsymbol{\sigma}(t, M)$. Any material plane is defined in terms of its normal vector, expressed as:

$$\mathbf{n} = \begin{pmatrix} \sin\theta \cdot \cos\varphi \\ \sin\theta \cdot \sin\varphi \\ \cos\theta \end{pmatrix} \tag{4.8}$$

where φ and θ are the Euler angles with respect to the Cartesian coordinate system. The range of the angles is $\varphi \in [0, 2\pi]$ and $\theta \in [0, \pi]$, defining a sphere.

The critical plane, defined by its normal, is the plane where a crack will open preferentially during the fatigue load cycle. The critical plane is defined by a maximization of a damage parameter over all possible normal directions. Several damage parameters for the critical plane have been proposed in the literature. Shear stress plays a central role in fatigue cracking, whereas normal stress influences the opening or closing of the crack [68]. Both magnitudes can be used in finding the critical plane. Some criteria such as Findley [116] define the critical plane as the plane where the linear combination of shear stress amplitude and normal stress is maximum. Other authors, for example Matake [72] or McDiarmid [73] [74], define the critical plane as the plane where the shear stress amplitude is maximum. Additional discussion can be found in papers like Papadopulus [64], where different criteria are compared. In the present study, the definition of the critical plane as the plane experiencing the maximum shear stress amplitude has been adopted. Nevertheless, the presented novel strategy for finding the critical plane can be easily adapted to Findley criterion, as will be shown in the next section. The problem of finding the orientation of the critical plane can then be defined as an optimization problem, the mathematical definition of the problem; is presented in Section 4.5.

Strategies for identifying the critical plane

Different strategies proposed for determining the orientation of the critical plane are now briefly reviewed. The classical approach is to make variations of φ and θ for each 20 degrees. This approach was first proposed by Bannantine and Socie [117]. With the increase of computational capabilities, this angular difference has been reduced to 10 degrees. Nevertheless, this approach does not guarantee to find the exact critical plane, although in most

cases it is able to find a good approximation to it. In any case, this method is not optimal, and even though it might find a plane very close to the critical plane, it requires a significant computational effort. Figure 4.3shows the distribution of the points that represent planes where the shear stress amplitude has to be computed in order to determine the critical plane.

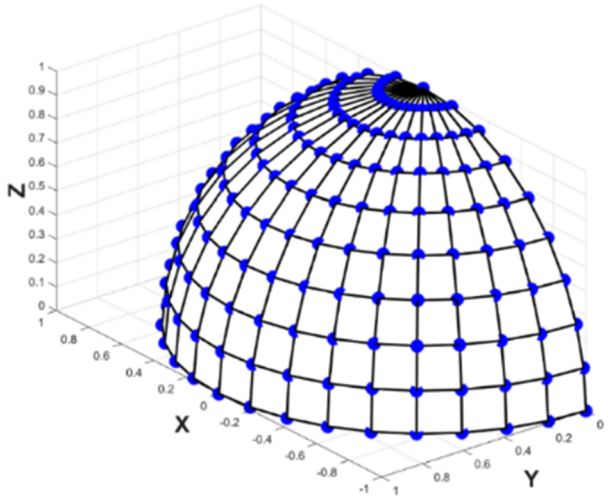

Figure 4.3 Classical Approach for locating the Critical Plane; the angle varies with 10° intervals

As already reported by Weber et al. [98], the resulting distribution is not optimal in that it gives very small areas for some elements, especially the elements located at the pole of the mid sphere. The method does not provide an equilibrated distribution of the planes to inspect with respect to the area. Weber et al. [98] proposed an improvement, to divide the quarter of sphere into equal parts. This method is more efficient; however, it does not guarantee to find the exact critical plane.

Susmel [99][118] proposed an efficient algorithm for locating the critical plane. Susmel defined the critical plane as the plane where the variance of the resolved shear stress is maximum, and performed multiple gradient searches using different starting points. The objective function (in this case, the variance in resolved shear stress) might have several local minima; by performing several optimizations with different starting points, the probability of finding the global

maximum is increased. In the optimization procedure, Susmel employed a constant step size, which is not very efficient, because far from the maximum the step sizes should be large and reduce as the maximum is approached.

Norberg and Olsson [119] proposed the use of a coarse mesh as an initial guess, and refinement of the grid at regions of interest. The authors did not employ optimization. As a final method to be considered, Svard [100] proposed a branch and bound algorithm for locating the critical plane according to Findley's Criterion. The performance of this algorithm is remarkable, although the implementation is not straightforward. Svard claimed that this method could also be implemented for other critical plane criteria.

4.4 Optimization of Functions

Optimization is a large field of numerical research, and its techniques are applied in different disciplines such as economy or operational research. A very simple definition of the problem follows: Given a function f (the objective function) that depends on one or more variable, find values for which f reaches a maximum. Sometimes the independent variables can only take values belonging to a certain interval (for example, mass cannot be negative); in such cases, the problem becomes constraint optimization.

Gradient methods such as BFGS need to be supplied with the gradient, whereas others, such as Simplex do not require information on the gradient. If the gradient is not known in an explicit form, its values can be derived numerically through finite differences. This supposes an increase in computational effort and in some cases, might not be very robust; therefore, finite differences method for deriving the gradient has been avoided. Methods that use the gradient should converge in fewer iterations, although this does not necessarily mean they are faster in terms of running time.

4.4.1 Simplex method

This method is also known as Nelder-Mead method. It was proposed by John Nelder and Joseph Mead [120]. Simplicity and robustness are among its strong points. It is a direct search method, it does not require the value of the gradient [121].

In an n dimensional problem, a simplex is a n+1 convex hull polyhedron, for example, in a 2D problem a simplex is a triangle or in 3D it is a tetrahedron. The simplex must fulfil the condition of non-degeneracy (that is, to be able to enclose a finite inner n-dimensional volumes). Starting with an initial simplex, the method carries out a series of transformations of the simplex, the aim being to decrease the function value at the vertices. At each step, the current simplex is updated through 3 possible transformations: reflection, reflection and expansion, contraction and multiple contraction. At each step, the worst vertex is located (where the function takes the higher value, with respect to the other vertices) and is moved by reflection through the centroid of the n remaining points. If the new location is better than the current one, the simplex is stretched along this line. On the contrary, if the new point is not much better, the simplex is shrunk towards a better point. The transformations of the initial simplex in a two dimensional problem are presented in Figure 4.4.

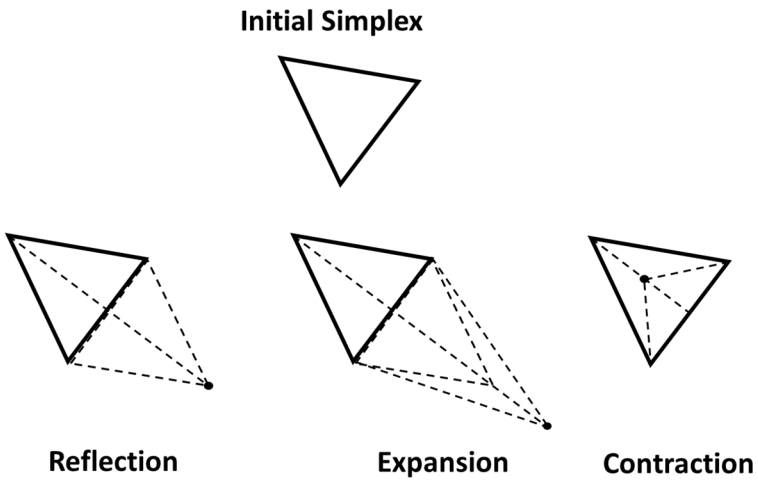

Figure 4.4 Possible movements of the Simplex method in 2D

The process stops when the simplex becomes sufficiently small, or the function values at the vertices are sufficiently close. Gradient based methods might require fewer iterations to achieve convergence than the Simplex method; nevertheless, this does not imply that such methods are faster in terms of running time. If a good initial simplex is provided, the number of iterations can be significantly reduced, hence the running time decreases.

MATLAB [122] has a built-in function of the simplex method that uses the simplex algorithm proposed by Lagarias [123].This built-in function has been used in the research presented in this chapter.

4.4.2 BFGS

The BFGS (Broyden–Fletcher–Goldfarb–Shanno) method for minimizing a smooth function is very popular among researchers [124]. Newton's method is commonly used for obtaining the roots of a function. It generates a sequence starting from an initial guess x_o. If the initial point is close enough, this method will converge to the minimum quadratically. In a one-dimension problem:

$$x_{n+1} = x_n + \frac{f(x_n)}{f(x_{n+1})} \tag{4.9}$$

The minimum of the function will be a root of the derivative, therefore, if we substitute the function by its derivative, we can use Newton's method for finding a minimum.

$$x_{n+1} = x_n - \frac{f'(x_n)}{f''(x_{n+1})} \tag{4.10}$$

Convergence to a minimum is guaranteed if $f''(x_n) > 0$. This expression can be generalized for n dimension:

$$\mathbf{x_{n+1}} = \mathbf{x_n} - \mathbf{A}_n^{-1} \cdot \nabla f(\mathbf{x_n}) \tag{4.11}$$

where:

$\nabla f(\mathbf{x_n})$ is the gradient evaluated at $\mathbf{x}_n$

$\mathbf{A}_n^{-1}$ is the inverse of the Hessian matrix evaluated at $\mathbf{x}_n$

If the Hessian matrix is positive-definite (let us recall that a positive-definite matrix is a symmetric matrix with all the eigenvalues positive [125]) the sequence will always move in a downhill direction (Therefore approaching the minimum). Nevertheless, far from the minimum, we might not be able to guarantee that the Hessian always remains positive-definite; if this is not the case, the sequence will not converge to a minimum.

In order to overcome this problem and the fact that the Hessian might not be available, Quasi-Newton methods (such as BFGS or LBFGS) do not use the exact value of the Hessian. Instead, they use an approximation that will always be positive-definite regardless how far the solution is from the minimum, as demonstrated in [124]. Because Quasi-Newton methods use the gradient (if it is not available explicitly it can be derived from finite differences) they tend to converge faster than direct search methods such as Simplex.

The method starts with a positive-definite approximation of the Hessian (usually the unity matrix) that, close to the minimum, will approach the true Hessian and achieve quadratic convergence. As in the case of Newton methods, a good initial approximation makes the algorithm very fast to converge [124]. Moreover, because quasi-newton methods do not evaluate the Hessian matrix, they can be faster than Newton methods. Instead of approximating the Hessian, an approximation of the inverse of the Hessian is computed, therefore avoiding the need of inversing the Hessian. A slightly similar version of BFGS is the LBFGS, which requires less memory and is usually used for problems of high dimensions.

The basic steps of the BFGS method are the following [124]:

For a given starting point $\boldsymbol{x_0}$, an initial approximation of the inverse of the Hessian $\boldsymbol{H_0}$ and convergence tolerance ε:

$n \leftarrow 0$

While: $||\nabla f(\mathbf{x_n})|| < \varepsilon$

1- Compute Search direction and step size

$$\mathbf{p_n} = -\mathbf{H}_n \cdot \nabla f(\mathbf{x_n}) \tag{4.12}$$

Perform a minimization to obtain the step size α_n from:

$$\mathbf{x_{n+1}} = \mathbf{x_n} + \alpha_n \mathbf{p_n}, \mathbf{\Phi}(\alpha_n) = f(\mathbf{x_n} + \alpha_n \mathbf{p_n}) \tag{4.13}$$

$$\min \mathbf{\Phi}(\alpha_n) \tag{4.14}$$

The one-dimensional problem is solved in two stages:

i. Bracketing of the Minimum: An interval [a,b] containing the optimal step length is found.

ii. Selection Phase: The step length belonging to the interval is obtained, this can be done using gradient information (for example cubic interpolation) or without (Fibonacci search or Golden search).

If the step length satisfies the Armijo condition (imposing a reduction of the function) and Wolfe condition (controlling the change in the gradient) it should decrease sufficiently the objective function [124]. Both aforementioned conditions are also known as Strong Wolfe Conditions (SWC). Most of the implementations of BFGS impose SWC. If *f* is smooth the existence of a step length satisfying SWC is guaranteed. For non-smooth functions, it is not possible to fulfil SWC [126].

2- The approximation of the inverse of the Hessian is obtained via:

$$\mathbf{s_n} = \mathbf{x_{n+1}} - \mathbf{x_n}, \mathbf{y_n} = \nabla f(\mathbf{x_{n+1}}) - \nabla f(\mathbf{x_{n+1}}), \rho_\mathbf{n} = \frac{1}{\mathbf{y_n}^T \mathbf{s_n}} \tag{4.15}$$

$$\mathbf{H}_{n+1} = (I - \rho_{\mathbf{n}}\mathbf{s_n}\mathbf{y_n}^T)\mathbf{H}_n(I - (I - \rho_{\mathbf{n}}\mathbf{y_n}\mathbf{s_n}^T) + \rho_{\mathbf{n}}\mathbf{s_n}\mathbf{s_n}^T \quad \textbf{(4.16)}$$

Originally, the BFGS method was intended to be used for smooth functions [127]. Implementations of the BFGS can be found in MATLAB [128] [95] [129], C++ [96] [130] or Python [97].

4.5 Mathematical Formulation – Objective Functions

Optimization of functions is a common operation throughout fatigue analysis. In this section, definitions of the objective functions for the problems described in Section 4.2 and Section 4.3 are presented.

4.5.1 SEB: Smallest Enclosing Ball (P1)

A ball B_i in $\mathbb{R}^n$ with radius such that $r_i \geq 0$ is the closed set $B_i = \{x \in \mathbb{R}^n : ||x - c_i|| \geq r_i\}$.

Given a set of balls $\mathbb{B} = \{B_1, B_2, ..., B_n\}$ in $\mathbb{R}^n$, the SEB problem is to find a ball of the minimum radius that encloses all the balls in $\mathbb{B}$.

Given a set of Points in $\mathbb{P} = \{P_1, P_2, ..., P_n\}$ in $\mathbb{R}^n$, a particular case of the SEB Problem is to find the SEB to all the points in $\mathbb{P}$, also known as the Minimum Enclosing Circle (MEC) problem. Each point represents a value of the discretized stress path. Nevertheless, each point could be considered as a ball instead; the radius of the ball would be a measure of the uncertainty of the calculation. For a two-dimensional case this concept is represented in Figure 4.5. This problem is frequently faced in multiaxial fatigue analysis, in two dimensions for deriving the shear stress amplitude and in 6 dimensions for computing the centre of the smallest hypersphere (Dang Van Fatigue Criterion).

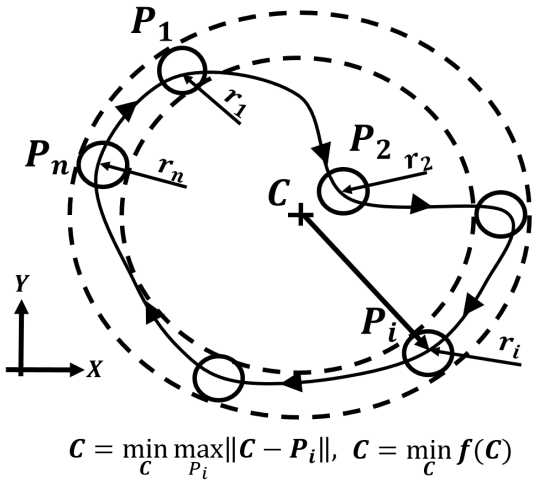

Figure 4.5 SEB Problem in 2D

There are two main strategies for solving the SEB problem to a set of Points:

1- ***Computational Geometry***: One of the most popular methods in this category is the randomized incremental algorithm. The method starts with the permutation of the set of points $\mathbb{P}$ and then adds one by one while the smallest circumscribed circumference is maintained [131]. A recent literature review regarding these techniques can be found in [132].

2- ***Optimisation***: The problem can be solved by minimizing the maximum distance between the centre of the ball and a given point. The Centre ($\mathbf{C}$) of the smallest enclosing ball can be obtained as follows:

$$\mathbf{C} \in \mathbb{R}^n, \mathbf{C} = \min_{\mathbf{C}} \max_{\mathbf{P}_i} ||\mathbf{C} - \mathbf{P}_i||, \mathbf{C} = \min_{\mathbf{C}} f(\mathbf{C}) \quad \textbf{(4.17)}$$

where $f(\mathbf{C})$ is the objective function, and for an *n* dimension problem is defined as follows:

$$f(\mathbf{C}) = \max_{\mathbf{P_i}} \sqrt{(c_1 - P_{i,1})^2 + (c_2 - P_{i,2})^2 + ... + (c_n - P_{i,n})^2} \quad \textbf{(4.18)}$$

For a given Centre C, the point for which the Euclidean norm is maximum is known and saved as $\mathbf{P}_{max} = (P_{max,1}, P_{max,2}, ..., P_{max,n})$. Once this point is determined, the calculation of the gradient is straightforward:

$$\nabla f(c_1, c_2, ...c_n) = \begin{pmatrix} \frac{\partial f(c_1,c_2,...,c_n)}{\partial c_1} \\ \frac{\partial f(c_1,c_2,...,c_n)}{\partial c_2} \\ . \\ . \\ \frac{\partial f(c_1,c_2,...,c_n)}{\partial c_n} \end{pmatrix} \quad \textbf{(4.19)}$$

where:

$$\frac{\partial f(c_1, c_2, ..., c_n)}{\partial c_i} = \frac{c_i - P_{max,i}}{\sqrt{(c_1 - P_{max,1})^2 + (c_2 - P_{max,2})^2 + ... + (c_n - P_{max,n})^2}} \quad \textbf{(4.20)}$$

A priori, we cannot guarantee the smoothness of the objective function [Eq. (4.18)], as has already been pointed out in the literature [133] (noting that a function is said to be smooth if it has continuous second order derivatives [125]). Therefore, the challenge of minimizing a non-smooth function has to be addressed. Different approaches based on optimization can be found in the literature, most of them using smoothing functions. Some authors propose to use Chen-Harker-Kanzow-Smale (CHKS) smoothing function and then application of the BFGS method [134], other authors use a smooth approximation (log-exponential aggregation) of *f* and then apply BFGS [135]. In this paper, a smoothing function proposed by Zhou et al [134] has been employed. The detailed mathematical formulation is given in Appendix A.

The BFGS method should strictly be used with smooth functions. Nevertheless, some authors have successfully used BFGS for non-smooth functions using Weak Wolfe Conditions (WWC) and inexact line search [126], [136], [137]. This approach does not require the use of a smoothing function. In general, the performance of minimization methods depends on the initial information provided to the algorithm and the tolerances imposed. For all methods, the centre of gravity (as in [112]) is provided as an initial point.

Different papers comparing optimization techniques for solving the SEM problem can be found in the literature. For example, Pan and Li [135] solved the problem for dimensions ranging

from 100 to 10000, and Zhou et al. [134] for dimensions greater than 100. These problems fall outside the scale of fatigue analysis, where the maximum dimension of the problem is 6.

4.5.2 Search of the critical Plane (P2)

The orientation of the critical plane is defined by its normal vector. At first, the use of constraint optimization could be considered. However, due to the possible existence of local maxima, such techniques might fail (trials performed with the MATLAB built-in constraint optimization algorithm showed that for complex loading histories this technique was not successful).

The orientation of the critical plane is defined as follows:

$$\boldsymbol{n}_{CriticalPlane} = \max_{\varphi,\theta\in\mathbb{R}} \tau_a \text{ subjected to } \begin{matrix} \varphi \in [0,\pi] \\ \theta \in [0,\frac{\pi}{2}] \end{matrix} \tag{4.21}$$

where the objective function is:

$$\tau_a = f(\boldsymbol{\sigma}(M,t),\boldsymbol{n}) \tag{4.22}$$

Recall that finding the maximum of a function is equivalent to finding the minimum of that function multiplied by -1. Consequently, Eq. (4.21) can be rewritten as a minimization:

$$\boldsymbol{n}_{CriticalPlane} = (-1)\cdot \min_{\varphi,\theta\in\mathbb{R}} \tau_a \quad \text{subject to } \begin{matrix} \varphi \in [0,\pi] \\ \theta \in [0,\frac{\pi}{2}] \end{matrix} \tag{4.23}$$

A novel strategy for finding the critical plane is now proposed**: Pre-Evaluation Grid + Simplex Optimization**. It comprises two distinct steps. First, an initial search is performed on planes located in a predefined grid. Each point of the predefined grid is associated with a plane defined by its normal vector. Then, the plane where shear stress amplitude is maximum is used

as initial guess of an optimization method. A more detailed description of the method is as follows:

0- Divide the quarter of sphere (represents all possible orientations of the critical plane) by meshing it with triangular elements to form an initial grid (as shown in Figure 4.6). The division of the quarter of the sphere is the same regardless of the load case. By doing this, we are sure to distribute homogenously the points where the shear stress amplitude is evaluated, as in Weber's proposal [98].

1- ***Pre-Evaluation***: Evaluate shear stress amplitude Eq. (4.22) at the points of the initial grid. Of all the nodes where the function has been evaluated, find the maximum value and store its position.

2- ***Optimization***: Perform a Nelder-Mead Simplex optimization (described in the previous section) using the previously saved maximum value as an initial guess.

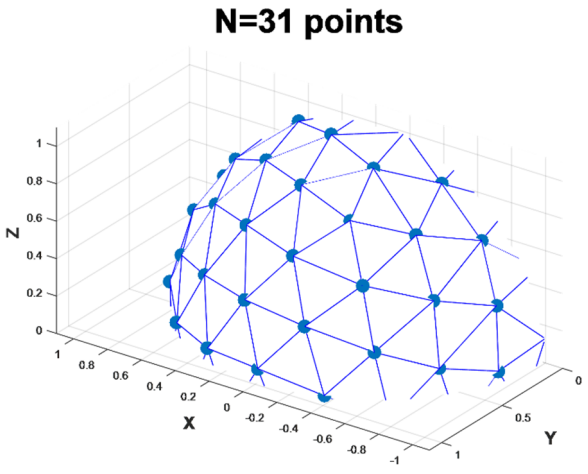

Figure 4.6 Pre-Evaluation Grid (31 Points)

The proposed strategy has several advantages, it is a modular approach and it does not rely on a particular definition or method for computing the shear stress amplitude. Furthermore, the approach is independent of the definition of the critical plane (unlike Susmel [99] [118] or

Svard [100]). Finally, there is no need to program a complex mathematical algorithm; instead the Nelder Mead Simplex optimization algorithm is already coded in several programming languages such as Python [97], MATLAB [138], C++ [96], among others. At first, BFGS could be used in the optimization stage; however, this method requires the gradient, whose expression is not known explicitly.

The number of points at which the function is Pre-Evaluated in Step 1 must be carefully calibrated. On the one hand, we want to evaluate the function in the fewest number of planes as possible. On the other hand, we need a good initial search so that the optimization algorithm does not require a large number of iterations to converge to the solution.

4.6 Results

In this section, the performances of different optimization techniques for solving the SEB problem (P1) and finding the critical plane (P2) are compared. All the calculations shown in this section have been performed using MATLAB R2015a on a standard laptop computer (Intel (R) Core (TM) i5 270GHz with 8GB of RAM Memory). All the presented running times have been measured in seconds and obtained as the mean over 10000 iterations.

4.6.1 SEB Problem in 2D-Shear Stress Amplitude

The performances of the following methods are compared:

1- *Randomized Incremental algorithm* as described in [139]. This method is based on computational geometry.

2- *Nelder-Mead simplex* implemented in the MATLAB built-in function.

3- *BFGS- HANSO*: At first the BFGS method using SWC was used, however, in many cases the line search failed because it was not able to fulfil SWC. The MATLAB code HANSO [140] [126] based on BFGS and Weak Wolfe Conditions (WWC) has

been used, this code can be used for smooth and non-smooth functions, as claimed by its authors. This code is available at [129].

4- BFGS with SWC using a smooth approximation of the function as described in [134]. Appendix A contains the formulation of the smoothing function.

5- Minmax built-in function in MATLAB, based on sequential quadratic programming [122]. This method was considered in previous studies for obtaining the shear stress amplitude [112], therefore it has been included in our study.

BFGS belongs to the quasi-Newton methods; these techniques require information on the gradient. Here, the gradient has been computed analytically, by means of Eq. (4.19) and Eq. (4.20).

Three different load paths (reported in Figure 4.7) have been selected for evaluating the performance of the available methods for computing the MCC (noting that regardless of the definition of the shear amplitude used, this is a compulsory step and remains the most computationally expensive operation). The load paths are similar to those used by Bernasconi [112] [113] in his comparison study. Each of the load paths has been discretized with a different number of points: 40, 75, 100, 150, 250 and 500.

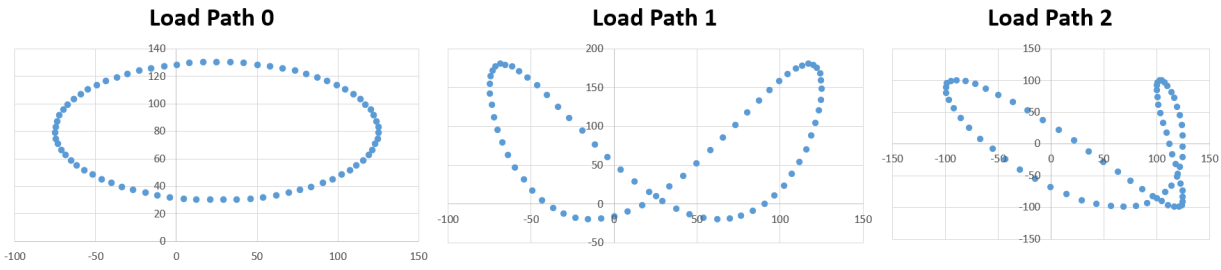

Figure 4.7 Load Paths used for comparing the performance of methods for deriving shear stress amplitude

A clear difference between Load Path 2 and the two others, is the complete lack of symmetry, Load Path 2 is the most complex problem (optimization methods need more iterations and

function evaluations to attain convergence). Indeed, a standard implementation of BFGS using SWC failed for this load path, and only an implementation using WWC (for example MATLAB code HANSO [140]) succeeded to converge for Load Path 1 and Load Path 2.

Figures 4.8 and 4.9 present the values of the recorded running times and function evaluations for the studied load paths for different numbers of points used to discretize the loadpath.

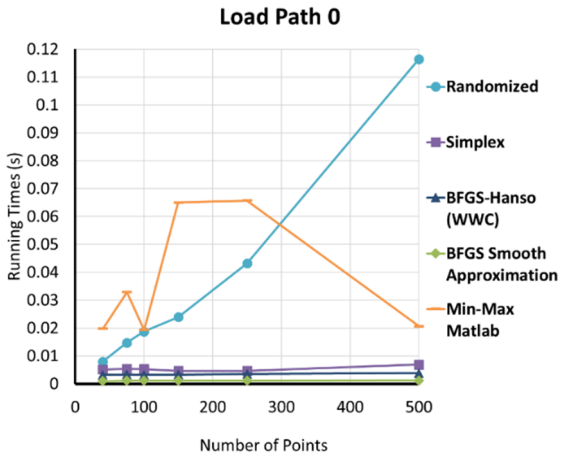

Figure 4.8 Recorded running times for Load Path 0

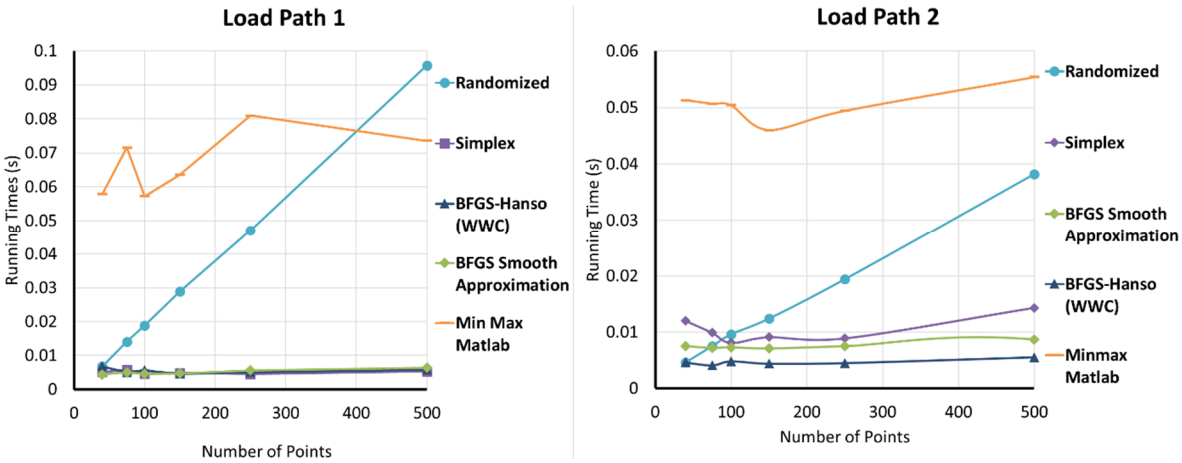

Figure 4.9 Recorded Running Times for Load Path 1 and Load Path 2

Figure 4.9 reveals that BFGS outperforms the other methods, in all the cases the run time was below 0.01 s. Also, the run time remained the same whatever the number of points used to

discretize the load path. Two different implementations of BFGS were compared, one using SWC and a smooth approximation of the function, and another without a smoothing function but WWC (Hanso). In terms of accuracy, both predicted similar results (less than 5% difference). When it comes to running time, both were similar except for Load Path 2 where BFGS-Hanso was slightly faster.

For Load Path 1 and Load Path 2 discretized with 40 points, Simplex, randomized and BFGS had similar running times, BFGS being the fastest. As expected, the run time of the Randomized algorithm remained proportional to the number of points. Furthermore, this method was faster than the Min Max built-in function in MATLAB as already reported by [112].

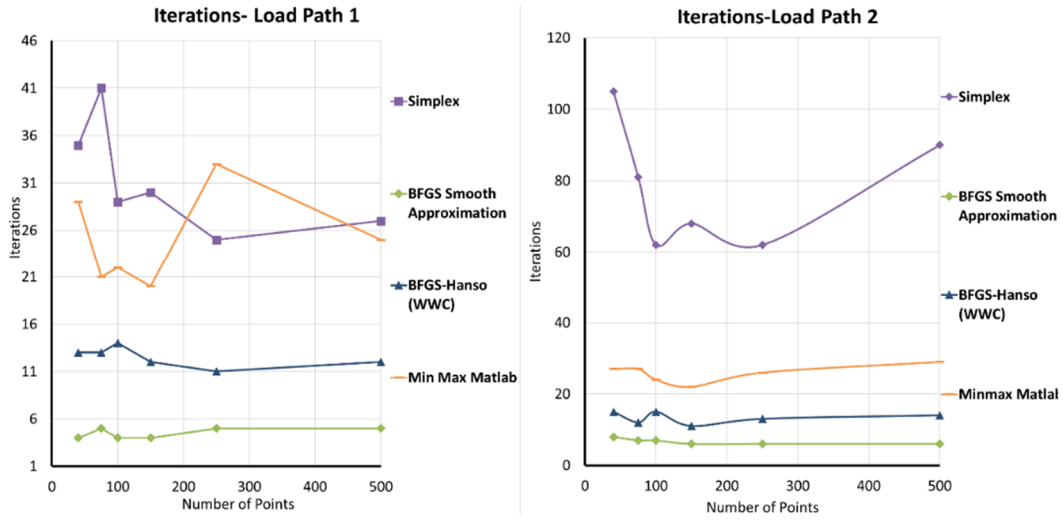

Figure 4.10 Iterations for Load Path 1 and Load Path 2

Figure 4.10 demonstrates that the Simplex Method requires a larger number of iterations than BFGS. This difference is not necessarily reflected in the run time. In fact, for Load Path 2, the numbers of iterations required by Simplex were between six and eight times more than those required by both BFGS implementations. However, this proportion was different in the case of the run time, which less than doubled. This should not come as a surprise, because BFGS uses information provided by the gradient and the approximation of the Hessian, and so it should

converge in fewer iterations than Simplex. However, each iteration of BFGS is computationally more expensive (involving the computation of the gradient, the approximation of the Hessian, and a line search) than a Simplex iteration; and because each function call is not time consuming, it is feasible that both methods could have similar run times despite requiring different number of function calls (This is the case of Load Path 1).

Figure 4.11 shows a contour plot of the objective function for Load Path 2 discretized with 75 points. As before, all the optimization methods had the same initial guess, the mean value. The circle markers represent the sequence of values of the solution at every iteration of BFGS, the cross markers the sequence predicted by Simplex. In the case of BFGS, the advantage of employing the gradient is evident; at each iteration it moves the next iterate in the direction of maximum change of the objective function (orthogonal to the contour lines). By contrast, Simplex always moves the next iterate in the same direction (this might not be the case for other problems), requiring more iterations to converge to a minimum. Another advantage of BFGS is that the time step is decreased when the value of the function is close to the minimum.

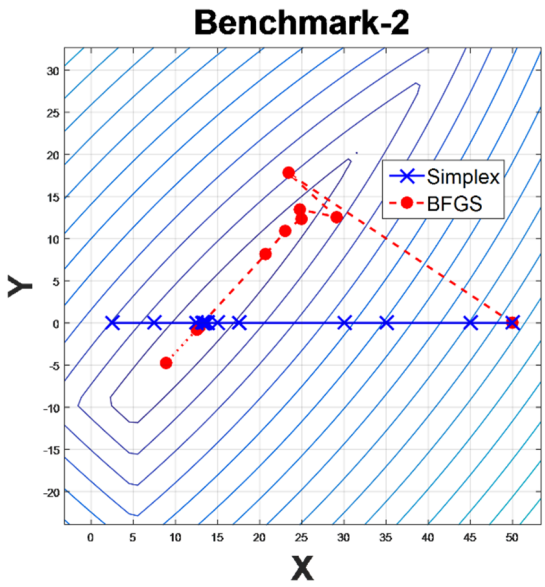

Figure 4.11 Contour Plot of the Objective function for Load Path 2, discretized with 75 points

It is found that an approach based on optimization using BFGS with weak Wolfe (WWC) conditions is the most efficient method for obtaining the centre of the MCC (mean shear stress). Regardless of the definition used, the computation of shear stress amplitude is straightforward once the mean shear has been obtained. It is worth reminding that the mean shear stress is the same for both definitions (MCC or MCE) of the shear stress amplitude.

4.6.2 SEB Problem in 6D-Center of the smallest hypersphere

In this case, we solve the SEB problem in 6 dimensions for computing the centre of the smallest hypersphere. This is required as part of the implementation of the Dang Van criterion. For this study, the following numerical methods have been employed:

1- Nelder-Mead simplex implemented in the MATLAB built-in function.

2- BFGS- Hanso: MATLAB code HANSO [140] [126] based on BFGS and weak Wolfe conditions (this tool can be downloaded from [129]).

3- Minmax built-in function in MATLAB.

A random non-proportional stress cycle has been chosen for the comparison study, as illustrated in Figure 4.12. As in the previous study, a sensitivity study has been carried out on the number of time increments defining the stress cycle.

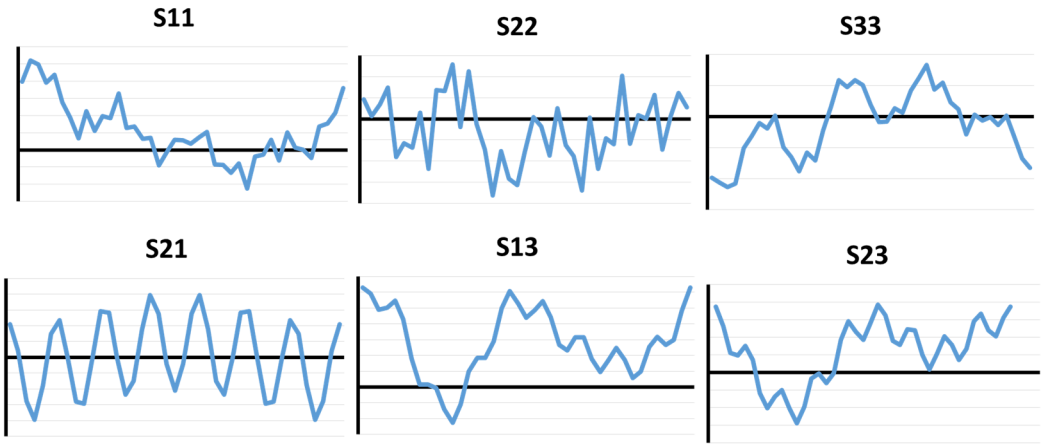

Figure 4.12 Components of the non-proportional stress tensor used for comparing the performance of numerical methods for solving the SEB problem in 6 dimensions

Table 4.1 confirms that BFGS is the fastest optimization technique for solving the SEB problem regardless of the dimension (for dimensions belonging to the scale of fatigue problems). In all cases, the run time is under 0.1 s.

Slightly more accurate results were obtained with BFGS and predefined minmax in MATLAB than with Simplex. Figure 4.9 and Table 4.1 provide evidence that the running time of the BFGS method does not change significantly with the dimension of the problem considered, and neither with the number of points used to discretize the path.

Table 4.1 Running Times for the computation of the smallest hypersphere for different numbers of points discretizing the load path

40 points					75 points				
Method	**Time**	**f**	**Iterations**	**Function Calls**	**Method**	**Time**	**f**	**Iterations**	**Function Calls**
BFGS	0.012	161.6466	37	98	**BFGS**	0.0141	165.0315	45	105
Simplex	0.0862	163.7465	1047	1667	**Simplex**	0.1155	166.7886	1332	2066
Min Max Matlab	0.1531	161.6653	53	708	**Min Max Matlab**	0.1543	165.0315	51	708
100 points					150 points				
Method	**Time**	**f**	**Iterations**	**Function Calls**	**Method**	**Time**	**f**	**Iterations**	**Function Calls**
BFGS	0.0088	165.5331	23	55	**BFGS**	0.0913	166.1813	127	359
Simplex	0.0654	169.5309	684	1114	**Simplex**	0.127	170.8687	1239	1965
Min Max Matlab	0.1524	165.5331	43	708	**Min Max Matlab**	0.1479	166.2416	42	657
250 points					500 points				
Method	**Time**	**f**	**Iterations**	**Function Calls**	**Method**	**Time**	**f**	**Iterations**	**Function Calls**
BFGS	0.0155	166.627	47	98	**BFGS**	0.0174	166.7159	48	92
Simplex	0.1418	171.3392	1218	1927	**Simplex**	0.2116	171.3932	1338	2098
Min Max Matlab	0.1721	166.6454	66	708	**Min Max Matlab**	0.1134	171.1796	22	437

4.6.3 Search of the critical plane

Two problems have been used for reviewing the performance of the novel strategy (Pre-Evaluation Grid+ Optimization). The first is a proportional stress cycle, the second is the same random non proportional stress cycle used in the previous study (already reported in Figure 4.12). The shear stress amplitude needs to be calculated for each plane, and so has been computed using BFGS implemented in MATLAB code Hanso [140].

Results

Two indicators have been chosen for evaluating the novel strategy, accuracy and run time. In order to study the accuracy, the results obtained have been compared with values computed through brute force (evaluation of the shear stress amplitude over a large number of candidate planes) for both stress cycles. Table 4.2 presents for each stress cycle, the shear stress amplitude at the critical plane computed by means of brute force (evaluating 260281 candidate planes) and by Pre-Evaluation Grid+ Optimization. The figures in brackets indicate the initial number of planes that conform the Pre-Evaluation Grid. It can be seen that for both stress cycles (Proportional and Non-Proportional) the novel strategy gives accurate results, the difference between the brute force method and the proposed strategy being less than 10E-3. Consequently, the accuracy of the proposed strategy (Pre-Evaluation + Optimization) has been verified.

For both problems, the best results were achieved with 12 and 19 pre-evaluation planes.

Table 4.2 Accuracy of the proposed strategy for obtaining the orientation of the critical plane

	Proportional Stress Cycle		Non Proportional Stress Cycle	
	Shear Amplitude	Function Calls	Shear Amplitude	Function Calls
Brute Force	252.6963	260281	119.0066	260281
Pre+Simplex (12)	252.6969	51	119.0065	44
Pre+Simplex (19)	252.6969	61	119.0067	56
Pre+Simplex (26)	252.6968	69	119.0066	58
Pre+Simplex (31)	252.6969	66	119.0066	68
Pre+Simplex (36)	252.6967	81	119.0065	62
Pre+Simplex (50)	252.6969	92	119.0066	83

With the purpose of assessing the computational cost, the novel strategy has been compared with the classical approach of searching at planes evenly spaced by 10 degrees. Table 4.3 presents measured values of the run time, shear amplitude at the critical plane, and number of function calls for both stress cycles and different numbers of points defining the stress tensor. SS10 stands for Sequential Search with 10 degrees variation between consecutive planes and

Pre+Simplex stands for Pre-Evaluation Grid (19 points) followed by Simplex Optimisation using as an initial guess the position of the maximum value found at the Pre-Evaluation stage.

Table 4.3 Comparison of different methods for obtaining the orientation of the critical plane for different number of points discretizing the load path

	Proportional Stress Cycle				Non Proportional Stress Cycle			
	Method	Time	Shear Amplitude	Function Calls	Method	Time	Shear Amplitude	Function Calls
40 Points	SS10	0.8231	249.9026	190	SS10	1.4144	118.4517	190
	Pre+Simplex	0.2708	252.7524	61	Pre+Simplex	0.3446	118.8209	55
75 Points	SS10	1.0013	249.8478	190	SS10	1.7863	118.7541	190
	Pre+Simplex	0.3289	252.6969	61	Pre+Simplex	0.4129	119.0067	56
100 points	SS10	1.1299	249.9026	190	SS10	1.7408	122.0531	190
	Pre+Simplex	0.3698	252.7524	61	Pre+Simplex	0.4467	122.1184	57
150 Points	SS10	1.3826	249.8478	190	SS10	1.9965	122.7857	190
	Pre+Simplex	0.4516	252.6969	61	Pre+Simplex	0.5147	122.816	56
250 Points	SS10	1.9045	249.8829	190	SS10	2.6543	122.631	190
	Pre+Simplex	0.6187	252.7324	61	Pre+Simplex	0.8507	122.6749	63

Table 4.3 reveals that the novel strategy (Pre+Simplex) requires a much lower number of function calls than SS10. An additional advantage of the novel strategy is that there is no significant difference either in the number of function calls or in the maximum shear amplitude with respect to the number of points used for defining the loading path. Moreover, for both stress cycles, the run time of the novel strategy was under 1 s. A practical consequence of the findings is that a structural member where 1000 different locations must be checked against fatigue damage using a critical plane approach, the fatigue analysis would require less than 15 minutes. Table 4.3 indicates that when the novel strategy (Pre+Simplex) is implemented to the Non-Proportional stress cycle, it requires less function calls to be solved than when implemented to the Proportional stress cycle. In other words, the Simplex optimization method requires more iterations for the Non-Proportional cycle than for the proportional one. This difference can be explained by looking at Figures 4.13 and 4.14. At the maximum, the optimized function (shear stress amplitude as a function of phi and theta) is smoother for the Proportional stress cycle than for the Non-Proportional one.

As already reported by several researchers (Susmel [99] and Svärd [100]), one of the problems of applying an optimization method is the ability to find the global maximum, and not a local one. Apart from reducing the number of iterations needed by Simplex algorithm in the optimization step, one of the purposes of the Pre-Evaluation Grid is to move the initial guess near the global maximum, therefore increasing the probability of finding it. In other words, it behaves like a filter that identifies the region where the global maximum is located.

Figure 4.13 and Figure 4.14 present three different plots for each stress cycle used for evaluating the performance of the novel proposed strategy, Pre-Evaluation + Simplex Optimization.

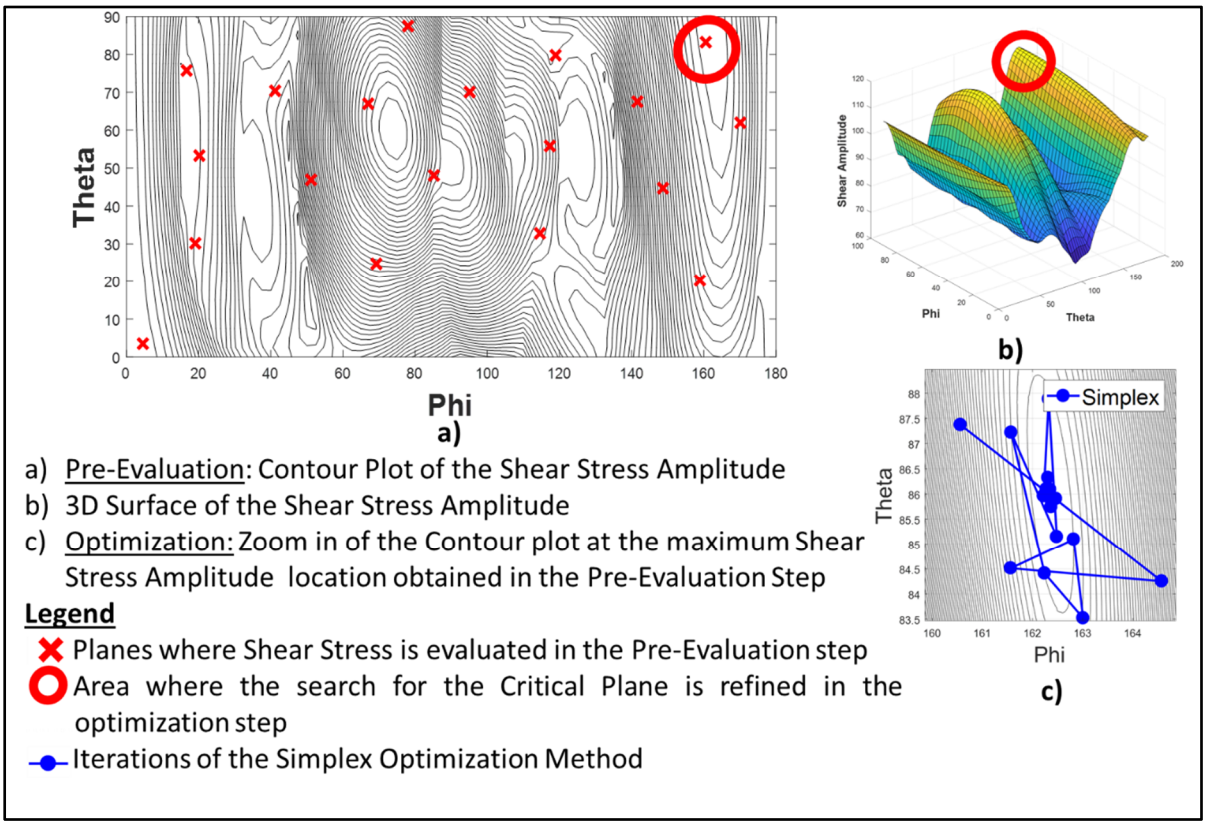

Figure 4.13 Critical plane location for a non-proportional Stress Cycle

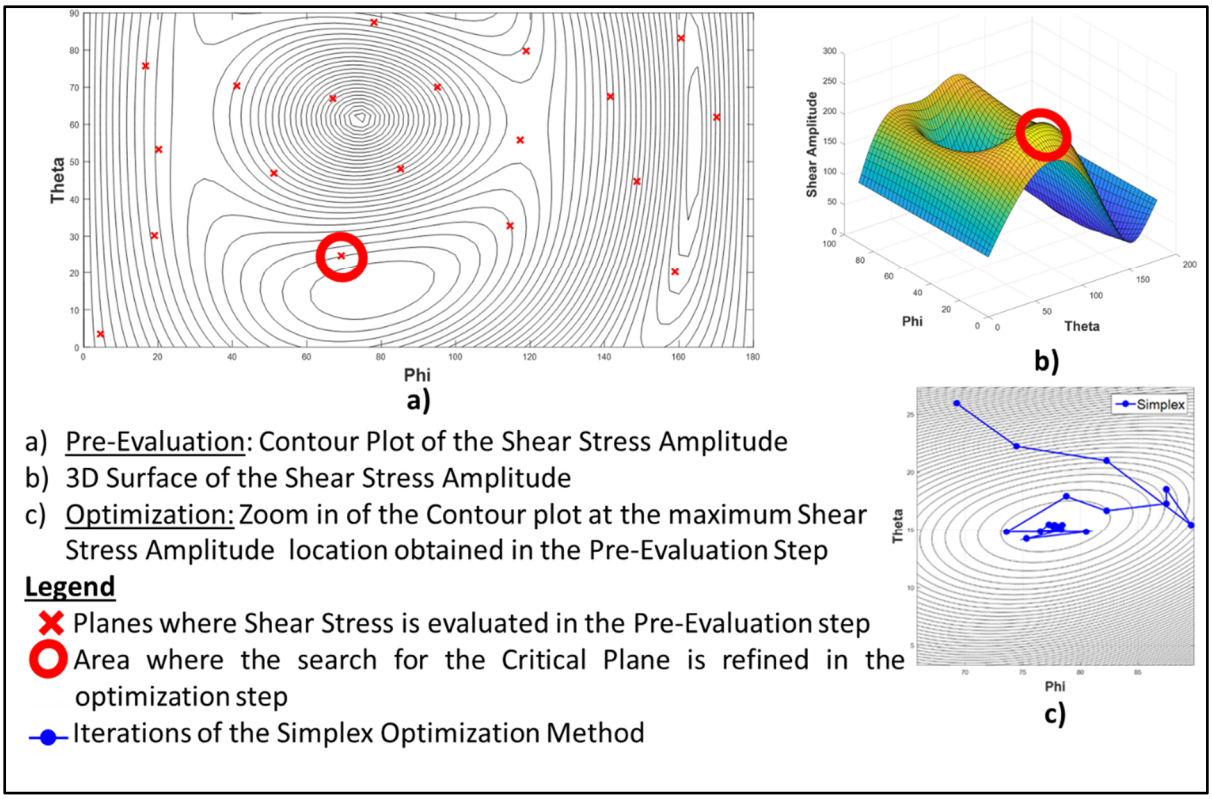

Figure 4.14 Critical plane location for a proportional stress cycle

4.7 Implementation in an industrial problem

Fatigue assessment of a chain link under OPB loading (described in Chapter 2) has been carried out using the numerical methods proposed in this chapter. The aim is to demonstrate their performance when applied to a practical problem faced by industry. The Dang Van fatigue criterion (presented in Chapter 3) was applied using BFGS-Hanso [129] (the best performing numerical method according to our research). The calculation was performed on a desktop computer (Intel (R) Core (TM) i7 340GHz with 12GB of RAM Memory). The criterion was applied at all the nodes of the surface of the chain link (**10384 Nodes**), with a run time of **170s**. This is particularly interesting because for complex cases, when the failure location is not known a priori, all the nodes must be considered in the fatigue analysis.

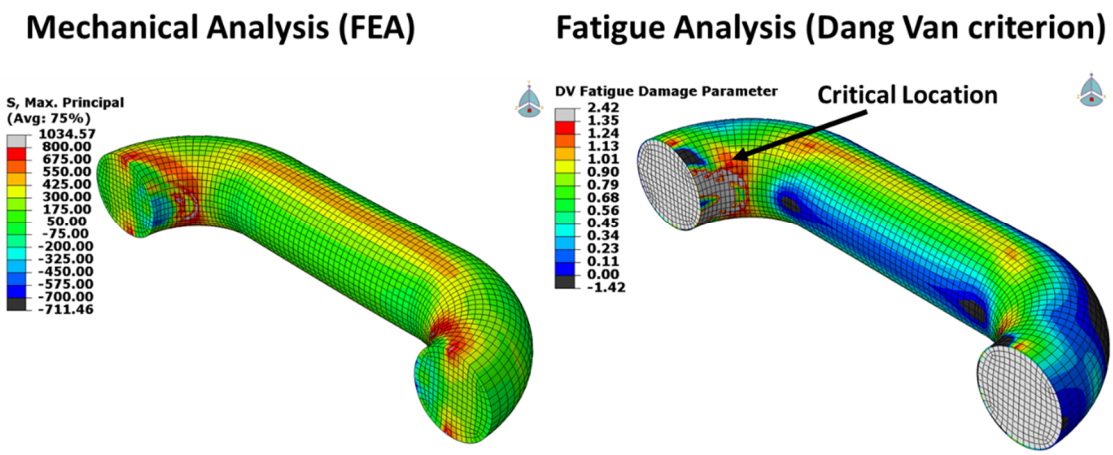

Figure 4.15 Fatigue Assessment of a mooring chain by means of DV criterion using fast numerical methods

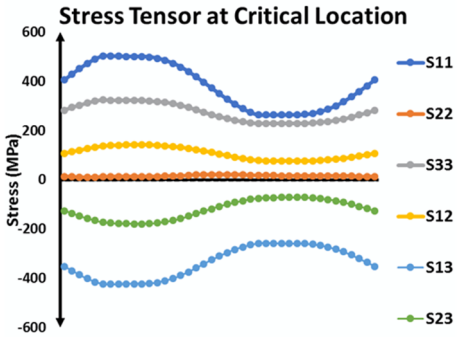

Figure 4.16 Stress Tensor at the Critical Location of the chain link

4.8 Chapter Summary

The fatigue assessment of structural members is frequently carried out using a computational fatigue method. The running time of the fatigue analysis depends on the optimization technique employed. Few recommendations or guidelines concerning optimization techniques for critical plane analysis have been found in the literature. This chapter has revisited different numerical methods at each of the stages of critical plane fatigue analysis that involve optimization. Preference has been given to methods that have proven robustness or performance in other applications. Comparison studies have been carried out to determine which of the methods is more efficient and a series of improvements to enhance precision and speed up computation

have been proposed. Based on the results obtained, the following recommendations for reducing the computational time are made:

- SEM Problem for Computation of shear stress amplitude (2D) or centre of the smallest hypersphere (6D): Use of the minmax approach by means of BFGS implemented along Weak Wolfe Conditions (For example HANSO MATLAB Code [140], available in [129]) or BFGS with Strong Wolfe Conditions applied to a smooth approximation of the objective function.
- Location of the Critical Plane: Perform a pre-evaluation at planes distributed homogenously along the surface, and then refine the critical plane search by means of Simplex optimization. Based on our experience, pre-evaluation of 13 or 19 planes is the most efficient.

Following these recommendations, the Dang Van fatigue criterion was applied to all the surface nodes of a mooring chain link, and critical locations for fatigue were identified in less than three minutes computational time.

Chapter 5: Prediction of Residual Stresses in Mooring Chains

In the previous chapter (Chapter 4) different numerical methods have been reviewed for performing multiaxial fatigue assessment in a reduced computational time. The chapter concluded by issuing a set of recommendations for applying the Dang Van fatigue criterion and proposing a novel strategy for locating the critical plane. The fundamentals of the numerical tools for fast fatigue assessment have been established. The present and following chapters address the fatigue assessment of mooring chains. The workflow of these chapters follows the lifecycle of mooring chains. First, in the current chapter, the manufacturing process is studied to predict the residual stress distribution remaining after the manufacture of mooring chains. Second, in the chapters 6 and 7, the fatigue assessment of mooring chains under tension and torsion loadings is performed.

5.1 Introduction

This chapter reports the results of a study conducted to investigate how residual stresses generated during the manufacturing process and subsequent proof loading may affect the fatigue life of mooring chains. Quantitative predictions of residual stress field obtained from finite element models of the fabrication process are presented, and their effect on the fatigue life of chain links depending on the loading mode is examined. The models combine heat transfer analyses for prediction of temperature histories during heat treatment (quenching and tempering), and stress analyses accounting for the thermo-mechanical history, including proof loading. The manufacturing conditions assumed for the models correspond to data obtained from a chain manufacturer (Vicinay Cadenas [141]). The predicted residual stress distribution is then combined with the fatigue stress range in service, due to either tension-tension loading

or Out-of-Plane Bending (OPB). The effect of the residual stress distribution on the fatigue damage is discussed, and a sensitivity study on the assumptions used in the residual stress prediction is carried out. This determines for which loading conditions modeling of the heat treatment stage can be neglected so that modeling of the proof loading step is sufficient for assessing the effect on fatigue life.

Fatigue life of a mooring chain can be altered by different factors including corrosion, anomalous loading modes (twisting or OPB), mooring layout, and residual stresses [142]. Some of these factors have already been studied (e.g. Joint Industry Projects on Out-of-Plane Bending [15], [18] and corrosion [143]). Residual stresses affect the fatigue life of a structure by modifying the mean stresses. For example, compressive residual stresses induced by shot peening lower the stress at the surface and are beneficial to prevent or delay fatigue cracking [29]. Previous publications have shown that self-equilibrating residual stresses in a chain link after proof loading are either tensile or compressive depending on their location. When the chain is subjected to tensile cycling loading (T-T), compressive residual stresses increase the resistance to fatigue failure at locations where the fatigue stress ranges are significant during service [27].

Fabrication of mooring chains involves for each of the links, a number of manufacturing steps that generate residual stresses: hot bending of the link's bar, welding, and heat treatment. For each of these steps, residual stresses are generated due to non-homogenous strains and/or thermal gradients. Furthermore, mooring chains have to undergo a mandatory proof load to check their strength and fitness for service. According to DNV-OS-302 [8], the proof load is specified to be about 70% of the minimum breaking load (MBL) of the links depending on the material grade and link's size. Because of the magnitude of the applied load, extensive yielding takes place in the link, resulting in additional residual stresses. The purpose of the proof load is to check the strength of the chain and its fitness for service. In particular, it also assures that

the chain is defect free at sensitive zones like the weld. Another important benefit of the proof load is the residual stress field it induces. Several authors (eg. [144]–[146] and more recently [27]) have shown the beneficial effects of compressive residual stresses at zones where high stress ranges can cause cracking. These studies concentrated on how residual stresses affect fatigue life when the chain is working under nominal loading, i.e. tensile loading. Furthermore, these studies only considered proof load as a source of residual stresses, and so neglected the residual stress distribution left after heat treatment. However, it is widely accepted that in quenched cylinders, heat treatment leaves considerable compressive residual stresses at the surface and tensile at the core [29], [147]–[149]. During heat treatment, residual stresses are created due to thermal gradients, while during proof loading by non-homogenous strains.

As already noted in Chapter 2, chains can experience undesirable loading modes, such as OPB. The latter was responsible for the failure of chain links at the *Girassol* buoy [14]. This incident launched a JIP (Joint Industry Project) with the objectives of understanding the mechanism of OPB, establishing recommendations for fatigue life design, among others [15] [18]. In this project, only residual stresses generated by proof loading were accounted for. Nevertheless, as already said, proof loading is not the only stage at which residual stress are generated.

As has been addressed in Chapter 3, residual stresses are self-equilibrating within the whole structure, meaning that in certain regions residual stresses are compressive and in other regions they are tensile. Then, it must be determined whether the regions where the residual stresses are tensile are also subjected to high applied stress ranges. Bastid and Smith [27] showed that the region in the boundary of the contact zone experiences tensile residual stresses after proof loading; nevertheless, under tensile loading, the stress range is not sufficiently large to cause fatigue cracking.

This chapter continues the work presented by [27] and looks upstream at the manufacturing process to see how residual stresses induced during manufacturing affect the fatigue life of a mooring chain depending on the service loading. Different models are presented for obtaining the residual stress distribution after manufacture, each of increasing complexity. Results predicted by the different models at the critical locations where fatigue failure is likely to occur (depending on the loading mode) are compared. This chapter also addresses the following question: if the residual stresses are to be taken in to account in the study of mooring chain fatigue life, is it necessary to consider the residual stresses generated during the heat treatment stage and proof loading, or just proof loading? In other words, which of the sources of residual stress has more weight on the resultant residual stress field, the heat treatment stage or proof loading? In order to answer these questions, finite element models have been used to model heat treatment stages and Proof loading for obtaining the resultant residual stress field. The values obtained have been introduced in models that study the response of the chain links when they are subjected to tension-tension and OPB service loading.

This chapter is divided as follows. First, the mechanical properties of mooring chain steel are outlined. Second, modelling of the manufacturing process is described. Third, two different FEA models are presented, the first accounts for heat treatment and proof loading whereas the second is solely for proof loading. Finally, the residual stress fields predicted by both models are presented and the results discussed.

5.2 Mooring Chain: Structure and Material

A mooring chain is composed of a series of interconnected links (see Figure 5.1) which transmit the applied load from one link to the next by direct contact. This section provides a brief overview of the material and geometry of mooring chain links.

Mooring chains are manufactured from hot rolled low alloy carbon steel. The steel has a fine grain microstructure formed of tempered martensite and bainite [32], [33], [150]. Engineering Standards (DNV-OS-E302 [8] and IACS W22 [151]) define different grades of mooring chain steel. The difference between each grade relates to the required mechanical properties. The newest material grades are R6 and R5S [152], although previous material grades, R5 and R4 are still widely used today. In addition, no chain made of R5S or R6 is yet in service today. Mooring chain steels have high yield strength compared to other low alloy carbon steels. The following table reports the mechanical properties for both steel grades measured by different authors and the minimum values required by the Standard DNV-OS-E302 [8]:

Table 5.1 Mechanical properties of mooring chain steel obtained from the literature and minimum values required by Engineering Standard DNV-OS-E302

Material Grade	$\sigma^{Y}_{0.2\%}$ [MPa]	σ^{U} [MPa]	Source	σ^{Y}_{min} [1)] [MPa]	σ^{U}_{min} [1)] [MPa]	ε_f [1)]
R4	896	959	[18]	580	860	12
	880	1000	[27]			
R5	970	1018	[150]	700	1000	12
	1000	1100	[27]			

1) Minimum values required by DNV-OS-E302 [8]

The nominal dimensions of the chain are given as a function of the diameter [151], as reported in Figure 5.1. This figure also illustrates the fatigue failure locations of chains under tensile loading [27] [40], [145], [153], [154]. At both locations, the stress concentration factor (defined as the ratio between the maximal principal stress and the nominal stress; the latter computed by dividing the total external force applied at the chain link by its cross section) has a value of about 4 [153].

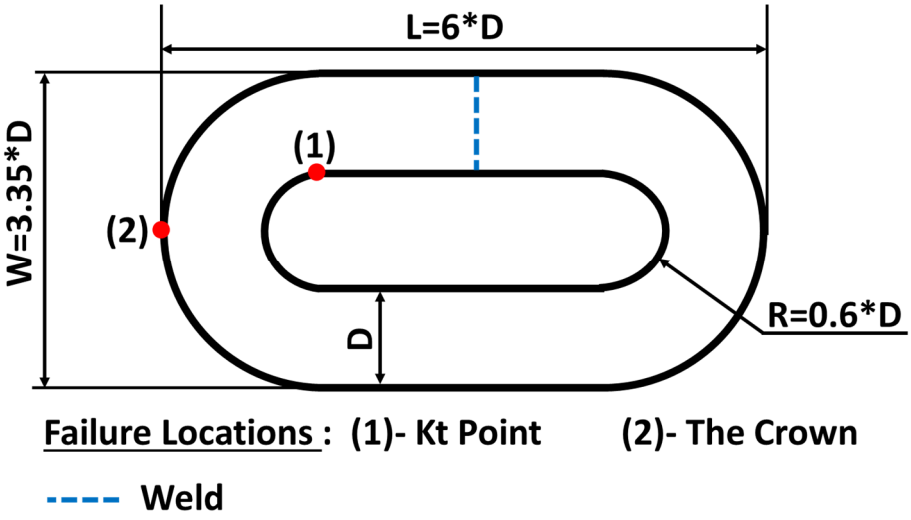

Figure 5.1 Nominal dimensions of a chain link and fatigue failure locations under tensile loading

As already mentioned in Chapter 2, chains can experience undesirable loading modes such as OPB. The following figure illustrates the failure location under OPB, and also displays a contour plot of the maximum principal stress. At the failure location (denoted as Point C in Figure 5.2, following the notation of Rampi et al. [15], [18]) the maximum principal stress attaints a maximum.

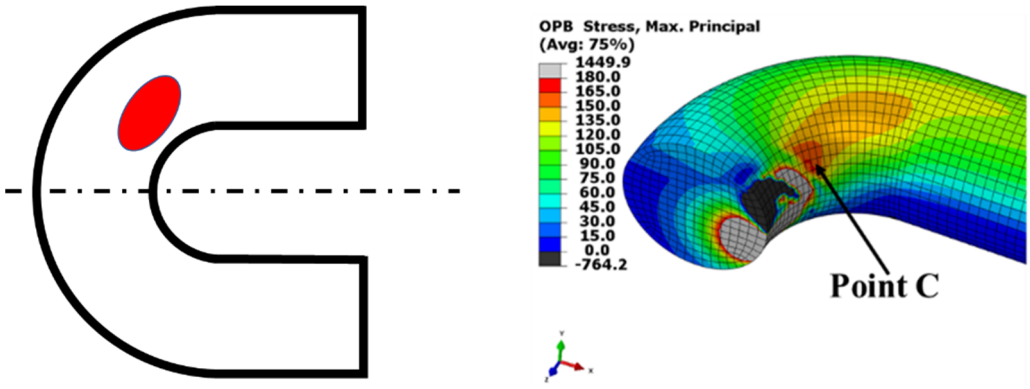

Figure 5.2 Fatigue Failure location under Out-of-Plane Bending

Different chain diameters are considered in this chapter and chapter 6: 76 mm, 127 mm, and 162 mm. The Minimum Breaking Load (MBL) is the minimum load that a chain segment of at

least 3 chain links must withstand during 30 s without fracture [151], and is a function of the material grade and the diameter of the chain. The following table presents the values of proof load and Minimum Breaking Load (MBL) for different diameters and material grades.

Table 5.2 Minimum Breaking Load and Proof Load for different chin diameters. Source DNV-OS-E302 [8]

Diameter (mm)	Material Grade	Proof Load (kN)	Minimum Breaking Load (MBL) (kN)	Nominal Stress (MPa)
76	R4	4205	6001	661.4
	R5	4484	7009	772.5
127	R4	10479	14955	590.3
	R5	12171	17466	689.4
162	R4	15641	22320	541.4
	R5	18166	26068	632.5

5.3 Modelling of the Manufacturing Process

The main steps in the manufacturing process of mooring chain links are hot bending of the link's bar, flash butt welding, heat treatment, and proof loading. The heat treatment stage comprises double quenching in water, tempering, and cooling in water. The temperatures of the first and second quench are 920 °C and 880 °C respectively [32], [33]. As a final operation, before being putted into service, chain links must undergo a mandatory proof load to check their strength and fitness for service. The value of the proof load is established by Standards [8], [151] for different chain sizes and diameters as presented in Table 5.2. In each of these steps, residual stresses are generated due to non-homogenous strains and/or thermal gradients. The resultant residual stress field is be the superposition of residual stresses from heat treatment and proof loading.

The second quench is performed at a temperature above the recrystallization temperature (Ac3, the temperature at which austenite stops forming), therefore, residual stresses generated during previous stages (hot bending, welding, and first quench) will be relaxed. Consequently, only heat treatment and proof loading is considered here. Quenching and tempering are multiphysics processes where the temperature field, microstructure, and stress/strain field interact with each other. Their coupling is complex, as shown in Figure 5.3 (adapted from [155]). Heat transfer is the main physical process; heat transfer triggers the phase transformation and the formation of thermal stress/strains.

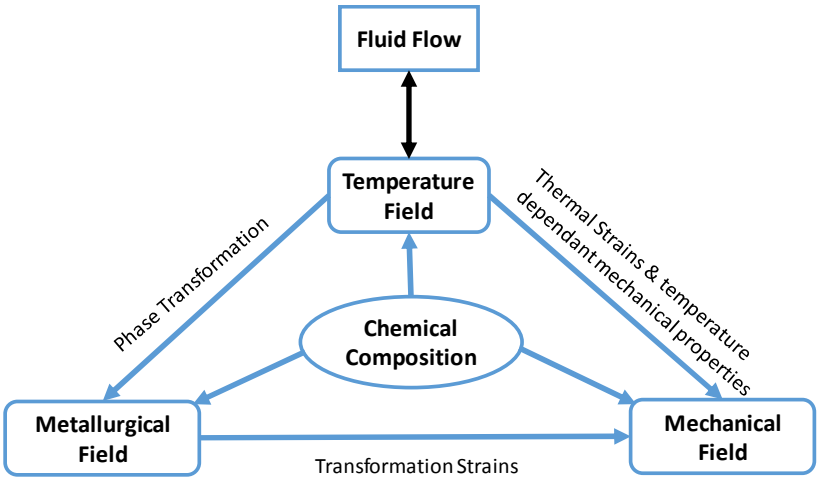

Figure 5.3 Coupling between physical fields during heat treatment

We are interested in determining how complex the simulation of the manufacturing process ought to be in order to obtain sufficiently accurate predictions of residual stress. The manufacturing process is complex involving quench, tempering, and proof load. Consequently, the models must be simplified in order to keep the computational cost below a reasonable level, while at the same time capturing the most significant effects. From an engineering point of view, residual stresses are relevant because they can have an important impact on fatigue life depending on whether they are tensile or compressive and are of special interest at the surface. Therefore, the residual stress distribution is of special interest at locations where fatigue failure

takes place (these locations have already been illustrated in Figure 5.1 and 5.2 for tensile and OPB loadings respectively).

The final residual stress field will be due to the thermal stresses, phase transformation stresses (both induced during the heat treatment stage) and mechanical stresses (induced during proof loading). However, because of the magnitude of proof loading (around 70% of the MBL depending on the material grade and the chain size, see Table 5.2), residual stresses due to proof loading might be the most relevant, especially taking into account that at the critical locations (see Figure 5.2) the stresses during proof loading reach large values. In this chapter two models, each of increased complexity, are presented for deriving the residual stress field:

- Model A: Accounts for solely proof loading.
- Model B: Takes into account both heat treatment and proof loading.

Model B does not account for solid state phase transformations (SSPT), this assumption keeps the computational burden below a reasonable level and enables the mechanical analysis to be decoupled from the thermal analysis. A ferritic steel transforms to austenite when heated above a certain temperature. Then, during quenching, austenite decomposes into a mixture of phases that may include martensite, bainite, ferrite, and perlite. The composition of the phases depends on the cooling rate and the transformation kinetics of the steel considered. During this transformation, a volume increase takes place due to the difference between the parent and product phases. This change of volume generates microscopic plasticity which interacts with thermal stresses resulting in thermal induced plasticity (TRIP). As mentioned earlier, in mooring chain steel, after heat treatment the microstructure is composed of martensite and bainite. Different models can be found for determining the phase composition at every discrete time instant during quenching. For modelling the transformation of austenite into martensite (which is diffusionless) the Koistinen-Marburger equation [156] is generally employed. For

the other transformations of austenite, which are diffusion controlled, the Johnson–Mehl–Avrami–Kolmogorov equation along with Scheil's additivity rule or the model proposed by Victor Li et al. [157] are popular among researchers. All of these models carry a significant computational overhead, which does not make them very appropriate for application to a structural member of the size of a mooring chain.

Although the influence of phase transformation on the residual stress field has been neglected, a theoretical discussion regarding the effects of transformation on the final residual stress field is presented in Section 5.5.3. All the models were performed using ABAQUS 6.14. For Model B, a heat transfer analysis was undertaken to obtain the transient temperature field, which was then imported to a stress analysis to obtain the final residual stresses field. Once the residual stress distribution was obtained, it was exported to the stress analysis that applied fatigue loading, tension-tension (T-T), and OPB.

5.4 Finite Element Models

Two different chain diameters have been chosen for this study: 76mm and 162mm. The material grade (R4) is the same for both diameters. First, the residual stress distribution was predicted with Model A and Model B. Recall that Model A accounts only for Proof loading and Model B for Heat treatment followed by proof loading. Second, the results were imported into the service loading models as an initial state, that takes into account the residual stress and plastic strain distributions. In order to import the distributions correctly, the same geometry (with the same number of chain links and symmetry planes) and mesh were used in both residual stress prediction and service loading models. Therefore, each manufacturing model has been run with two different geometries: one for T-T loading and the other for OPB loading. For the stress analysis, the chain links were meshed with 3D solid quadratic elements with reduced integration (C3D20R). Quadratic elements capture stress concentrations better and are

more accurate than linear elements when subjected to bending. For the heat transfer analysis, 3D solid linear elements were used (DC3D8). In Model B the contact nodes between chain links were tied in (no contact interaction was considered during heat treatment) to avoid interpenetration of the chain links and solid rigid movement. This boundary condition is not compatible with OPB fatigue loading, and so different models have been used for modelling the manufacturing and the service loadings.

5.4.1 Model A: Proof loading

This model predicts the residual stresses due to proof loading. The material has been modelled with elastic plastic properties with isotropic hardening. The geometry of this model is presented in the Figure 5.4:

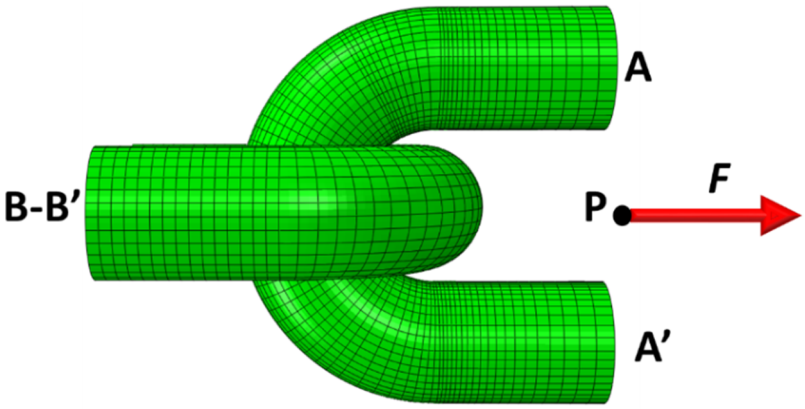

Figure 5.4 Geometry and Boundary Conditions of Model B

The boundary conditions are the following:

- Sections B-B': Symmetry boundary conditions.

- Sections A-A' are coupled with the reference point *P*. The coupling is enforced in an average sense. That is, the degrees of freedom of the nodes at Sections A-A' are not eliminated. The

constraint is enforced by distributing loads such that: the resultants of the forces at the coupling nodes (nodes at Sections A-A') are equivalent to forces and moments at point *P* (the reference node). The displacements of this point are restrained in all directions except that of the applied load *F*. The external loading is applied at reference point *P*. The value of the proof load has been specified in Table 5.2.

An important characteristic of this model is the formulation of the contact between chain links. From a physical point of view, when contact takes place, a normal force to the surface of contact and a shear force are transmitted. Contact is intrinsically a nonlinear phenomenon. The contact pressure between the contact surfaces is defined as a function of the penetration distance between the contact surfaces. Hard contact definition has been chosen, it does not allow the transfer of tensile stress across the interface nor penetration between contact surfaces. Two options are available for enforcing the hard contact definition. The first one strictly enforces hard contact; therefore, it does not allow any penetration between surfaces. Nevertheless, its convergence rate is slow since there is an abrupt change in the contact stiffness (as illustrated in Figure 5.5). The second one, the penalty method, allows some small penetration, consequently improving the convergence rate. Moreover, the penetration distance is generally negligible. Figure 5.5 illustrates the difference between these two contact enforcement methods. Convergence was not achieved using the strict enforcement of the hard contact definition (denoted in ABAQUS as "Direct"). Instead, a penalty method has been used providing, a good convergence rate.

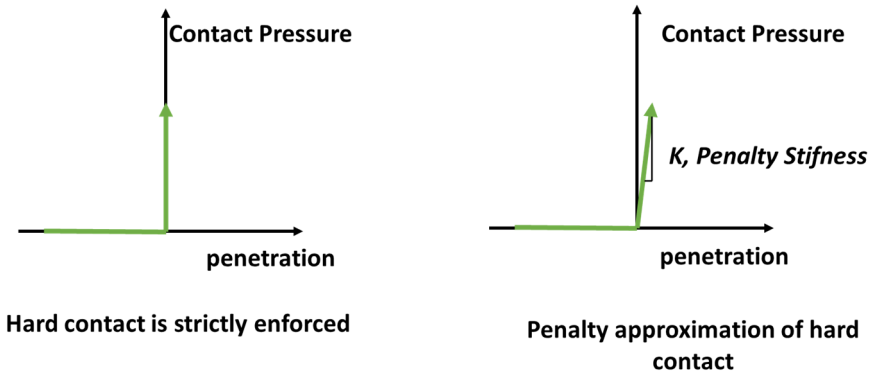

Figure 5.5 Contact enforcement methods

Shear force is defined by the frictional model. Fiction between chain links has been modelled as an isotropic Coulomb law. Experiments have illustrated that friction coefficient μ is close to 0.3 in salt water and 0.5 in air [49]. A friction coefficient of 0.3 has been used in this study.

Recall that the geometry has been meshed with 3D solid quadratic elements with reduced integration (C3D20R). Compared to linear elements, quadratic elements have a higher computational burden, although when subjected to bending they capture stress concentrations better and are more accurate. As shown in Figure 5.4, the right hand side link (where the load is applied) has been meshed with a finer mesh, especially at the potential fatigue failure locations (Kt Point, the Crown, these locations are reported in Figure 5.1). This has two advantages, the first is that it reduces the memory requirements of the analysis, the second is that it improves the contact convergence rate between chain links, since a finer mesh of the slave part will avoid penetration and improve convergence.

5.4.2 Model B: Heat Treatment and Proof Loading

As described previously, mooring chain manufacturing involves several steps during which residual stresses are generated due to non-homogenous strains and/or thermal gradients. This model accounts for heat treatment and proof loading. The initial temperature of the second quench is above the temperature at which austenite stops forming (Ac3); it can be assumed that the residual stresses created in the previous stages (hot bending of the chain, welding, and first

quench) are relaxed. Consequently, only the last stages of the manufacturing process, second heat quench, tempering and, proof loading have been modelled:

- Step 1: Quenching. The chain is cooled in water. Because the water bath is continually refrigerated, the temperature of the water (around 20 °C) has been considered to be constant.

- Step 2: Tempering. The chain is heated until the tempering temperature is reached.

- Step 3: Water Cooling. The chain is cooled in water until room temperature is reached.

- Step 4: Proof Load. The value of the proof load depends on the material grade and the chain diameter, as indicated in Table 2.

- Step 5: Unload. Proof load is removed and residual stresses from heat treatment and proof load remain in the chain.

This model accounts for the interaction between the fluid flow, temperature field, and mechanical field, as displayed in Figure 5.6.

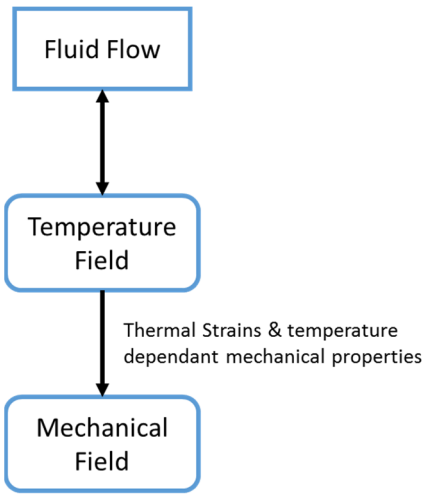

Figure 5.6 Interaction between physical fields during heat treatment

Fluid Interaction: The interaction between the quenching fluid and the surface of the chain is complex. Once immersed, a water blanket appears, then nucleate boiling takes place and

finally, convective cooling occurs. Therefore a temperature dependent heat transfer coefficient taken from the literature [147] has been used in order to take into account these phenomena. Because the quenching liquid (water) is agitated and continuously cooled, the water temperature in the surroundings of the chain is assumed constant.

Temperature field: First, a heat transfer analysis has been run for obtaining the thermal profile in each step. In the heat transfer analysis, no heat sources have been considered. Heat generation due to plasticity and the heat transfer through conduction between chain links have been neglected. The only heat transfer mechanism considered refers to the chain links with the quenching fluid (water) through convection and radiation. Therefore, the heat transfer analysis is independent of the stress analysis.

Mechanical Field: The thermal profile obtained was exported to a stress analysis for predicting the resultant residual stress field. The mechanical fields are defined by an elastoplastic constitutive law under the hypothesis of small strains and the equilibrium equation:

$$\mathrm{div}\sigma = 0 \tag{5.1}$$

The mechanical field is defined as follows:

$$\boldsymbol{\sigma} = \boldsymbol{C} : (\boldsymbol{\varepsilon} - \boldsymbol{\varepsilon}^{P} - \boldsymbol{\varepsilon}^{Th}) \tag{5.2}$$

$$\dot{\varepsilon} = \gamma \nabla f(A_p) \tag{5.3}$$

where ε_{th} and ε_p are the plastic and thermal strain tensors respectively, C is the fourth order elasticity tensor (defined by the Young's modulus and the Poisson ratio). The plastic strain rate is given by Eq. (5.3). The values of γ and A_p are defined by a von Mises equivalent stress yield criterion and the assumption of isotropic hardening behavior:

$$A_p = \mathrm{dev}\sigma \tag{5.4}$$

$$\gamma = \sqrt{\frac{3}{2}}\langle J_2(A_p)\rangle \tag{5.5}$$

where $J_2(A_p)$ is the second invariant of the deviatoric stress tensor.

The elasto-plastic behaviour law is defined by the Young modulus (E)and the yield limit. Overall, the following properties have been used to define the material behaviour at high temperatures: density (Temperature dependent), conductivity (Temperature dependent), expansion coefficient (Isotropic), specific heat (Temperature dependent), Young Modulus (Temperature dependent), and Yield Strength (Temperature dependent).

Mooring chains are made from low alloy steels. The chemical composition of R4 and R5 steel grade (carbon content less than 0.30%) is mainly formed by the following alloys: manganese, chrome and nickel, among others [33], [150]. R4 and R5 are low alloy steels, hence the sum of all of the alloying elements is under 5%. The alloying elements and the heat treatments increase the yield strength. The chemical compositions of R4 or R5 grades have some similarities with the composition of high strength structural steels. Both steels have high yield strengths compared to other low carbon steels (for example, S355).

The elastic properties of R4 steel grade at room temperature have already been presented in Table 5.1. Thermal stresses are dependent on the variation of the yield strength and Young modulus with temperature. High-temperature measurements are complex and more expensive than those undertaken at room temperature.

Chen et al. [158] studied how the elastic-plastic properties of mild and high strength structural steels vary with temperature. They performed tensile tests at different temperatures (from room temperature up to 940 °C) and established ratios between each property at room temperature and at high temperatures. These ratios were similar for both steel families and have been used

for estimating the material properties of R4 steel at high temperatures. The values showed good agreement with calculated ratios for other low alloy steel data obtained from high-temperature, testing available from the NIMS Database [159]. Figure 5.7 displays the mechanical properties used for modeling the mechanical behavior of R4 grade at different temperatures. The values at ambient temperature where taken from [27], at higher temperatures they were estimated using the ratios published by Chen et al. [158].

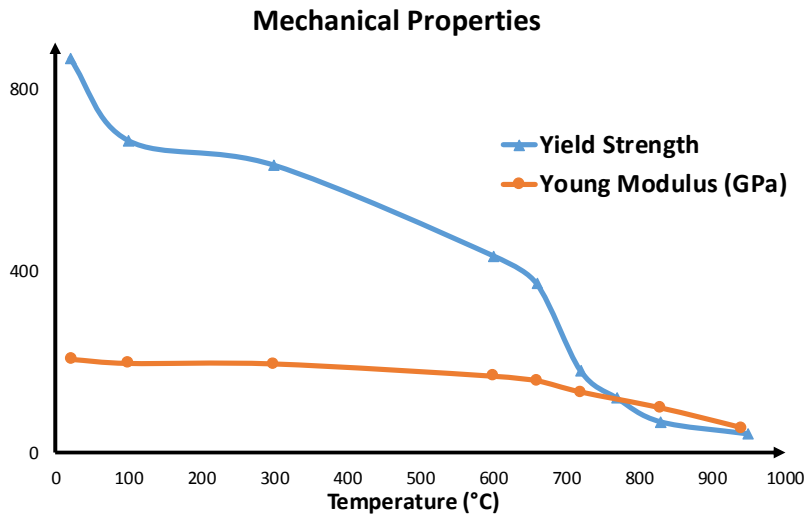

Figure 5.7 Estimated mechanical properties of R4 steel as a function of temperature

In summary, the main parameters of Model B are:

- Mechanical properties at different temperatures (Figure 5.7). As already said, high-temperature mechanical tests are complex and more expensive than those undertaken at room temperature. This parameter is a source of uncertainty; nevertheless a good estimation has been made using data from the literature.

- Data from the manufacturing process (i.e. quenching temperatures, proof load).

- Temperature dependent heat transfer coefficient between steel and quenching fluid (water).

From the above list, the first two parameters have the greatest impact on the results.

Validation of Model B: To the author's knowledge no measurements of residual stresses in mooring chains are available in the public domain. Quenching of mooring chains can be considered similar to quenching of cylinders. The development of numerical methods for studying distortion and residual stress distributions of quenched cylinders has been the aim of many investigations in the last 40 years [160]. Most of the results presented in the literature are for small cylinders (around 20 mm of diameter); and so a validation model consisting of cylinder of 20 mm diameter with the same properties as Model B was created for comparing the obtained results with experimental measurements available in the literature.

Schröder [148] studied the residual stress distribution of cylinders after quenching for different diameters (from 10 to 40 mm), and concluded that qualitatively, the stress distribution was the same for all the diameters, but the magnitude of the stresses increased for bigger diameters. According to [148],[19],[161],[149],[162] and [163], at the end of the quenching process, tensile residual stresses can be found at the core and compressive stresses at the surface of the cylinders.

As shown in Figure 5.8, at the beginning of the quenching process, the surface cools down faster than the core. The contraction of the surface is resisted by the core (where the specific volume is higher). As a result, the surface is in tension and the core in compression. When the temperature difference between the core and the surface is greatest, the core starts to cool down faster than the surface, therefore it contracts faster than the surface. At different time instants the thermal stress at the core and the surface reach their respective zero values. Because of plasticity, these thermal stresses cannot be zero simultaneously. Further cooling leads to tensile residual stresses in the core and compressive stresses at the surface. This behavior was reported by [29], [164], and [165] among others. Similar behavior was observed during quenching of mooring chain links.

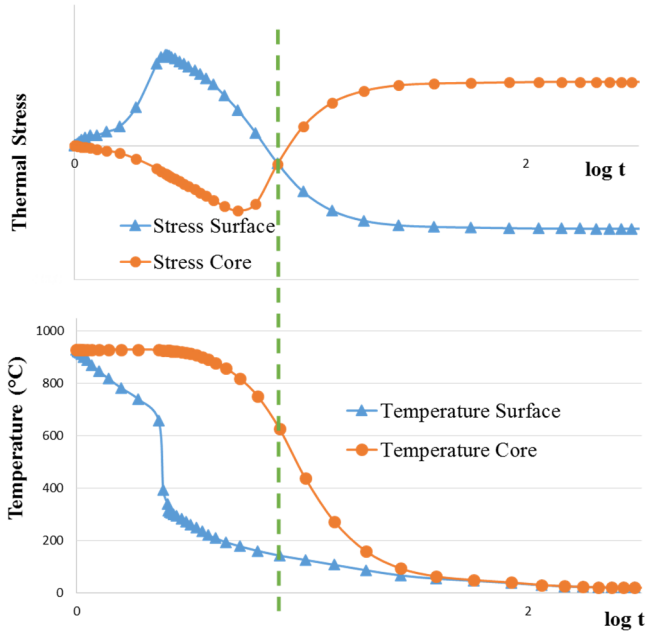

Figure 5.8 Evolution of temperature and thermal stresses at the core and at the surface during quenching

Predicted residual stress values at the surface of the validation model (20mm quenched cylinder with the same properties as Model B) were compared to experimental data available in the literature from Ariza [161], Inoue [162], and Schröder [166]. Table 5.3 indicates that the value of the residual stress depends on the type of steel, the initial temperature and the quenching liquid. The predicted values are higher than the measured ones, the closest being for S45C. This might be explained by the fact that the initial temperature is higher, and that phase transformation has not been taken into account. Figure 5.8 shows that phase transformation occurs at the surface before the time instant (dashed line) at which the thermal stresses at the core and at the surface take the same value. Consequently, according to [165], transformation would reduce the compressive thermal stresses at the surface. Regarding the quenching of mooring chains, for the studied diameters, the effect of phase transformations at the surface would be similar, that is to reduce the magnitude of compressive residual stresses.

Table 5.3 Comparison between predicted and measured (from literature) residual stresses

		Experimental Data				
	Own results	Inoue	Inoue -2	Ariza	Ariza-2	Schröder
Axial Residual Stresses [(MPa)Surface]	-619.30	-539.55	-343.35	-350 ± 20	-350 ± 30	-225
Technique	Numerical Simulation	X-Ray Difraction	X-Ray Difraction	X-Ray Difraction	X-Ray Difraction	Neutron Diffraction
Steel	R4	S45C	SCM3	AISI 4140	AISI 4340	Ck45
Diameter (mm)	20	20	20	25.5	25.5	20
Quenchant	Water	Water	Water	Water	Water	Oil
Initial Temperature (°C)	930	850	850	850	850	680

5.4.3 Tensile Loading Model

This model has the same geometry, material properties and boundary conditions as Model A: Proof loading.

5.4.4 Out-of-of-Plane Bending Model

As already described in Chapter 2, OPB is due to the interlocking of the chain links; consequently, they behave like a bending beam, causing high stresses at certain locations of the chain link. The model used for studying OPB is similar to the model presented by [15], [18]. Three chain links have been represented, one complete and two half links. One symmetry plane has been used.

Figure 5.9 presents the geometry and boundary conditions of the OPB model. Link 3 applies a rotation to the central chain link, while Link 1 prevents the central link from moving. The stress distribution will be studied in the central chain link (Link 2). Therefore, Link 2 has a finer mesh, which also helps contact convergence; Link 2 is the slave surface for both contact

formulations with Link 1 and Link 3, being both master surfaces. A friction coefficient of 0.3 has been used, this value has been obtained from [49].

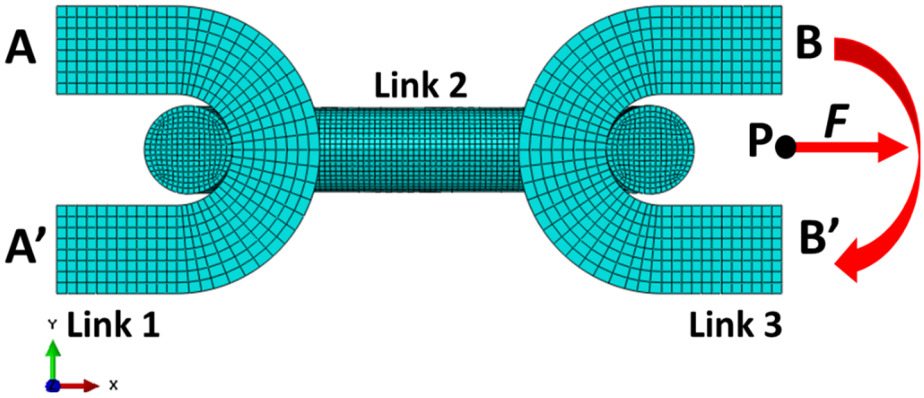

Figure 5.9 Geometry and Boundary Conditions of the OPB service loading model

The boundary conditions are the following:

- Symmetry Plane: Symmetry boundary conditions have been applied at the symmetry plane

Sections A-A': All the displacements have been restrained.

- Sections B-B' are coupled kinematically with the reference point *P*. Displacements of this point are restrained in all directions except that of the applied load *F*. After applying a pretension of 20% MBL, rotation is imposed at the reference point for rotating Link 3, which through the locking of contact surfaces imposes a bending moment at Link 2.

For both chain sizes, an interlink angle of 1.5 degrees and a pretension of 20% MBL have been applied. The contact formulation is the same as Model A, already presented.

5.5 Results

First, the predicted residual stress field by both models is presented. Second, the predicted values by both modes at the fatigue failure locations are compared. The aim is to answer the

question formulated at the beginning of this chapter: if residual stresses are to be taken into account in the study of mooring chain fatigue life, is it necessary to consider the residual stresses generated during the heat treatment stage and proof loading, or just proof loading?

5.5.1 Model A: Proof loading

This model only predicts the residual stresses generated by proof loading. After proof loading significant compressive residual stresses remain at the crown and the kt point, as illustrated by Figure 5.10. Note that the crown and Kt point are the locations where fatigue failure take place. In addition, residual stresses are more compressive at the Kt point than at the Crown. Unlike the von Mises stress, the hydrostatic stress gives information about the nature of the stress distribution, whether it is compressive or tensile. Figure 5.10 also reveals that high tensile residual stresses are present at the boundary of the contact zone and at a location midway between the intrados and the extrados of the link's axis. Those locations with high tensile residual stresses have already been identified by Bastid and Smith [27].

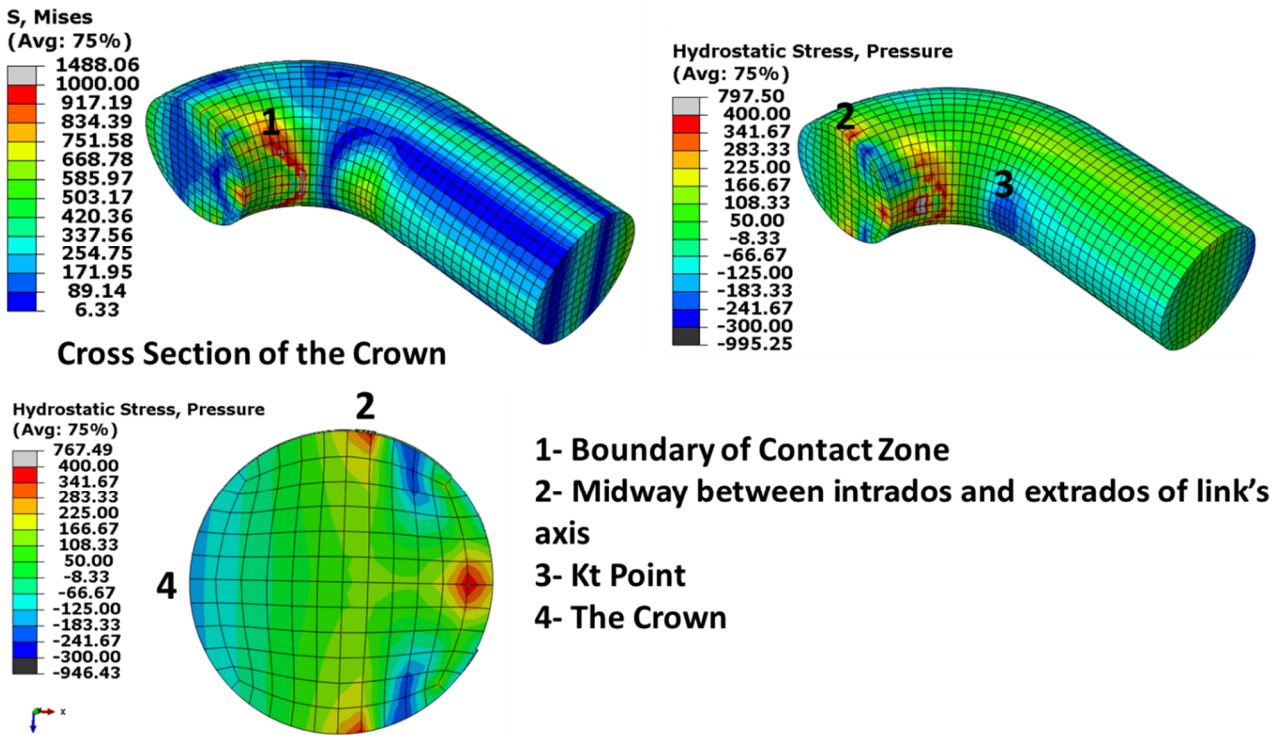

Figure 5.10 von Mises and hydrostatic residual stress distribution predicted by Model A for a 76mm diameter chain

Figure 5.11 highlights that as expected, there is no relative displacement between the contact surfaces of the chain links during proof load. Furthermore, it also shows that high normal contact forces occur.

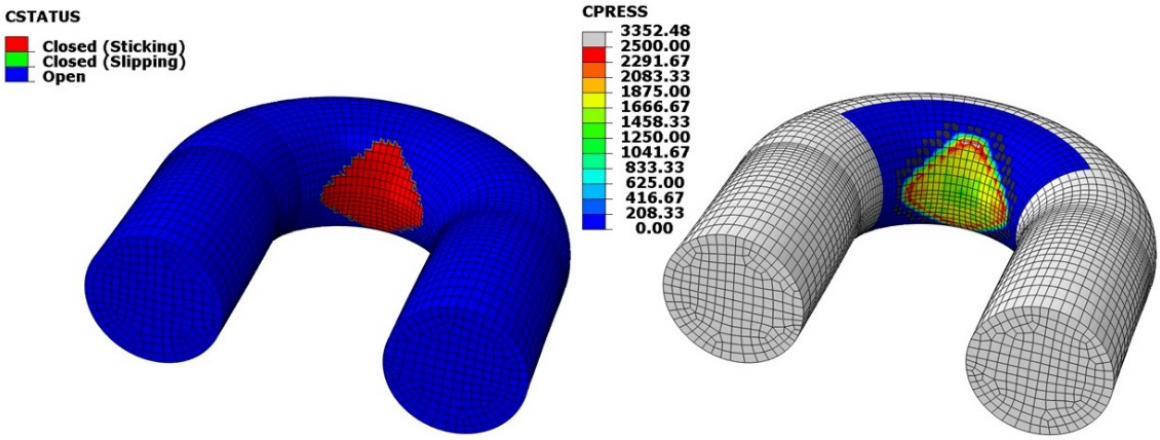

Figure 5.11 Contact between chain links during Proof load

5.5.2 Model B: Heat Treatment and Proof loading

This model accounts for residual stresses induced by heat treatment and proof loading. A contour plot of the hydrostatic stress (note that it is defined as the average of the trace of the stress tensor) after quenching is displayed in Figure 5.12. The figure highlight's that, after quenching, high compressive residual stresses (with values near the yield strength of the steel, reported in Table 5.1) remain at the surface while tensile at the core. As already said, this distribution is characteristic of quenched cylinders. Aligned with this, Figure 5.13 presents the residual stress distribution in a cross section of the chain link, expressed in local cylindrical coordinates. Again, compressive residual stresses are found at the surface and tensile at the core. This figure highlights the multiaxiality of the residual stress tensor.

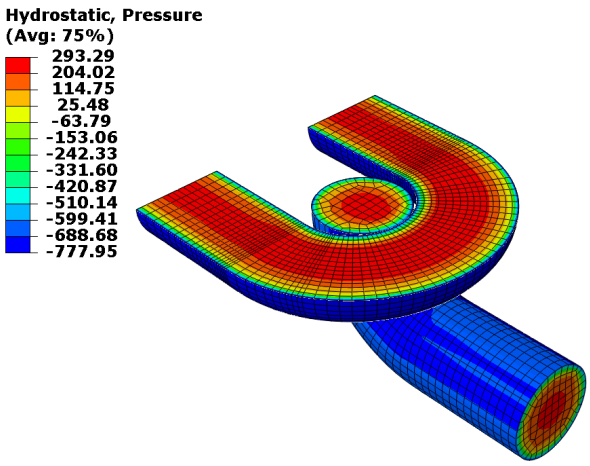

Figure 5.12 Hydrostatic residual stress distribution after quench

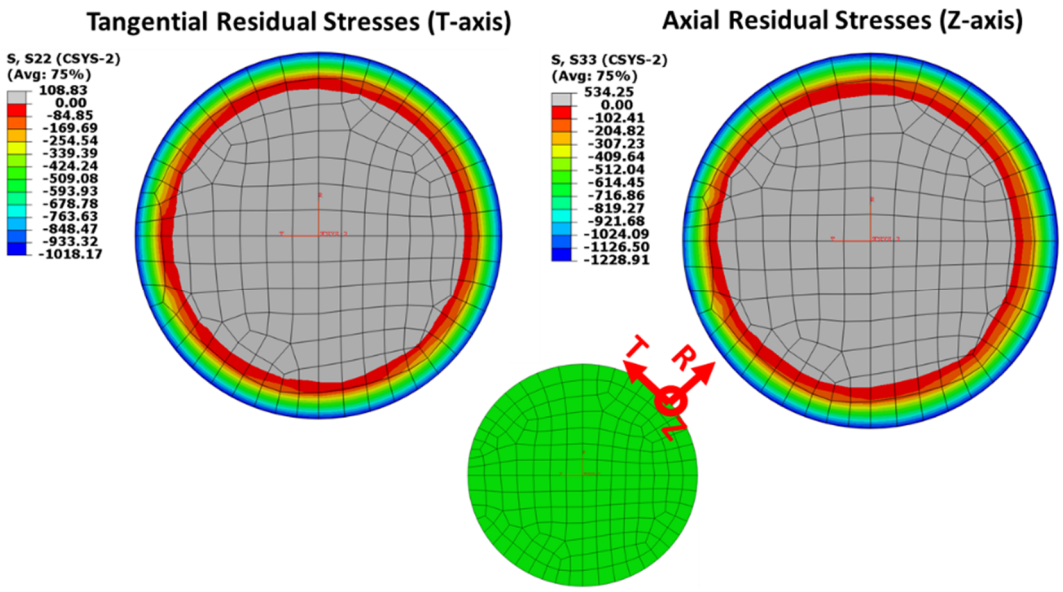

Figure 5.13 Residual Stress distribution at the mid-section of the chain link expressed in local cylindrical coordinates

Figure 5.14 reports the evolution of thermal stresses in the axial direction of the chain links during the heat treatment processes. During quenching, tensile thermal stresses are generated at the core whereas compressive stresses develop at the surface. When the chain is heated, the material softens, and the stresses are partially relaxed. After the second quench, the chain is tempered and cooled in water.

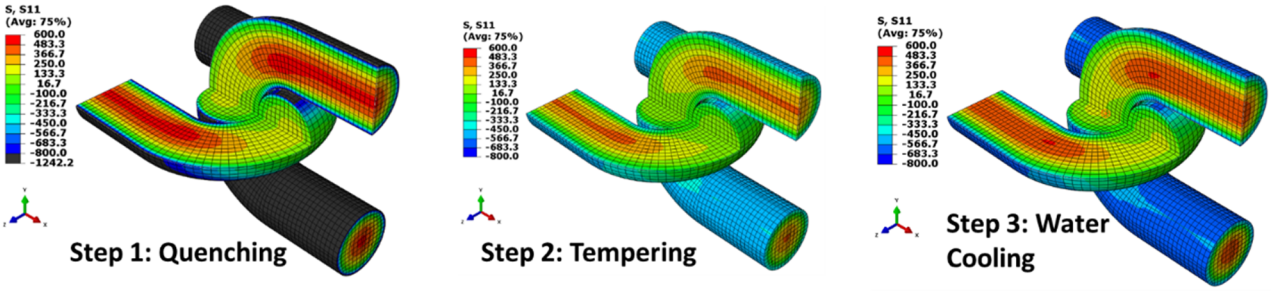

Figure 5.14 Evolution of thermal stresses in the axial direction of the chain during heat treatment

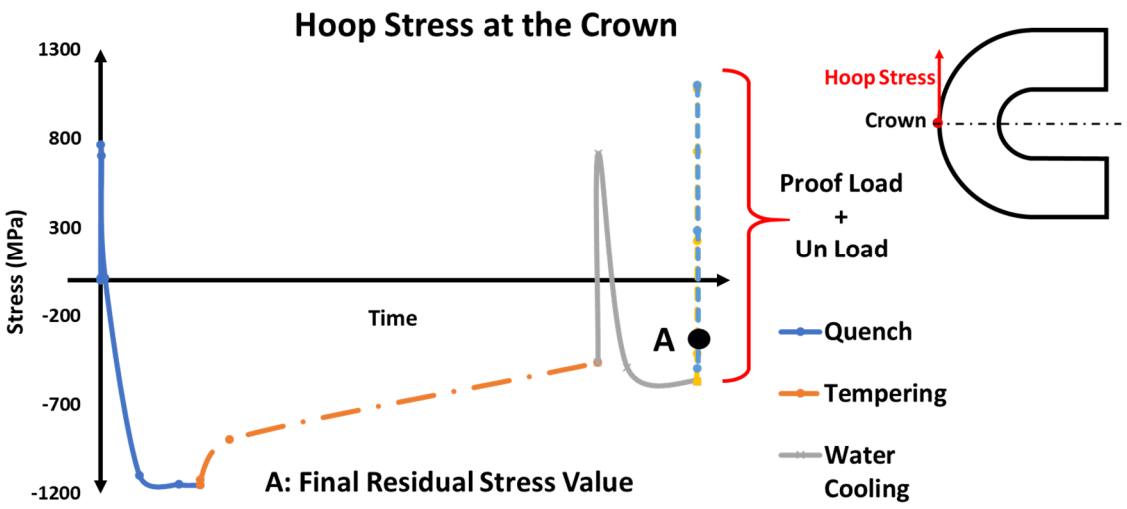

Figure 5.15 Evolution of the stress at the Crown in the hoop direction during heat treatment and proof loading

Figure 5.15 presents the evolution of the stress at the Crown in the hoop direction. After quenching, high compressive residual stresses are generated, which are partially relaxed during the following heating cycle. Similarly, after water cooling from the tempering temperature, the residual stresses will be lower than after the quench. During proof load, the hoop stress takes high tensile values (it is a stress concentration location), and after unloading compressive residual stress remain, which are beneficial for fatigue life.

5.5.3 Comparison between Model B and Model A

As mentioned in the introduction, the value of residual stress is particularly interesting at locations where fatigue failure may occur. Therefore, at those locations, the residual stress distribution predicted by each model will be compared

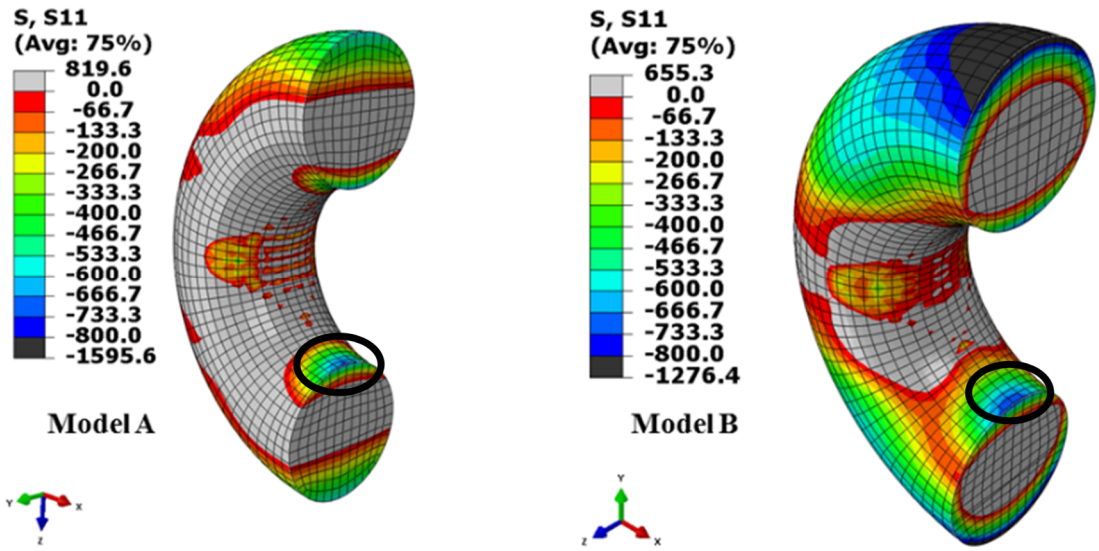

Figure 5.16 Comparison between residual stress field in the axial direction predicted by Model A: proof load and Model B: heat treatment and proof load

K_t point: Model A predicts a residual stress distribution characteristic of structural members subjected to bending. The upper region of the cross-section has compressive residual stresses, whereas the bottom one tensile. On the other hand, Model B predicts a circular distribution of residual stress due to the thermal gradients experienced during the heat treatments. However, at the K_T location (shown by the black circle) the residual stress values predicted by both are similar. Nevertheless, at regions near K_T, the distributions are different. This difference might have an effect on fatigue crack propagation since the effective stress intensity factor range will be smaller due to crack closure as a result of compressive residual stresses.

Crown: both models predict similar residual stress field at the crown

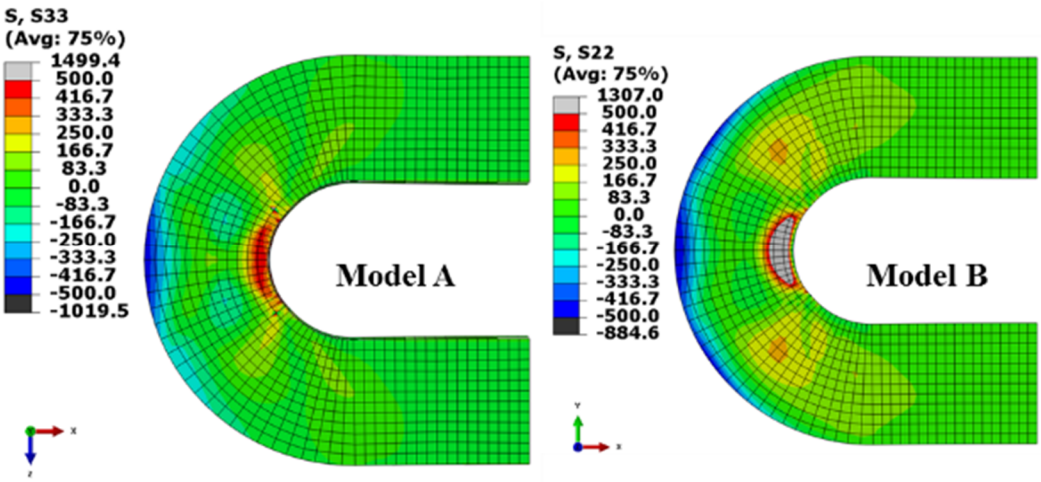

Figure 5.17 Comparison between residual stress field in the hoop direction predicted by Model A: Proof load and Model B: Heat treatment and proof load

Region near the contact zone: Figure 5.18 shows the residual stress distribution predicted by both models at the location where OPB is likely to occur. Model A predicts a tensile residual stress distribution over the majority of the surface whereas Model B predicts compressive residual stresses.

This difference in the residual stress state predicted by both models has an influence on the stress distribution after an OPB loading cycle as illustrated in Figure 5.19. If only the tensile residual stress from the proof load are taken into account (as in Model A) the stresses after a fatigue load cycle are higher than when the compressive residual stresses predicted by Model B are considered.

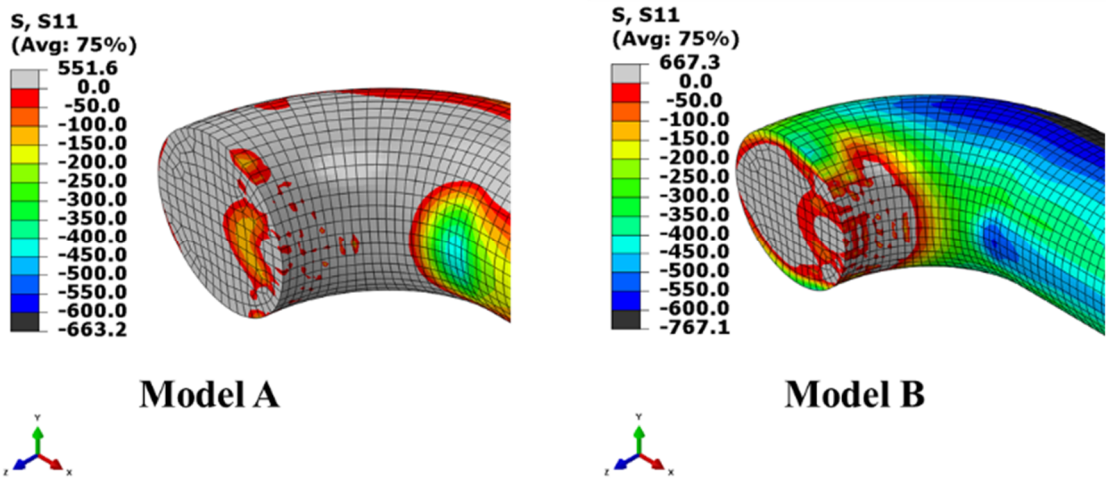

Figure 5.18 Residual stress field in the axial direction predicted by Model A and Model B in the boundary of the contact zone. D=162mm

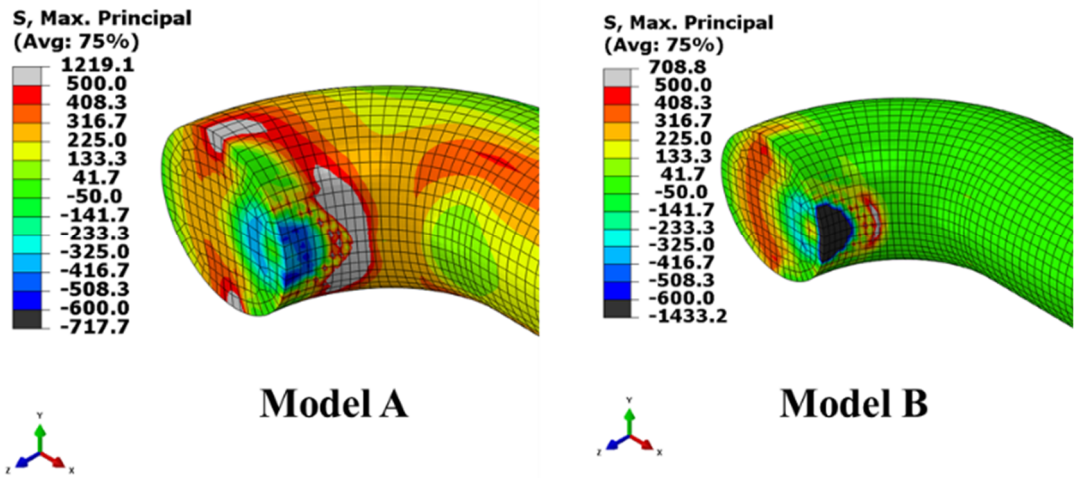

Figure 5.19 Maximum principal stresses under an OPB cycle for different residual stress distributions. D=162mm

5.5.4 Influence in the fatigue behavior

Table 5.4 illustrates the predicted values of maximum principal residual stress and stress range after a tension load cycle at Kt point and the crown. Table 5.4 presents the predicted values of maximum principal residual stress and the maximum hydrostatic stress (during an OPB load cycle) at Point C. For both diameters studied, Model B predicts lower residual stresses (hence more compressive) than Model A. As expected, the effect of residual stresses on the stress range is negligible, nevertheless, they have an important effect in the maximum hydrostatic stress during the fatigue load cycle.

Table 5.4 Residual stress and stress range predictions by Model A and Model B at Kt and the crown

	Model	D	Maximum Principal Residual Stress [MPa]	Stress Range [MPa]
K_T	Model A	76mm	-734	252
	Model B	76mm	-753	249
	Model A	162mm	-449	207
	Model B	162mm	-517	206
Crown	Model A	76mm	-502	246
	Model B	76mm	-515	241
	Model A	162mm	-439	211
	Model B	162mm	-548	209

Table 5.5 Residual stress and maximum hydrostatic stress predictions by Model A and Model B at Point C

	Model	D	Maximum Principal Residual Stress [MPa]	Maximum Hydrostatic Stress [MPa]
Point C	Model A	76mm	280.6	310.5
	Model B	76mm	153	178
	Model A	162mm	104	88
	Model B	162mm	-63	-132

5.6 Chapter Summary

Modeling of the manufacturing process is a complex task and requires elastic plastic material data at high temperatures. Two models for predicting the residual stress field after the manufacturing process have been presented, each of them with increasing complexity. The first (Model A), only takes into account the last stage of manufacture: proof loading. The second, Model B, considers the heat treatment and proof loading stages.

5.6.1 Tension-Tension

The predicted values at K_T and the crown by the different models do not differ significantly, the difference being below 15%. However, the stress distribution in the vicinity of these locations is different (as shown in Figures 5.16 and 5.17). This might have an impact on crack propagation. The reason for the similarity between the predicted values is that the yield produced by proof load at these locations (where stresses reach high values during proof load) is large enough to partially wash away the residual stresses left by the heat treatment stages. The influence of heat treatment increases with the chain diameter.

For a tension-tension load cycle, only the residual stresses generated by proof loading can be taken into account without leading to significant error.

5.6.2 Out-of-Plane Bending

Similar to tension-tension, Model A predicts higher values of residual stress than Model B (at Point C, Figure 5.18), although the difference between the values predicted by both models is larger than for K_t and the crown. The maximum Hydrostatic Stress after an OPB load cycle is lower when the residual stress distribution from Model B is considered.

Finally, the answer to the question formulated in the Introduction (i.e. which source of residual stress has more weight in the resultant residual stress field, the heat treatment or proof loading) depends on the diameter. For small diameters proof loading has more influence whereas, for large diameters, heat treatment plays a major role in the final residual stress distribution. Consequently, the next question worth asking is as follows: given the complexity of modeling the heat treatment processes, should it be considered for large diameter chains? For both loading modes, if only the residual stress distribution from proof loading is considered, a conservative assumption is made. This assumption is more conservative for OPB than for tension-tension, as well as for big diameters (162 mm).

It is worth reminding that Model B does not take into account phase transformations during quenching. On the surface, the effect of transformation strains would be to reduce the magnitude of compressive residual stress field. These observations are based on numerical analysis that has been validated qualitatively against experimental data from the literature.

Chapter 6: Fatigue Assessment of mooring chains under Tension loading

In the previous chapter the residual stress field after manufacture was predicted by means of Finite Element Analysis (FEA). This chapter presents a computational fatigue assessment method for mooring chains under tension loading. The method comprises of a mechanical calculation followed by a fatigue analysis. The mechanical analysis takes into account the residual stress field, obtained using the model described in the previous chapter, and applies service loading to derive the stabilized stress cycle. Finally, the Dang Van fatigue criterion is applied to estimate the lifetime. The effect of mean load is discussed, this aspect is not currently taken into account in the Engineering Standards. The described computational fatigue assessment method is complex and carries a substantial computational overhead, which does not make the method very appropriate for routine use in an industrial environment. Therefore, a simplified assessment method based on the Dang Van fatigue criterion is proposed. This method, once calibrated, does not require the use of FEA software, and has been successfully implemented in an Excel spreadsheet (presented in Annex B). Validation of the simplified method by comparing the predicted results with experimental data obtained from fatigue testing of mooring chains is presented.

6.1 Introduction

It is widely accepted among researchers that the mean stress has an effect on the fatigue behavior of engineering components, different papers studying its influence can be found in the literature, for example [75], [167], [168]. Nevertheless, neither in previous studies reported in the literature, nor in current standards (DNV-OS-E301[8] and API-RP-2SK[9]) the question of the influence of mean load on the fatigue performance of mooring chains under tension loading has been addressed in detail. However recently it has been pointed out that the dependency of the fatigue behavior of mooring chains under tension loading with respect to the mean load should be investigated [10]. Current standards (DNV-OS-E301[8] and API-RP-2SK[9]) provide S-N curves derived from experimental work without specifying the mean load for which they have been obtained or proposing a mean load correction function.

All of this indicates that we are still missing a comprehensive and robust numerical design method for the lifetime prediction of mooring chains under tensile loading. The design method must include the combined effect of mean load and residual stresses. The latter should be measured experimentally or predicted accounting for all the relevant manufacturing stages, and not only the last manufacturing operation (proof load). This chapter proposes a computational fatigue assessment methodology for mooring chains under tension loading accounting for residual stresses. They were predicted considering all stages in the manufacturing process. Multiaxial fatigue criteria enable to account directly for complex phenomena, such as residual stresses, mean stress, and non-proportionality of the stress tensor. A multiaxial fatigue criterion has been applied as part of a computational fatigue assessment method. In a computational method, as commonly practised in the industry [169], one can distinguish two steps:

Mechanical analysis based on knowledge of the geometry, the constitutive law, the boundary conditions, the manufacturing process and the service loading, which will provide the cyclic response of the structure in terms of strain and stress.

Fatigue analysis based on study of the stress-strain response computed before for each geometric point of the structure and assessment of the local elastic or plastic shakedown state or a ratcheting state, and the application of an appropriate lifetime criterion.

The next question that ought to be asked is which fatigue criterion should be used? Mooring chains are designed for an expected lifetime of 20 years; therefore, their fatigue lifetime falls within the high cycle fatigue regime. Previous work [32]-[33] has shown that in the giga cycle fatigue regime, most of the fatigue lifetime of mooring chains is spent on crack initiation. This finding was observed after multiple fatigue tests performed on corroded specimens tested in air and specimens tested under seawater flow of R5 Steel Grade. Consequently, it seems sensible to use a fatigue criterion based on crack initiation, for the present study. The Dang Van fatigue criterion is chosen; this criterion has already been used for the fatigue assessment of mooring chains under OPB [15]. The computational assessment method is summarized in Figure 6.1.

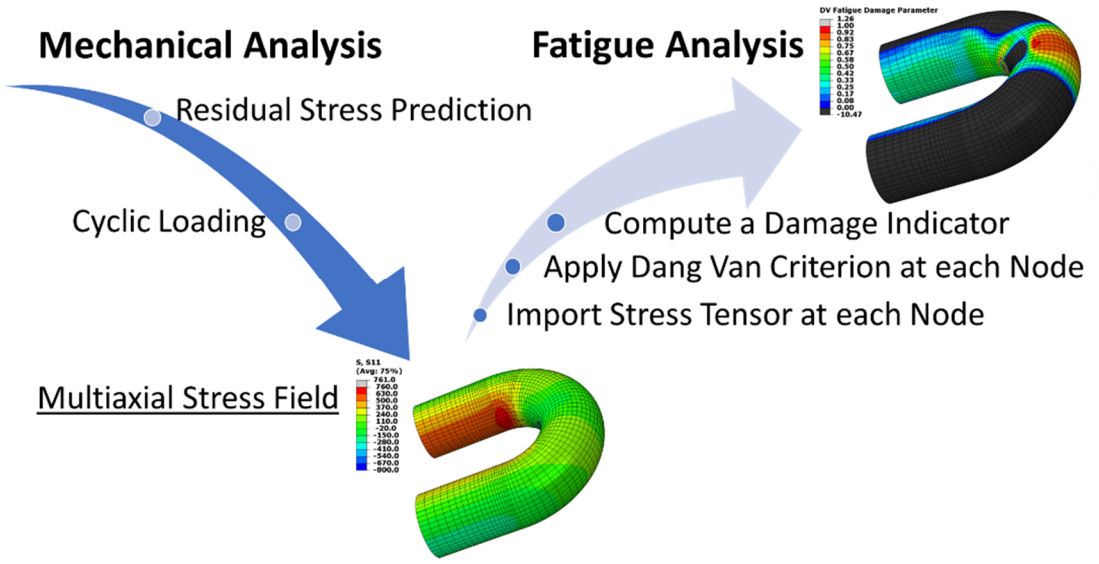

Figure 6.1 Workflow of the Computational Fatigue assessment method

This chapter is divided into two distinct parts: The first illustrates the computational fatigue assessment method illustrated in Figure 6.1 and presents the results obtained. It commences by describing the mechanical analysis. Noting that the residual stress prediction model from heat treatment has already been introduced in the previous chapter, only the constitutive law of the model applying proof load and service loading is presented. Then, the fatigue analysis is described. Two different loading conditions with the same amplitude but different mean loads are analyzed with the aim of assessing the effect of the mean load on the lifetime. This section ends with a discussion of the effect of the mean load on the fatigue lifetime and a discussion of the formulation of the Dang Van locus for the region of high compressive hydrostatic stresses.

The assessment method presented above incurs a substantial computational overhead, which does not make it appropriate for routine use in industry. To overcome this drawback, in the second part of this chapter, a simplified method is proposed. This method uses different mathematical tools and assumptions to simplify considerably the fatigue assessment using Dang Van fatigue criterion and has been implemented successfully in an Excel Spreadsheet. This section ends by comparing the predicted fatigue lifetimes obtained using the simplified assessment method against fatigue lifetimes recorded from tests performed in seawater. These tests were carried out at TWI Ltd as part of a Joint Industry Project whose sponsors were: American Bureau of Shipping (ABS), BP Exploration Operating Co Ltd, Shell Projects and Technology (former BG group), Equinor (former Statoil), Ramnäs Bruk (in kind) and Vicinay Cadenas (in kind). The author is grateful to these companies for the permission to use these results. Their contribution has been of great value for the validation.

6.2 Computational Fatigue Assessment of Mooring Chains under Tension loading

The fatigue analysis of a R5 127mm mooring chain is presented. Two loading conditions have been selected; both have the same load amplitude, 8%MBL, but different mean loads, 10%MBL and 20%MBL respectively. The aim is to determine the influence of the mean load.

6.2.1 Mechanical analysis

The mechanical analysis comprises two parts: residual stress prediction and service loading. The result is the stabilized stress cycle which is imported into the fatigue analysis. In order to derive it, two different models have been employed:

(i) Heat Treatment Model: This model was presented in the previous chapter.

(ii) Tensile Loading Model: Simulates proof load and service loading.

Both models were implemented using ABAQUS 6.14 and have the same geometry: two chain links accounting for one symmetry plane. Nevertheless, the models have different constitutive laws, the main characteristic of the heat treatment model is that it uses temperature dependent material parameters, whereas the tensile loading model accounts for combined nonlinear hardening. This section described the tensile loading model, followed by illustration of the stabilized response of the chain when subjected to service loading.

Tensile Loading Model: Proof Load and Service Loading

This model predicts the final residual stresses field after proof load and the stabilized stress cycle when service loading is applied. The predicted residual stress field from the heat treatment stage is incorporated as an initial state before the proof loading step. This model has several similarities with Model A, presented in the Chapter 5. Both models have the same

geometry, mesh, boundary conditions and contact formulation. Nevertheless, the mechanical behaviour of the material has been represented using a different constitutive law than Model A. The main outcome of Model A was the residual stress distribution after proof load, whereas in this chapter the outcome is the stabilized response of the chain links when subjected to service loading. Consequently, the material behaviour has been modelled as elastic-plastic with combined non-linear isotropic and non-linear kinematic hardening. The yield surface is given by the von Mises equivalent stress yield criterion:

$$F = f(\sigma - \alpha) - \sigma^0 \tag{6.1}$$

Isotropic hardening is given by:

$$\sigma^0 = \sigma\big|_0 + Q_\infty[1 - \exp(-b\bar{\varepsilon}_p)] \tag{6.2}$$

where σ^0 is the flow stress, $\sigma|_0$ is the initial yield stress and Q_∞ the asymptotic value of the flow stress and b the isotropic hardening exponent.

Kinematic hardening is described by:

$$\dot{\alpha} = C\frac{1}{\sigma\big|_0}(\sigma - \alpha)\dot{\bar{\varepsilon}}_p - \gamma\alpha\dot{\bar{\varepsilon}}_p \tag{6.3}$$

where C and γ are material parameters and $\dot{\bar{\varepsilon}}_p$ represents the equivalent plastic strain rate and can be written as a function of the plastic strain rate as follows:

$$\dot{\bar{\varepsilon}}_p = \sqrt{\frac{2}{3}\dot{\varepsilon}_p : \dot{\varepsilon}_p} \tag{6.4}$$

The combined kinematic hardening is defined by Eq. (6.3) and Eq. (6.2), it is composed of five material parameters, $\sigma|_0$, Q_∞ , b, C, and γ. For R4 steel grade the values of the parameters were obtained from [18].

Table 6.1 Non-linear combined hardening parameters. Source [15]

Parameter	Value
$\sigma\|_0$	723.6 MPa
Q_∞	-141.6 MPa
B	1.42
C	2.4410E+5 MPa
γ	1379 MPa

For a description of the geometry, mesh, boundary conditions, and contact formulation of this model, please see the description of Model A presented in Chapter 5. Moreover, the final residual stress distribution after heat treatment and proof load is also presented in Chapter 5 .

Results: Service loading

The aim of this analysis is to derive the asymptotic response of the chain when subjected to fatigue loading. Service loading is defined as the external force applied to the chain links and characterized by a periodic function. It is referred to as a percentage of the MBL of the chain. Figure 6.2 presents the hoop stress versus strain at the crown under proof loading, unloading, and service loading. The figure was obtained from the mechanical analysis (which, as already said, was performed in ABAQUS). Service loading is defined by a mean load of 20% MBL and a load amplitude of 8% MBL; 5 fatigue cycles were simulated. The graph highlights that the cyclic response of the chain remains macroscopically elastic. Figure 6.3 highlights that the cyclic stress tensor at Kt position is mainly uniaxial.

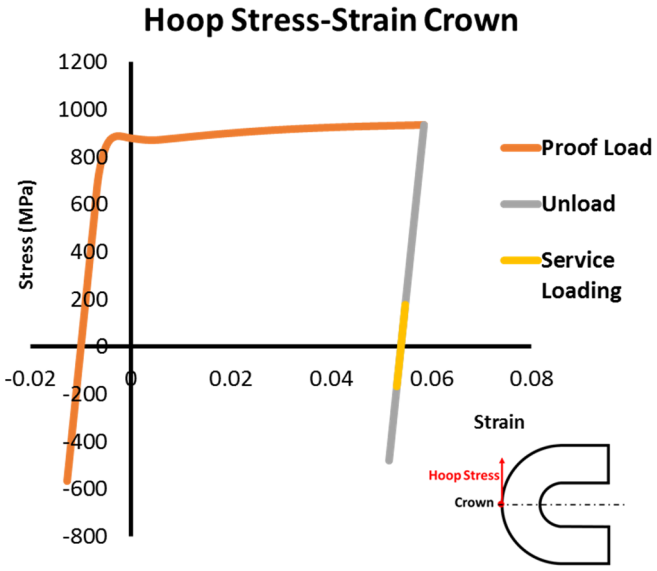

Figure 6.2 Stress-strain curve during proof load and service loading

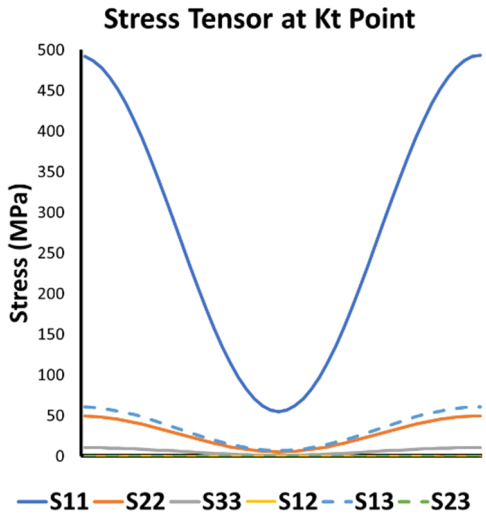

Figure 6.3 Cyclic Stress Tensor at Kt Point

6.3 Fatigue Analysis

The Dang Van fatigue criterion has been selected for the fatigue analysis (one of the conditions for applying it, is that the stabilized cyclic response must be elastic). This criterion has already been used for the fatigue assessment of mooring chains under OPB [15], [18]. A strong point of this criterion compared to others, is its graphical representation, which enables to understand

intuitively the role of residual stresses and mean stresses in the fatigue lifetime. Given that the Dang Van fatigue criterion has been described previously in Chapter 3, only the mathematical formulation is presented here. The fatigue assessment is performed in two stages. First the stress tensor at the point of interest is represented in the Dang Van diagram (hydrostatic stress vs mesoscopic shear stress). Second, the Dang Van locus intersecting the load path exclusively at one point is reported in the diagram. The predicted fatigue lifetime is then derived from the locus.

6.3.1 Dang Van Fatigue Criterion

The Dang Van criterion [76] defines the fatigue damage as a linear combination of maximum mesoscopic shear stress and the hydrostatic stress. It states that fatigue failure will not take place if the following inequality is satisfied.

$$\max_t[\tau(t) + a \cdot \sigma_h(t)] < b \tag{6.5}$$

where:

- $\tau(t)$ is maximum mesoscopic shear stress.

- $\sigma_h(t)$ is hydrostatic stress

- *a* and *b* are material parameters

Dang Van criterion is an endurance criterion. Nevertheless, it can be also be implemented for finite fatigue life ([78]–[80]) by defining material parameters *a* and *b* as a function of the number of cycles to failure. Engineers work with macroscopic stresses (for example obtained from FEA calculations). Under the assumption of elastic shakedown and based on Lin-Taylor homogenization, Dang Van derived a change of scale expression that enables the derivation of mesoscopic stresses from macroscopic ones:

$$\tilde{\sigma} = \sigma(t) - \mathbf{s}^* \tag{6.6}$$

where:

- $\tilde{\sigma}$: Stress tensor at mesoscopic level

- $\sigma(t)$: Stress tensor at the macroscopic level

- $\mathbf{s}^*$ Represents the local residual stress state, which characterizes the local stress fluctuation at the mesoscopic level. Under elastic shakedown, it is time independent and can be computed as the centre of the smallest hypersphere that circumscribes the path of the stress deviator.

6.3.2 Implementation of the fatigue criterion

The fatigue analysis has been carried out by post processing the results from the mechanical analysis using MATLAB. Attention has been paid to the aspects regarding accurate application of the criterion in reduced computational time. The first aspect relates to the mathematical points at which the criterion is applied. The second to how to derive mesoscopic stresses from macroscopic ones. And the third concerns the calibration of the material parameters *a* and *b* of the fatigue criterion.

Because of the high stress gradient predicted in the region of the Kt point (already shown in Chapter 5), the value of the stress at the integration point is not representative of the peak stress at the element. The stress values extrapolated at the nodes of the elements with quadratic interpolation were thought to be more reliable for this analysis. Consequently, in this study, the fatigue criterion has been applied at the nodes, rather than at the integration points.

From a calculation point of view, when solving Eq. (6.6) the main challenge is to obtain $\mathbf{s}^*$. It can be calculated through computational geometry[101] although most of the applications in the literature use optimization methods (for example [80], [102]–[104]) or in textbooks [105], and obtain $\mathbf{s}^*$ solving:

$$\mathbf{s}^* = \min_{s^*} \max_{t} ||\mathbf{s} - \mathbf{s}^*|| \tag{6.7}$$

In Chapter 4 it was concluded that the BFGS optimization method was the most efficient method for deriving the center of the smallest hypersphere circumscribing the load path of the stress deviator. Following the recommendations for fast fatigue assessment issued in Chapter 4, the MATLAB code HANSO [140], available at [129] has been employed. This method enabled a fast fatigue assessment of the chain link, taking less than 4 minutes to apply the Dang Van fatigue criterion at the 11960 nodes of the surface of one of the chain links.

A final aspect to be considered, is the calibration of the criterion. The predicted lifetimes depend on the material parameters *a* and *b*. These parameters can be obtained from simple tests on small specimens; for example, alternating tension and alternating torsion. In this case, the parameters are expressed by:

$$a(N) = \frac{\tau_N - \frac{\sigma_N}{2}}{\frac{\sigma_N}{3}} \quad b(N) = \tau_N \tag{6.8}$$

where:

τ_N is the alternating torsion fatigue strength for *N* cycles.

σ_N: is the alternating tension fatigue strength for *N* cycles.

Mooring chains are located in seawater which is a corrosive environment. Consequently, fatigue properties accounting for corrosion should be introduced in Eq (6.8) for deriving material parameters *a* and *b*. The assumption that *a* remains constant with the number of cycles has been made. This assumption is commonly made when applying Dang Van for finite fatigue life [78], [80]. For mooring chain steel under, when corrosion is not accounted, *a* takes a value of 0.34 [18]. On the contrary, if corrosion is accounted, *a* takes a value of 0.55 [18]. The

conclusions that can be drawn from this difference between the values of *a*, is that the material is more sensitive to mean stresses in corroded conditions than in uncorroded ones.

Once *a* is known, only *b* remains to be calculated, and can be rewritten as a function of a and the alternated fatigue strength as follows:

$$b(N) = a \cdot \frac{\sigma_N}{3} + \frac{\sigma_N}{2} \tag{6.9}$$

Fatigue strength is obtained through the testing of small specimens and should account for corrosion. Determination of the fatigue properties under corrosion is not as straightforward as in a corrosion free environment. There are two approaches: the first is to test the specimens under constant sea water flow, the second is to pre-corrode the specimens (for example following the standard EN ISO 9227) prior to fatigue testing in air. Different fatigue properties of R5 steel accounting for corrosion can be found in the literature. Fernandez et al. [170] and Arredondo et al. [35] presented fatigue testing under sea water of small specimens of R5 grade at frequencies varying between 0.5 and 10 Hz. These tests were conducted with a R ratio (defined as the minimum peak stress divided by the maximum peak stress) of 0.1. The alternated fatigue strength (for zero mean load, R_{-1}) can be derived using the Dang Van fatigue criterion as follows:

$$\sigma_{R-1} = \frac{\frac{\sigma_a}{2} + \frac{a}{3}(\sigma_m + \sigma_a)}{\frac{a}{3} + \frac{1}{2}} \tag{6.10}$$

where:

σ_a is the stress amplitude.

σ_m is the mean stress.

a is the material parameter of Dang Van criterion.

Eq. (6.10) has been derived from the geometric effect of a mean load in the Dang Van plane (see Figure 6.7 for more details). Perez Mora [32],[150], obtained fatigue properties of R5 steel of small specimens under sea water flow tested at 20 kHz and small pre-corroded specimens tested on air (note that their tests were carried out in very high cycle regime). Both series were tested with a null mean load (R= -1). The obtained alternated fatigue strengths (for 1E6 cycles) are compared with the alternated fatigue strength derived from the data of Fernandez et al. [170] (whose data were interpolated using a slope m=3) and Arredondo et al [35].

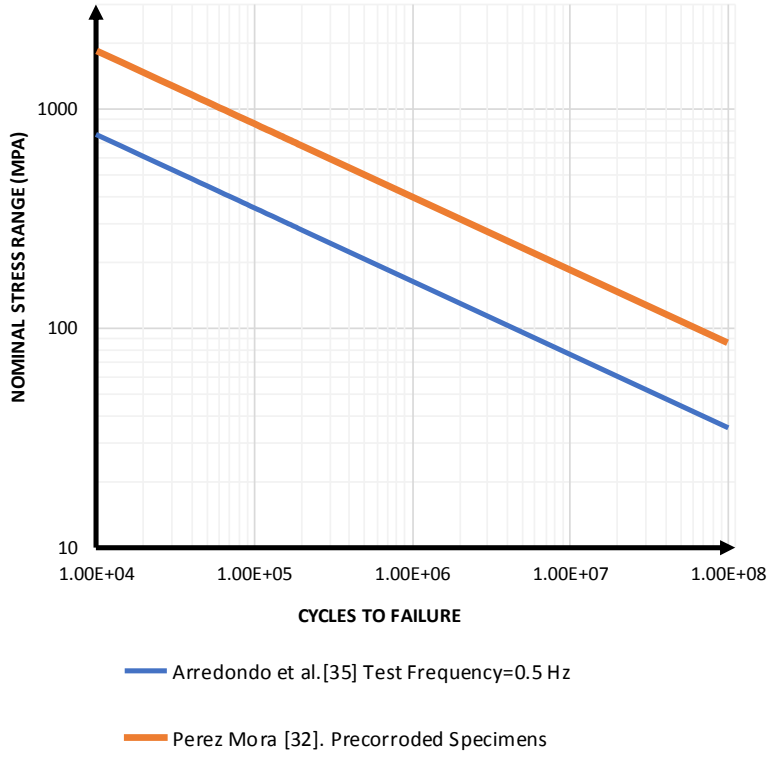

Figure 6.4 S-N Curves derived from small specimens

Table 6.2 Alternated fatigue strengths for 1E+06 cycles

Source	Fatigue strength (1E+06 cycles)	Conditions	Testing Frequency
Fernadez et al. [170]	154.5 MPa	Tested under sea water	0.5 Hz
Arredondo et al. [35]	164.4 MPa	Tested under sea water	0.5 Hz
Arredondo et al. [35]	286.6 MPa	Tested under sea water	10 Hz
Perez Mora [32]	400 MPa	Pre-corroded specimens	N/A
Perez Mora [32]	~400 MPa	Tested under sea water	20 kHz

Table 6.2 reveals that there is an important difference between the fatigue properties obtained from specimens tested under sea water flow and pre-corroded specimens. Furthermore, the testing frequency has a non-negligible effect on the obtained fatigue strength. This phenomenon has already been pointed out in the literature. Endo and Miyao [171] performed fatigue testing of carbon steels in aqueous saline solution in the high cycle fatigue regime and test frequencies below 100 Hz. They concluded that an increment of a factor of 10 of the test frequency resulted in augmentation by 50% of the fatigue strength. Table 6.2 highlights an important difference in the obtained fatigue strength depending on the conditions under which fatigue testing has been carried out. The fatigue tests that represent better the mechanisms of corrosion and fatigue are those performed at low frequencies under sea water flow.

The predicted fatigue lifetime by the Dang Van fatigue criterion depends on the value of the alternated fatigue strength used for its calibration. As an example, the predicted fatigue lifetime using Perez Mora's data [8] is 14,4 times higher than predicted using Arredondo et al. [35] for a test frequency of 0.5 Hz.

6.3.3 Results

Two load conditions have been studied; both with the same mean load but different load amplitudes. The aim is to determine the influence of the mean load. The fatigue lifetime corresponding to a mean load of 20% MBL was reduced approximately by a factor of 2.6 with respect to the fatigue lifetime for 10% MBL. As expected, mean load has a non-negligible effect on the fatigue lifetime of mooring chains. Figures Figure 6.5 and Figure 6.6 present the Dang Van diagram for both load conditions and the load paths at the Kt point and the crown. The first aspect highlighted by both figures, is that failure occurs at the crown for both loading conditions. Moreover, one important feature shown by these figures is that at both locations, the maximum mesoscopic shear stress takes similar values. Shear stress plays a primary role in the formation of fatigue cracks [6], although normal or hydrostatic stress has an essential role in opening or closing the crack. The difference between the fatigue lifetime at different locations is due to the difference in the hydrostatic stress between them. Hydrostatic stress is the addition of residual stresses (that can be treated as a mean stress) and mean stress from mean load. As previously mentioned, heat treatment and proof loading leave high compressive residual stresses, although they are more compressive at the Kt point than at the crown, this is in accordance with results from other authors, for example [27], [172], [173].

Figure 6.7 has been obtained by post processing the results of the mechanical analysis. The figure reveals that in the Dang Van diagram the effect of increasing the mean load is to translate the Dang Van plot towards higher hydrostatic stresses, therefore reducing the predicted fatigue lifetime. Residual stresses have the same effect in the Dang Van diagram as mean stresses. The translated distance is slightly higher for the Kt point than for the crown.

It can be concluded that the main difference between a failure occurring at Kt or at the crown is due to the superposed effect of mean load and residual stresses, although residual stresses have a greater influence than mean load.

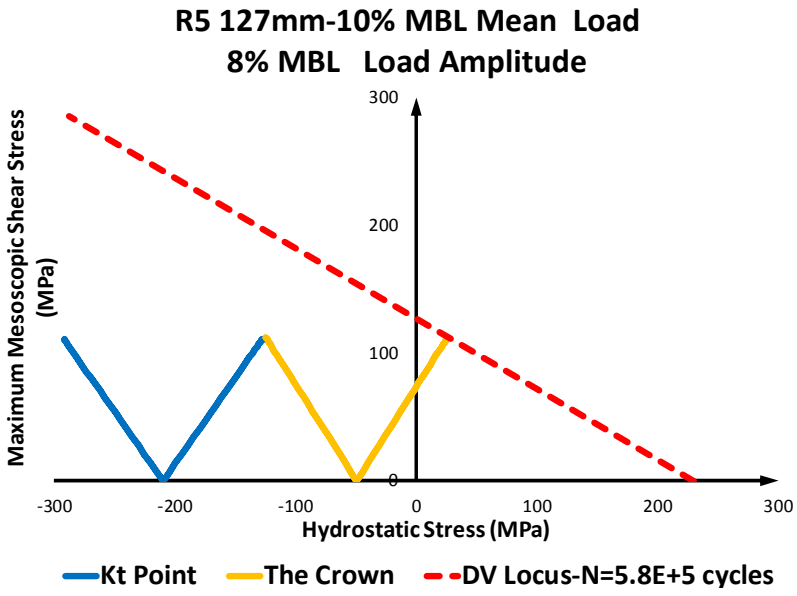

Figure 6.5 Dang Van diagram for 10%MBL Mean Load

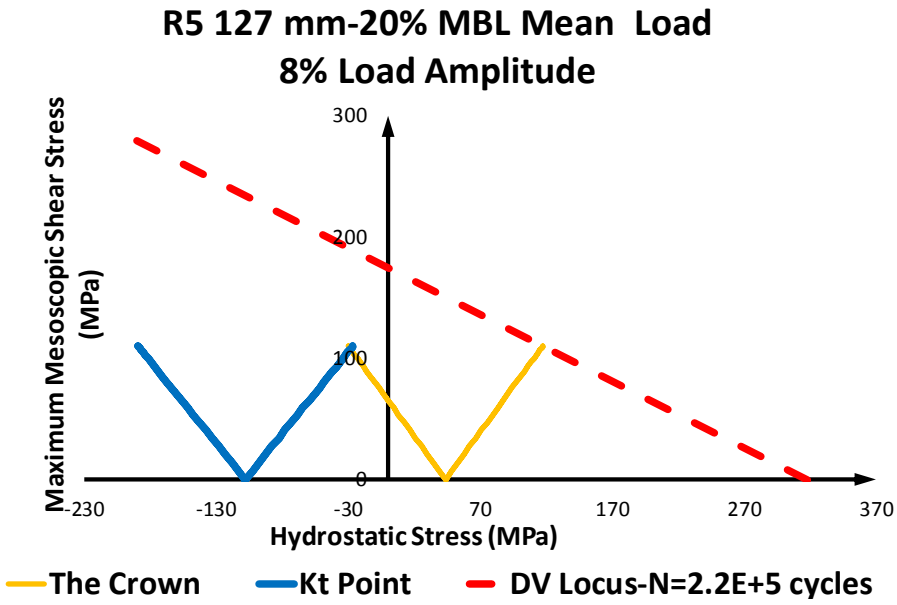

Figure 6.6 Dang Van diagram for 20%MBL Mean Load

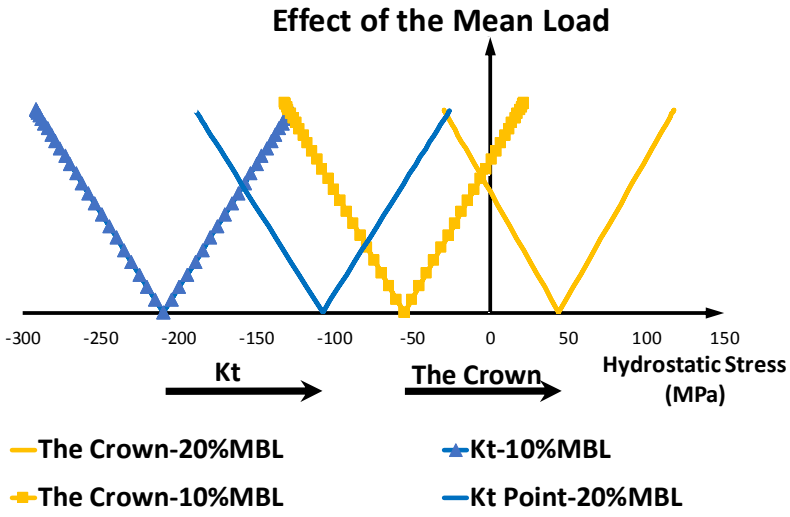

Figure 6.7 Mean load effect in the Dang Van diagram

6.3.4 Comparison of the failure locations predicted by Dang Van fatigue criterion with experimental observations

Before comparing the predicted fatigue lifetimes with experimental data (this comparison is reported in Section 6.4) a qualitative comparison has been performed. The criterion has been applied at all nodes on the surface of the chain link. The aim is to check whether the predicted fatigue failure locations, by the Dang Van criterion, correspond to the locations where chains are known to fail (the Kt point and the crown). For each node, the following damage indicator was computed:

$$C_{DV} = \left[\frac{\max[\tau(t) + a(N) \cdot \sigma_H(t)] - b(N)}{b(N)}\right] \tag{6.11}$$

Figure 6.8 presents a contour plot of the Dang Van fatigue damage parameter [Eq. (6.11)] obtained from post processing the results of the mechanical analysis with MATLAB. Surprisingly, it unveils that the two most critical locations were neither the Kt point nor the crown; they are the region at the boundary of the contact zone (Region 1) and the region

midway between the intrados and the extrados of the link axis (Region 2). Figure 6.9 illustrates the Dang Van diagram for the locations reported in Figure 6.8.

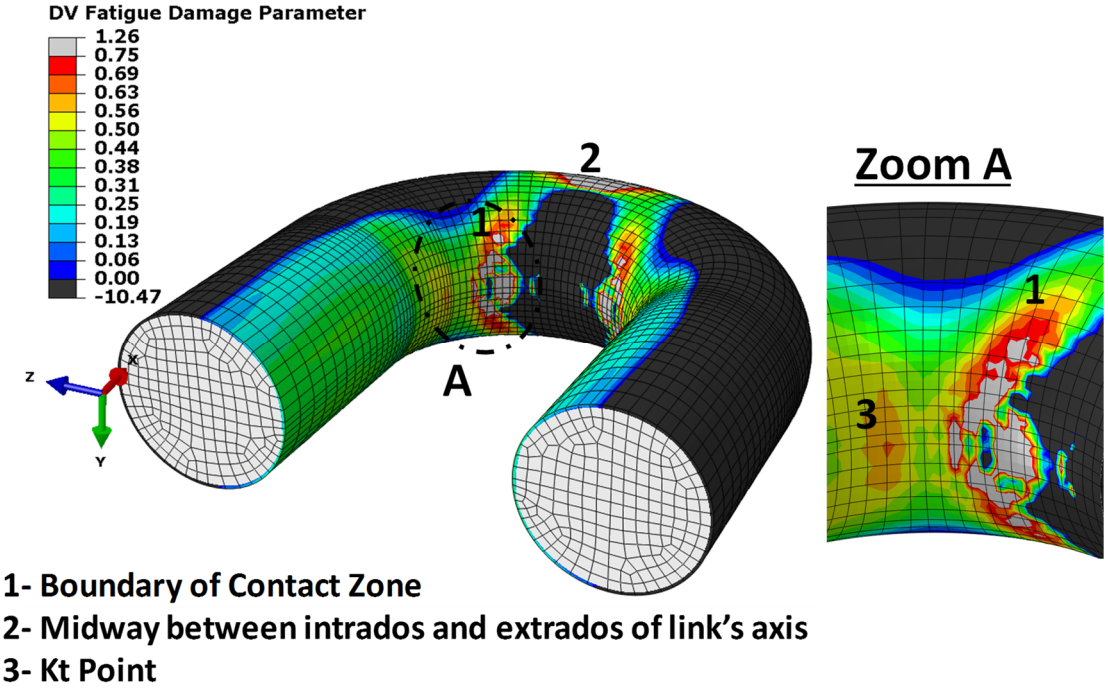

Figure 6.8 Contour plot of the Dang Van Fatigue damage parameter and zoom in at the boundary of the contact zone

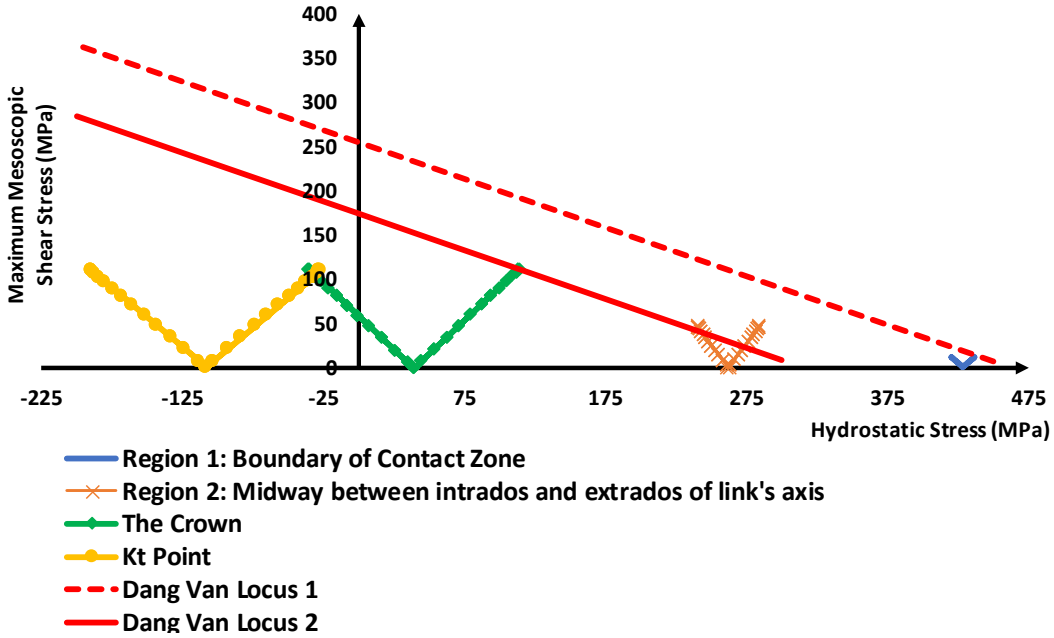

Figure 6.9 Dang Van load paths of the predicted fatigue failure locations

Figure 6.9 highlights that at the boundary of the contact zone (Region 1) and midway between intrados and extrados of link's axis (Region 2) the hydrostatic stress is significantly bigger compared to the mesoscopic shear stress amplitude. This can be explained by analyzing the values of residual stresses at these locations. As already reported in Section 5.5, residual stresses take high tensile values at Region 1 and Region 2. Moreover, this is in agreement with the results from Bastid and Smith [27], who predicted principal residual stresses of 1512 MPa and 710 MPa at Region 1 and Region 2 respectively, by means of elastic-plastic finite element analysis. Bastid and Smith only accounted for residual stresses from proof loading. At first, it could be considered that these high values were predicted because heat treatment was not being accounted for. In fact, when heat treatment is considered, these values are reduced, but are still important. For a 127mm R5 chain the predicted residual stress values accounting for heat treatment and Proof loading are 625 MPa and 450 MPa at Region 1 and Region 2 respectively. In other words, even if heat treatment is considered in the prediction of residual stresses, high tensile residual stresses are still predicted at both regions.

The Dang Van Fatigue criterion is of a phenomenological nature. Similar to critical plane methods, the criterion is based on the mechanisms that govern fatigue crack initiation. The criterion considers that crack initiation is driven primarily by shear stress amplitude, with hydrostatic stress playing a secondary although important role. Susmel et al. [93] found that when the ratio between maximum normal stress and shear stress amplitude relative to the critical plane attains an upper threshold, critical plane criteria no longer have physical sense. In other words, failure is not governed any more by the mechanisms which underpin critical plane methods. The critical plane stress ratio is defined as follows:

$$\rho = \sigma_{n,max}/\tau_a \tag{6.12}$$

The mechanisms that govern static failure are different from those of fatigue failure. When ρ takes high values, we are closer to a static problem rather than to a fatigue problem. In such cases, the lifetime will not be governed anymore by shear stress amplitude. Critical plane approaches or Dang Van fatigue criterion can be applied as long as the critical plane stress ratio remains below a certain value, in other words, as long as the shear stress amplitude is significant compared to mean stress. Susmel et al. [93]. derived an equation to obtain the limit value of the critical plane stress ratio. Although this ratio might change from one critical plane criterion to another, it gives an initial approximation to the threshold at which critical plane approaches can be used. The limit value depends on material fatigue material properties, and is defined as follows:

$$\rho_{lim} = \frac{\tau_{A,\infty}}{2 \cdot \tau_{A,\infty} - \sigma_{A,\infty}} \tag{6.13}$$

In the case of R5 grade for corroded specimens and a fatigue lifetime of 10E6 cycles, the limit value obtained using Eq. (6.13) is around 1.81. The critical plane stress ratio was calculated for Region 1 and Region 2, giving values of 35 and 6.5 respectively. At these locations shear stress amplitude is small compared to normal stress, as already reported in Figure 6.9. Moreover, at these locations, there is a competition between the negative effect of damage and the beneficial effect of hardening [174]. In addition, the Dang Van locus should be modified at the high hydrostatic region, it should be derived from fatigue tests performed on notched specimens and account for the positive effect of hardening [175].

Excepting Region 1 and Region 2, the most critical locations according to the Dang Van fatigue criterion are located at the Crown and Kt. In fact, for a 20% MBL mean load, the crown was found to be the location governing the fatigue lifetime of the mooring chain links. This was confirmed by fatigue testing, where most of the fatigue failures occurred at the Crown. Figure

6.10 and Figure 6.11 show fatigue cracks that led to failure at Kt point and the crown respectively.

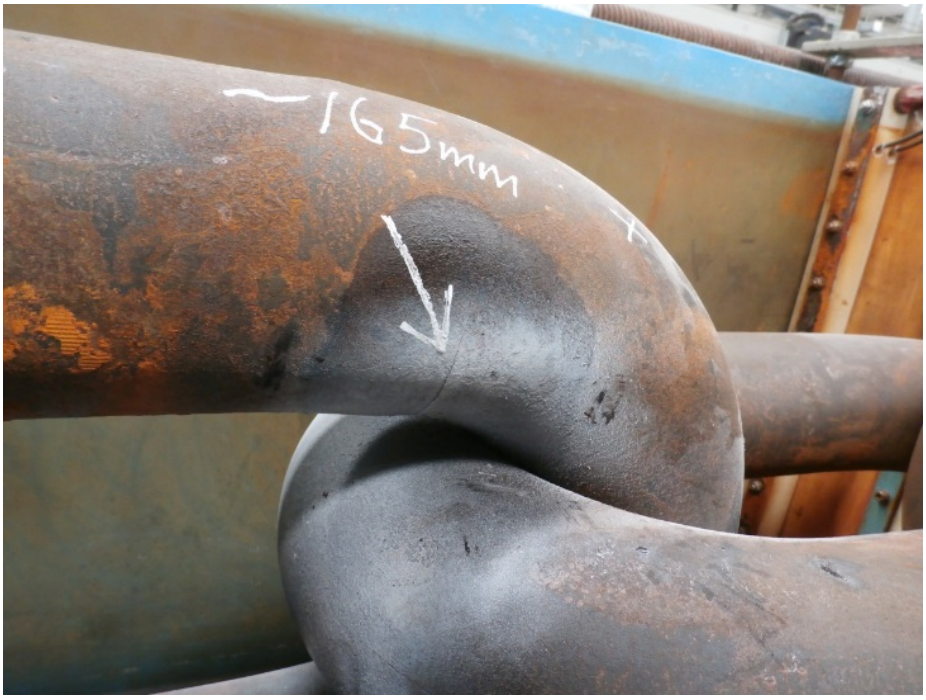

Figure 6.10 Fatigue crack at the Kt position

Figure 6.11 Fatigue crack at the Crown

6.4 Modification of the Dang Van fatigue criterion for high compressive hydrostatic stresses

The Dang Van criterion is widely applied for studying fatigue caused by fretting or rolling contact fatigue. In these applications, high compressive hydrostatic stresses are present. Desimone et al. [176] performed fatigue testing of a quenched and tempered steel (grade 27MnCrB52 denominated as EN-10083-3) with a yield strength of 1230 MPa. Desimone et al. performed fatigue tension tests for different R ratios, -2, -1,0.1 and 0.3 and concluded that there was no difference in the fatigue strength for R=-2 and R=-1. In other words, the compressive mean stress did not have any effect on the fatigue strength. Based on these results, Desimone et al. [177] proposed to modify the Dang Van locus by dividing it in two parts. For positive hydrostatic stresses the locus remains unchanged, whereas for lower hydrostatic stress values the locus becomes horizontal (Reported in Figure 6.12). This modification is a conservative approach which avoids overestimating the predicted fatigue lifetime for high compressive mean stresses, a drawback of the Dang Van fatigue criterion, which has already been pointed by different authors [178]–[180].The modified Dang Van locus has been applied by different authors for studying Rolling Contact fatigue [180],[181].

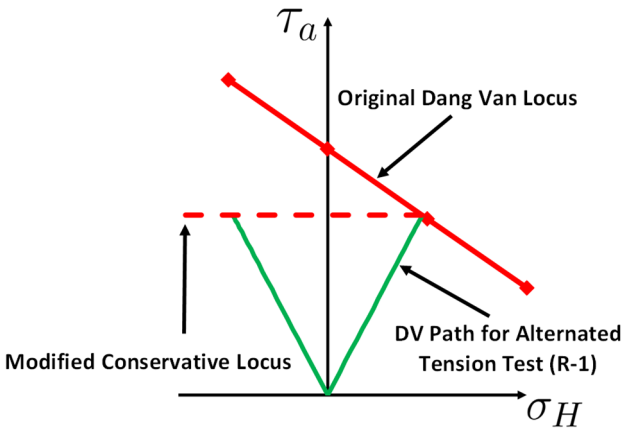

Figure 6.12 Conventional and Modified Dang Van

The original Dang Van locus needed to be adapted to account better for high compressive hydrostatic stress values. The resulting Modified Dang Van locus is based on experiments on a steel with different material properties than mooring chain steel. Tests of mooring chain steel accounting for corrosion with negative mean stresses should be performed to confirm that negative mean stresses have small influence on the value of alternating fatigue strength. Furthermore, in the case of mooring chains, and only for low mean loads, the Dang Van path at the Kt point is located in the high compressive hydrostatic regions (as highlighted by Figure 6.5 and Figure 6.6), which means that the modified Dang Van locus would be only conservative for low mean loads, remaining the same when applied for high mean loads.

For the load case corresponding to a low mean load (10 % MBL), the fatigue lifetimes predicted by both the original locus proposed by Dang Van [77] and the modified locus proposed by Desimone [177] are reported in Figure 6.13. This figure, obtained after postprocessing the results of the mechanical analysis, highlights the difference between the fatigue lifetimes predicted by both locus. When the modified conservative locus proposed by Desimone et al. [176] is applied, the definition of the failure location is ambiguous, because at both locations the maximum mesoscopic shear stress takes similar values. In other words, the chain is likely to fail indistinctly at the crown or Kt. Considering the scatter that characterizes fatigue, the difference in the fatigue lifetimes predicted by both loci not significant. The fatigue lifetimes predicted by both loci can be viewed as two bounds of the fatigue lifetime. Fatigue testing of specimens of mooring chain steel accounting for corrosion with different R ratios, for example R= -1 and R=- 2, should be performed in order to modify more accurately the Dang Van locus for compressive hydrostatic stresses.

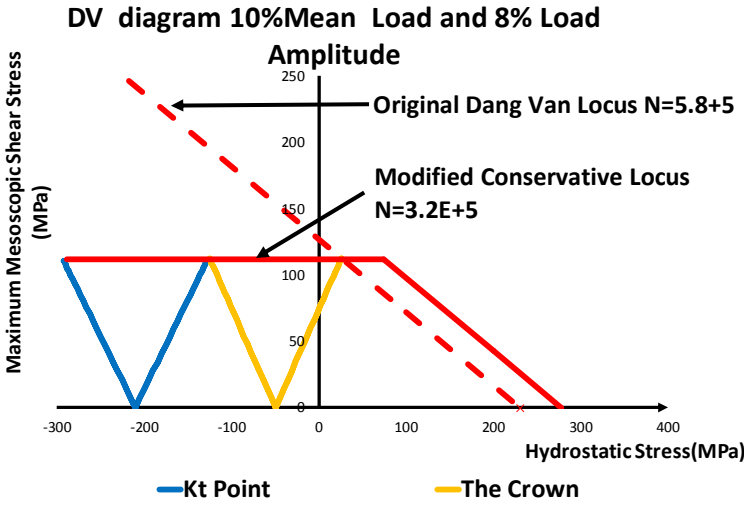

Figure 6.13 Comparison between the original Dang Van locus and the modified locus

6.5 Simplified Fatigue Assessment

In the previous section, the effect of mean load on the fatigue lifetime of mooring chain links has been illustrated by the cases investigated. On one hand, the methodology presented in the previous section is robust and accounts for complex phenomena such as residual stresses and multiaxiality of the stress tensor, among others. On the other hand, the methodology incurs significant computational cost which does not make it very appropriate for routine use in an industrial environment. This section presents a series of simplifications that can be applied to reduce the computational effort required to apply the Dang Van fatigue criterion. For example, a ratio between the fatigue lifetimes for two loading conditions with same load amplitude and different mean load has been derived using the geometrical properties of the Dan Van diagram. A simplified fatigue assessment method is then proposed and has been successfully implemented in an Excel Spreadsheet. Finally, the lifetimes predicted by the simplified method are compared against fatigue data from tests performed at TWI Ltd as part of a JIP.

6.5.1 Ratio between two fatigue loadings with the same load amplitude but different mean loads

A ratio relating directly the lifetimes of two loadings of different amplitudes is derived analytically. This ratio is based on the Dang Van fatigue criterion. Consequently, it accounts for multiaxiality of the stress tensor, unlike other mean load correction functions like Goodman or Gerber. The latter were obtained from uniaxial fatigue tests and are only applicable to uniaxial load cases.

Two load conditions are defined, *Loading 1* with a fatigue lifetime of N_1 cycles and *Loading 2* with the same load amplitude as *Loading 1* but with a higher positive mean stress. *Loading 2* has a fatigue lifetime of N_2 cycles. A higher mean stress has a negative effect in the fatigue lifetime, and so, *Loading 2* will have a shorter fatigue lifetime than *Loading 1* ($N_2<N_1$). This is equivalent to the effect of a tensile residual stress. Figure 6.12 presents a zoom in of the Dang Van paths for both loadings.

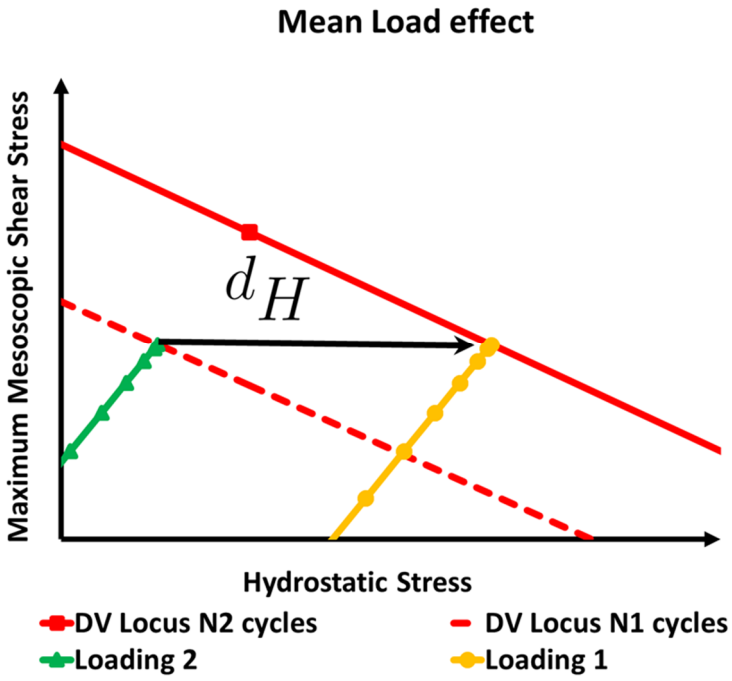

Figure 6.14 Zoom in of Dag Van paths for Loading 1 and Loading 2

We want to compute the ratio between N_1 and N_2 as a function of the translated distance d_H and a set of material properties **C**, such that:

$$N_2 = \rho \cdot N_1 \quad \rho = f(d_H, \mathbf{C}) \tag{6.14}$$

For a uniaxial stress state, stress amplitude and number of cycles to failure are related through the Basquin Equation. For example, as reported in DNV-RP-C203:

$$\log N = \log a - m \cdot \log \Delta\sigma \tag{6.15}$$

where:

N is the number of cycles to failure.

M is the negative inverse slope of the S-N curve.

A is the intercept of the design S-N curve with the log N axis

$\Delta\sigma$ Is the stress range

The Stress range can be replaced by the stress amplitude:

$$\sigma_a = \frac{\Delta\sigma}{2} \tag{6.16}$$

We can define ρ as a function of the fatigue strength for two different fatigue lifetimes, N_1 and N_2, as follows:

$$\rho = \frac{N_2}{N_1} = \left(\frac{\sigma_{N1}}{\sigma_{N2}}\right)^m \tag{6.17}$$

Let's recall the expression of the Dang Van Locus is given by:

$$\tau(t) = b - a \cdot \sigma_h(t) \tag{6.18}$$

The material parameters *a* and *b* are dependent of the alternated tension fatigue strength and alternated torsion fatigue strength, and can be defined as a function of *N*, the number of cycles:

$$b_N = a_N \cdot \frac{\sigma_N}{3} + \frac{\sigma_N}{2} \tag{6.19}$$

The assumption that a remains constant with the number of cycles has been made. This assumption is commonly made when applying Dang Van for finite fatigue life [78], [80], [18] and enables the translated distance between *Loading 1* and *Loading* to be written as:

$$d_H = \frac{b_{N2} - b_{N1}}{a} \tag{6.20}$$

Substituting for each fatigue lifetime Eq. (6.19) in Eq (6.20).

$$d_H = (\sigma_{N2} - \sigma_{N1}) \cdot \frac{2 \cdot a + 3}{6 \cdot a} \tag{6.21}$$

Rearranging Eq. (6.21) and combining it with Eq. (6.17):

$$d_H = (\rho^{-1/m} - 1) \cdot \sigma_{N1} \cdot \left(\frac{2 \cdot a + 3}{6 \cdot a}\right) \tag{6.22}$$

Rearranging Eq. (6.22) gives:

$$\rho = \left[\frac{\sigma_{N1} \cdot (2 \cdot a + 3)}{6 \cdot a \cdot d_H + \sigma_{N1} \cdot (2 \cdot a + 3)}\right]^m \tag{6.23}$$

The ratio depends on the fatigue strength in alternated tension for N_1 cycles, the translated distance d_H , and material constants. The value of the fatigue strength in alternated tension (R_{-1}) of R5 steel for pre-corroded specimens tested in air and specimens tested under sea water can be found in [32], [33], [150]. The value of a obtained from tests in air is 0.34 and obtained from pre-corroded specimens tested in air is 0.55 [18]. As said before, this parameter is an indicator of the sensitivity of the material to mean stresses, therefore it can be concluded that the material is more sensible to mean stresses in corroded conditions than in the absence of

corrosion. The value of *m* under corrosion recommended by both standards, API-RP2SK [9] and DNVGL-OS-E302 [8] is 3.

The translated distance d_H, measured in the Dang Van diagram, can be computed directly from elastic cyclic stresses if it is assumed that there is no residual stress relaxation between Loading 1 and Loading 2. For the loading cases studied previously (Load Amplitude of 8% MBL and a variation of the Mean Load of 10% MBL) at the locations reported in Figure 5.1, d_H takes the following values listed in Table 6.3.

Table 6.3: Translated distance in the Dang Van load path for Kt point and the crown

Location	d_H
The Crown	91.7 MPa
Kt Point	101.64 MPa

It is important to keep in mind that the ratio has to be computed for each location susceptible to fatigue damage. As a result, we obtain the corrected fatigue life for each location where fatigue failure is likely to occur; the final predicted fatigue lifetime for the whole component will be the lowest of the fatigue lifetimes at each of the critical locations. As already noted, in the case of mooring chains, the locations governing fatigue are the Kt point and the Crown.

As shown in Figure 6.15, for low mean loads, the hydrostatic stress due to the mean load at Kt and the crown are almost the same, with the difference increasing for high mean loads, reaching of 13 MPa at 20% MBL. This supports the conclusion presented in the previous section, the difference in the fatigue lifetime at the crown and Kt is due to residual stresses. Figure 6.15 can be used for computing d_H ; the graph has been obtained from elastic analysis.

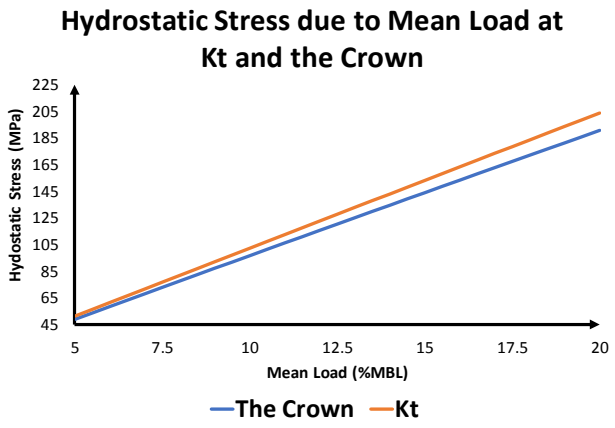

Figure 6.15 Hydrostatic stress due to mean Load at Kt and the crown

Figure 6.16 presents the mean load ratio, Eq. (6.23), plotted as a function of the translated distance (d_H) for different fatigue lifetimes. The plot reveals that the influence of mean load depends of the fatigue life time of Loading 1 (Note that Loading 1 is the loading with a lower mean load). For low fatigue lifetimes (1E+5), the relation between the translated distance (which is proportional to the variation of the mean load) is nearly linear, whereas for high fatigue lifetimes (1E+7) the relation is exponential.

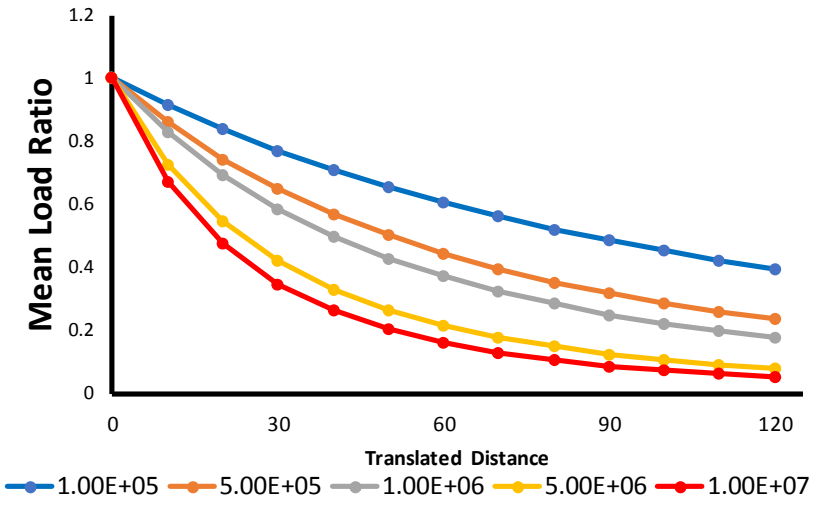

Figure 6.16 Mean load ratio for different fatigue lifetimes

6.5.2 Decoupling of Residual Stresses from Fatigue Analysis

The effect of residual stresses on fatigue life can be easily assessed using the Dang Van diagram by translating horizontally the Dang Van load path in the diagram. If residual stresses are tensile, they move the Dang Van load path towards the right, on the contrary, if they are compressive, they move the load path towards the left. Figure 6.17 reports the effect of compressive residual stresses at the crown, avoiding fatigue failure by shifting to the left the Dang Van load path.

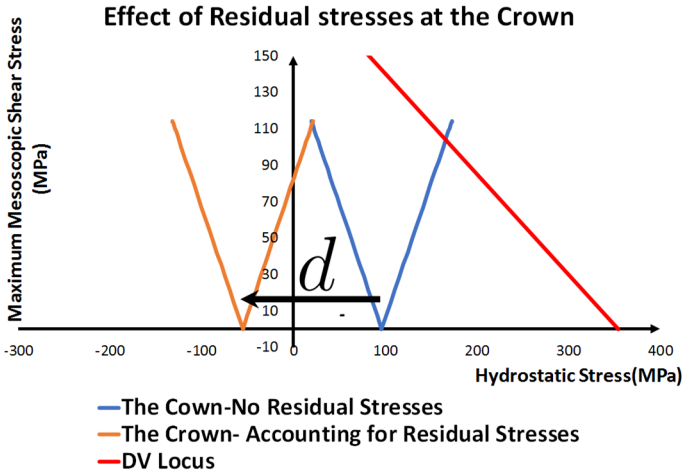

Figure 6.17 Effect of Residual Stresses

The translation magnitude *d* can easily be calculated analytically as follows. Let the residual stress tensor at a particular point be known, and defined as:

$$\boldsymbol{\sigma}_{Residual} = \begin{pmatrix} S11 & S12 & S13 \\ S21 & S22 & S23 \\ S31 & S32 & S33 \end{pmatrix} \tag{6.24}$$

Then, the magnitude *d* can be computed as:

$$d = \frac{1}{3} \cdot [S_{11} + S_{22} + S_{33}] = \frac{1}{3} \cdot trace[\boldsymbol{\sigma}_{Residual}] \tag{6.25}$$

If *d* takes a positive value, it will move the Dang Van path to the right, if it is negative, it will move the path towards the left. An important consequence of this property is that residual stresses can be decoupled from cyclic stresses and taken into account a posteriori in the fatigue analysis. Furthermore, if experimental measurements are available, they can be included in the fatigue study independently of cyclic stresses. Consequently, a residual stress prediction model would not be needed, only an analysis for computing cyclic stresses.

6.5.3 Computation of stresses due to service loading

Under nominal loading conditions, stresses in a mooring chain are elastic. For example, for the load case considered in this study, the stresses have been reported in Figure 6.2. Therefore, for computing cyclic stresses, only an elastic FEA model should suffice. Elastic analysis is less computationally expensive than elastic-plastic. Another advantage is that elastic material properties possess less uncertainty than elastic-plastic ones. Elastic properties are defined by Young's Modulus and the Poisson ratio.

Moreover, since cyclic stresses are elastic, the stress tensor at critical locations of the chain can be characterized with simple trigonometric functions, for example sines functions, which are defined by their mean and amplitude values. Therefore, for a given load cycle and at a particular location the stabilized cyclic stress tensor is defined by 12 parameters, 6 stress amplitudes and 6 mean stresses. Defining the external loading as:

$$\text{Mean Load}{=}c \cdot \%MBL \qquad \text{Load Amplitude}{=}d \cdot \%MBL \tag{6.26}$$

The stress tensor at a generic point *M* can be defined as:

$$\boldsymbol{\sigma}_M(c,d) = \begin{pmatrix} f_{S11}(c,d) & f_{S12}(c,d) & f_{S13}(c,d) \\ f_{S21}(c,d) & f_{S22}(c,d) & f_{S23}(c,d) \\ f_{S31}(c,d) & f_{S32}(c,d) & f_{S33}(c,d) \end{pmatrix} \tag{6.27}$$

where:

$$f_{Sij}(c,d) = A_{ij} \cdot \sin(wt) + B_{ij} \tag{6.28}$$

A_{ij} and B_{ij} are constants that depend on the point considered and on the loading conditions (Load Amplitude and Mean Load). Within the elastic regime, these parameters will depend linearly on the load conditions. A set of linear functions that relate the values of A_{ij} and B_{ij} to the load amplitude can be obtained from elastic FEA models. These functions that fit Eq. (6.27) can be introduced in a spread sheet, enabling computation of the cyclic stress response for any generic load conditions. For a given diameter, once these parameters have been computed, the stress cyclic stress tensor at the critical locations can be derived without employing FEA.

6.5.4 Simplified Fatigue Assessment of mooring chains under tension loading: Methodology

A simplified multiaxial approach is proposed based on the previous simplifications, Figure 6.18 present the workflow of the assessment method.

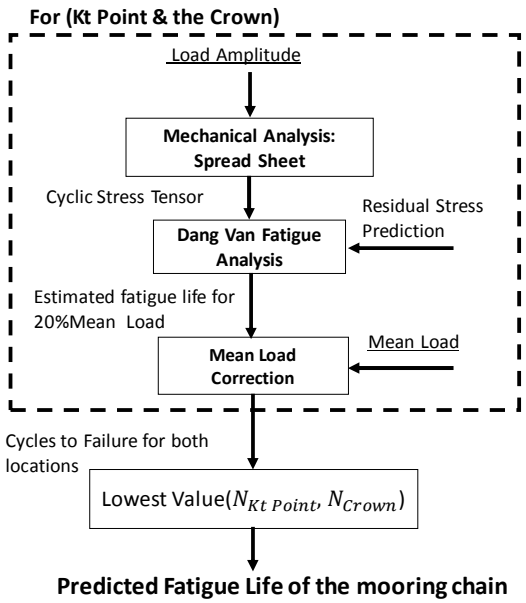

Figure 6.18 Workflow of the Simplified Fatigue assessment methodology

As noted previously, the fatigue assessment has two parts. The first involves obtaining the Dang Van load path from the stress tensor at a point of interest. The second is the prediction of the fatigue lifetime using the locus. If the modified Dang Van locus is implemented (for high compressive hydrostatic stresses), the first step of the simplified fatigue assessment remains unchanged. The Dang Van load path for a given mean load is derived by translating the load path corresponding to a mean load of 20% MBL a certain magnitude *d* (obtained from Figure 6.14). Finally, the fatigue lifetime is derived using the following expression:

$$N = \frac{a_{S-N}}{(2 \cdot \max[\tau(t)])^m} \tag{6.29}$$

where:

- *m* is the slope of the S-N curve (for mooring chain steel accounting for corrosion *m* takes a value of 3).

- a_{S-N} is the intercept of the log N-axis by S-N curve (the stress variation is defined as the stress amplitude)

Alternatively, if the original Dang Van locus is used, Eq. (6.23) is used to account for the effect of mean load.

6.5.5 Simplified fatigue assessment of mooring chains under tension loading: Implementation in an Excel Spreadsheet

The proposed simplified method described previously has been successfully implemented in an Excel Spreadsheet. This Software is simple, flexible and extensively used in industry. In addition, its cost is considerably lower compared to ABAQUS or MATLAB. However, its capabilities for performing complex calculations, such as matrix operations, are very poor because it is not intended to be used for numerical analysis. As part of the application of the Dang Van fatigue criterion, the maximum mesoscopic shear stress (Tresca stresss) has to be derived at every discretized time instant of the load cycle. The mesoscopic Tresca stress can be easily obtained by subtracting the maximum and minimum values of the principal stresses, derived from the eigenvalues of the stress tensor.

Microsoft Excel does not have a built-in function for calculating eigenvalues of a 3x3 matrix, unlike MATLAB, Sci-Py or other numerical analysis software. Nevertheless, Excel offers the possibility of writing custom functions using Visual Basic programming language. A numerical method for deriving the eigenvalues of a 3x3 matrix has been programmed. Especial attention has been paid to choosing the most appropriate method, which should be numerically robust and efficient in terms of computational time.

The problem to be solved is to compute the eigenvalues of a symmetric low dimension matrix (3x3). The eigenvalues of a given matrix **A** are defined as the solution of the following equation:

$$| \mathbf{A} - \lambda \mathbf{I} | = 0 \tag{6.30}$$

The strict definition of the problem consists of finding the roots of a n^{th} degree polynomial, where n is the dimension of the matrix. Although it is straightforward, root searching is not a

very good computational method [121]. A complete review of the different numerical methods available for solving this problem falls out of the scope of this section; here only the method chosen is briefly outlined, and more information can be found in [121], [182], [183]. Taking advantage of the fact that the matrix is symmetric, an efficient method is to perform iteratively QR decompositions [184], [185]. The QR decomposition derives a sequence of matrixes $\mathbf{A}_k$ that converge to a diagonal matrix similar to **A**. The eigenvalues are the elements in the diagonal of $\mathbf{A}_k$. The QR decomposition factorizes the matrix A, such that:

$$\mathbf{A} = \mathbf{Q} \cdot \mathbf{R} \tag{6.31}$$

where:

Q is an orthogonal matrix

R is an upper triangular matrix

The iterative process is as follows:

Initialization: $$\mathbf{A}_0 = \mathbf{A} \tag{6.32}$$

QR factorization: $$\mathbf{A}_k = \mathbf{Q}_k \cdot \mathbf{R}_k \tag{6.33}$$

Reverse product: $$\mathbf{A}_{k+1} = \mathbf{R}_k \cdot \mathbf{Q}_k \tag{6.34}$$

The process [Eq. (6.33) and Eq. (6.34)] is repeated until $\mathbf{A}_k$ is a diagonal matrix; that is, all the elements of the matrix outside the diagonal are smaller than a specified tolerance. Two modifications have been implemented to improve the convergence rate and reduce the computational effort of the QR factorization [182]. The first is to transform matrix **A** into a

tridiagonal form using Householder [186] decomposition prior to QR factorization. The second is to accelerate the convergence rate of QR factorization by introducing shifts [183]. Overall the algorithm programmed in Visual Basic, has two steps:

1- Householder reduction of the stress tensor into a tridiagonal matrix

2- QR decomposition introducing shifts for accelerating the convergence rate

A complete description of this method for deriving eigenvalues of a symmetric matrix can be found in [183]. It is important to keep in mind that this method is especially efficient for symmetric matrixes, which is always the case in our problem.

6.6 Quantitative Validation: Comparison with Experimental results

The final step towards an industrial application of the simplified assessment method is its validation with experimental data. As part of a Joint Industry Project (JIP) led by TWI Ltd, fatigue testing of mooring chains under saline solution flow has been performed. The fatigue results have been compared with the predicted fatigue lifetimes by the simplified fatigue assessment implemented in an Excel Spreadsheet.

A 127mm R5 chain has been tested at different mean loads and load amplitudes ranging between 3.75% MBL and 8% MBL. In the JIP, full-scale fatigue testing of mooring chains was carried out in air and 3.5% NaCl solution under tension-tension loading, at loading frequencies between 0.2-0.5 Hz at a temperature around 10°C. Each chain segment was composed of seven links. Once a link failed, it was replaced with a Kenter link to continue the tests until three link failures in each segment had been achieved. Most tests were achieved at a mean stress equal to 20% MBL, and one test at 10% MBL.

Fatigue lifetimes predicted by the computational fatigue assessment have been compared with experimental results. Fatigue testing was performed at two different mean loads, 20% MBL and 10% MBL.

Mean load 20% MBL

Different load amplitudes have been tested at a 20% MBL mean load. In total 48 tests were carried out for this mean load value. The difference between the logarithmic values of the lifetimes is presented as a histogram in Figure 6.19. The distribution of the error has been fitted to a normal distribution. The mean value of this distribution is 0.05 whereas the standard deviation is 0.13. Consequently, on average Dang Van fatigue criterion tends to predict fatigue lifetimes that are 1,12 times lower (therefore conservative) than the experimental fatigue results. Moreover, a small standard deviation indicates that the estimation error tends to be concentrated near the mean value.

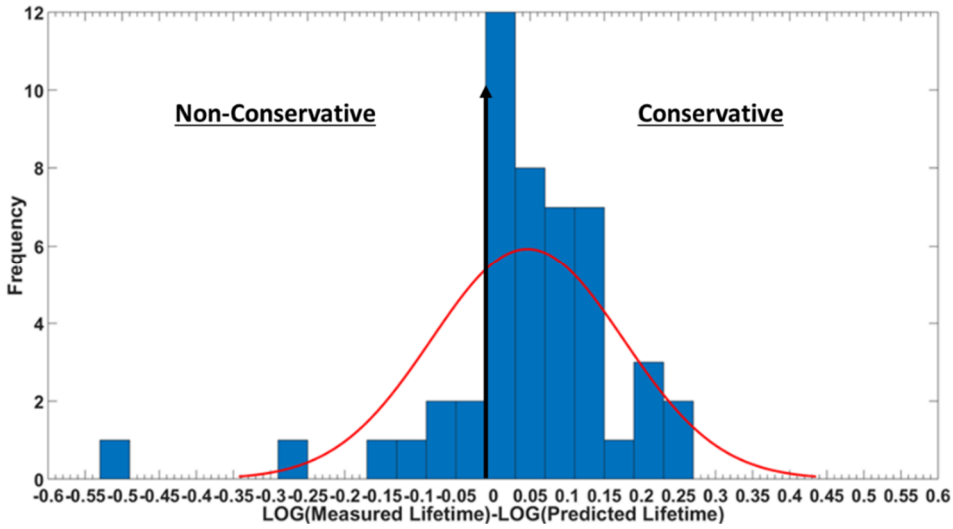

Figure 6.19 Histogram of the Dang Van Prediction for a 127mm R5 chain link under a 20%MBL mean load

Mean load 10%MBL

A single fatigue test at low mean load was performed. The Modified Conservative Locus proposed by Desimone et al. [176] matched better with the experimental result, with the difference in logarithms of the predicted and measured fatigue lifetime being less than 0.075. Nevertheless, this is not sufficient to validate the Modified Conservative Locus proposed by

Desimone et al. [176]. In addition, fatigue testing of small specimens with compressive mean stress should be carried out to define the Dang Van locus in the high compressive hydrostatic stress region.

6.7 Chapter Summary

This chapter has presented a computational fatigue assessment method of mooring chains accounting for residual stresses created during the manufacturing process. In addition, the chapter has addressed the question as to whether mean load should be considered when studying the fatigue performance of mooring chains. By applying the computational fatigue assessment, for a 127mm R5 chain, it has been demonstrated that increasing the mean load from 10% MBL to 20% MBL reduces the fatigue life by a factor ranging between 1.5 and 2.6. The factor depends on which definition of the Dang Van locus is used for the assessment of the 10% MBL mean load case. If the traditional Dang Van locus is implemented, the ratio between fatigue lifetimes is 2.6; whereas if the modified Dang Van locus is used, the ratio becomes 1.5. Although the modified Dang Van locus might be over-conservative, it is more accurate for low mean loads than the original locus. It is worth noting that for the load case where mean load is 20% MBL, the original Dang Van locus should be used. Its accuracy has been proved by comparing the predicted lifetimes with 48 fatigue tests.

A common drawback of the applied methodology is that it is computationally expensive and time consuming. To overcome this, a simplified assessment method based on the Dang Van fatigue criterion is proposed. This method has successfully been implemented in an Excel Spreadsheet.

Apart from the ease of implementation, the proposed method has several advantages. Although it needs to be calibrated for each chain diameter, it is valid for several steel grades, since cyclic

stresses depend exclusively on elastic properties. Another important feature is that this method, which is composed of two steps, a mechanical and a fatigue analysis, identifies the main sources of uncertainty of each of them. The mechanical analysis has two parts: cyclic stress computation, and residual stress prediction. The main source of uncertainty comes from residual stress prediction, which should account for heat treatment and proof loading. The proposed methodology enables residual stresses to be taken into account a posteriori, and if experimental measurements are available, they can be introduced directly in the fatigue analysis. In the fatigue study, the main source of uncertainty arises from the calibration of the criteria with material properties rather than the method itself, as shown in Table 6.2.

Future work should involve a better understanding of the role of compressive mean stresses in the fatigue performance under corrosion conditions. Experimental validation of the modified Dang Van locus proposed by Desimone et al. [176] should be carried out. Combined with fatigue data obtained from small specimens tested under sea water flow at low frequencies, the accuracy of the fatigue predictions using Dang Van fatigue criteria would improve significantly.

Chapter 7: Fatigue Assessment of mooring chains working under twisted conditions

The previous chapter presented a computational fatigue assessment of mooring chains under tension loading. In this chapter, the same methodology is employed to study fatigue behaviour under another loading mode, tension loading in a twisted configuration (also known as twist).

7.1 Introduction

Twisting may occur during the installation of a chain or during service due to torque generated in the near-by elements of the mooring (for example wire cables). During installation, effort is made to avoid twisting a chain, nevertheless marginal twist is inevitable (around two or five degrees per link). To the author's knowledge, this loading mode has not caught the attention of industry, with the exception of studies analyzing the torsional response of chains [21]–[23] and fatigue testing of small-scale chains working in twisted conditions [19]. The opinion from different chain operators consulted, is that installation is the most frequent source of twisting compared to twist generated by torque in near-by elements. Fatigue of mooring chains working in twisted conditions is not addressed by current standards. Nevertheless, DNV-OS-E301 [3] recommends to avoid twist and limits the twist angle to 5 degrees. However, as will be shown in this chapter, this recommendation might not be sufficient.

The assessment method has already been presented in the previous chapter (see Chapter 6). Note that is based on a two step analysis: a mechanical and a fatigue analysis. The mechanical analysis accounts for the initial residual stress state of the chain after manufacturing. The result

is the stabilized cycle of the multiaxial stress field which is obtained through elastic-plastic three-dimensional Finite Element Analysis (FEA). Then, the fatigue analysis is performed to determine the lifetime. The mechanical analysis has shown that the stabilized cycle of mooring chains under twist is of an elastic shakedown. Consequently, the Dang Van Fatigue Criterion [21] has been chosen for the fatigue analysis. Moreover, in the previous chapter, the fatigue lifetimes predicted by this criterion have shown good agreement with experimental results.

For the research reported in this chapter, three different chain diameters have been considered, 162 mm, 127 mm and 114 mm, all of them R4 grade. These diameters are representative of big and medium size chains used by the industry. Initially, the aim was to determine whether there is a scale effect in the influence of twists on fatigue performance. The first two diameters (162mm and 127 mm) have been twisted an angle of 5 degrees and have been applied with a service loading characterized by mean load and load amplitude of 15% MBL and 5% MBL respectively. While working on this chapter, the author was shown a picture of a chain recovered from field in the North Sea after more than 15 years in service. This picture (Courtesy of Equinor, former Statoil. See Figure 7.8) showed a chain link with fatigue cracks at the same locations predicted by Dang Van fatigue criterion when the chain is working twisted. This finding motivated a more in-depth analysis of the phenomenon. The chapter ends with a more detailed fatigue analysis of this chain, moreover, a small sensitivity analysis is carried out to investigate the effect of twist angle, mean load and load amplitude.

Overall, this chapter shows how the computational methodology developed in Chapter 6 can be adopted for different loading modes. This is especially interesting for loading modes that are not currently covered in the standards (DNV-OS-E301 [8] and API-RP-2SK [9]).

7.2 Mechanical Analysis

The mechanical analysis comprises two different parts: residual stress prediction (accounting for all the relevant stages of the manufacturing process) and service loading. The first analysis has already been described in detail in Chapter 5. Consequently, only the second part is discussed here.

The FEA model employed for studying the mechanical response of the chain when subjected to twist presents similarities with the model that simulates tensile loading (presented in Chapter 5 and Chapter 6). Both have the same geometry and have been meshed with the same type of elements, 3D solid quadratic elements with reduced integration (C3D20R). These elements capture stress concentrations better and are more accurate than linear elements when subjected to bending. Furthermore, in both models the mechanical behaviour has been represented using the same constitutive law, which has already been illustrated in the previous chapter (see Chapter 6, Section 6.2.1) and accounts for combined non-linear hardening. Moreover, both models share the same contact formulation.

Figure 7.1 presents the geometry mesh and boundary conditions of the FEA model that studies the mechanical response of the chain under twist.

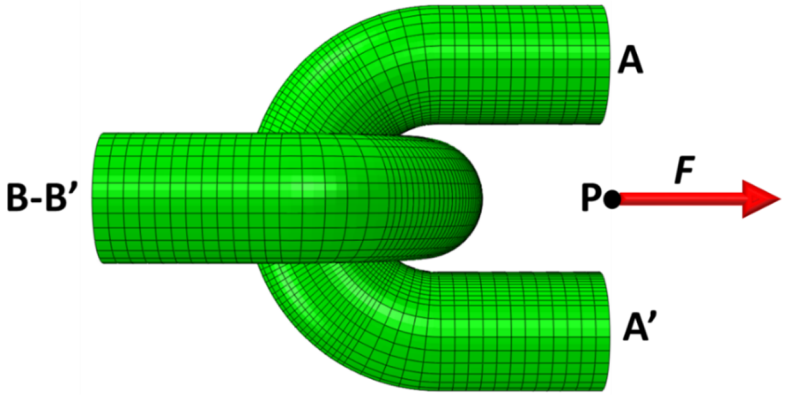

Figure 7.1 Geometry and boundary conditions of the FEA model

The boundary conditions are the following:

- Sections B-B': Symmetry boundary conditions.

- Sections A-A' are coupled with the reference point *P* using ABAQUS option "Continuum distributed coupling". The coupling is enforced in an average sense. The degrees of freedom of the nodes of Sections A-A' are constrained such that the resultant of the force and momentum are equivalent to the forces and momentums at the reference point *P*. The displacements of this point are restrained in all the directions except that of the applied load *F*. The chain is twisted by applying a rotation at point *P*.

The simulation comprises the following steps:

Step 1: Initial Step: The residual stress values after heat treatment are imported.

Step 2: Proof load is applied

Step 3: Proof load is removed. The final residual stress distribution after manufacturing is derived in this step

Step 4: Twist of the chain links without external loading (As displayed in Figure 7.2)

Step 5: Service loading is applied under twisted conditions.

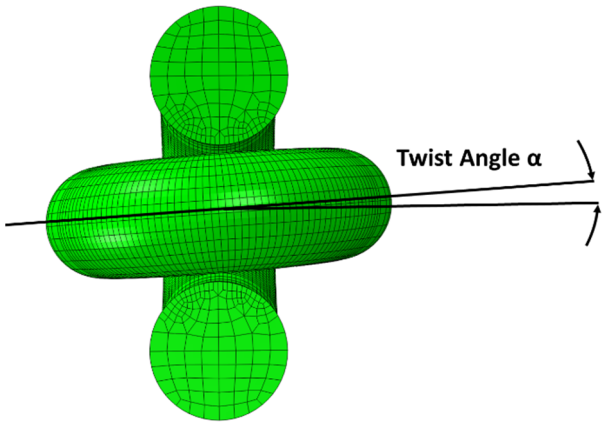

Figure 7.2 Chain in twisted condition

Results

A key difference between tension and twisting loading modes is the contact between chain links. Figure 7.3 presents contact stresses for the tension and twist loading modes due to the mean component of the cyclic loading. It is important to remind that proof loading causes significant yielding in the contact zone, and therefore leaves high residual stresses. Due to the plastic deformation of the contact zone remaining after proof loading, in the case of twisting, two separated regions define the contact between chain links.

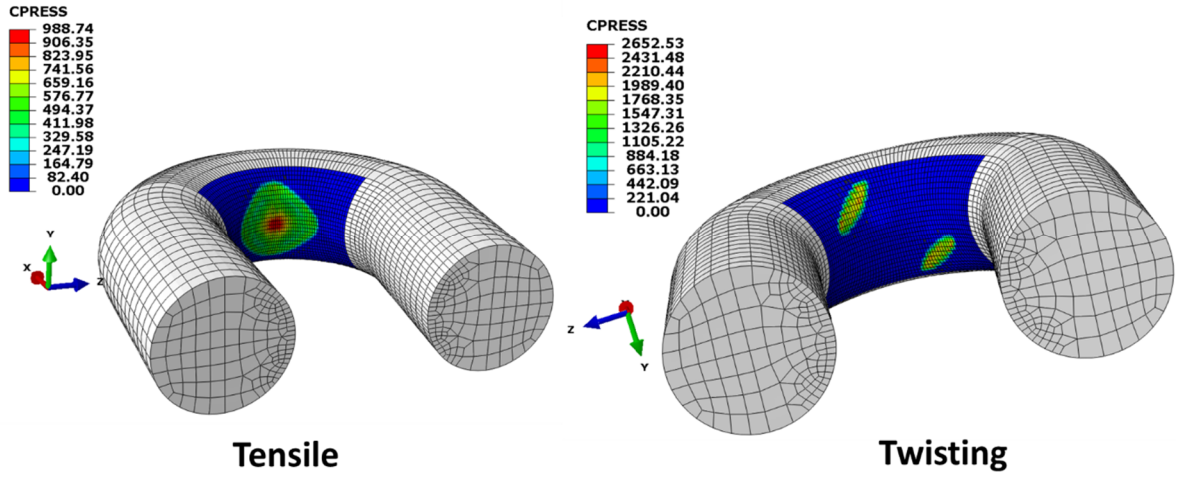

Figure 7.3 Contact Stresses of tensile and twisting loading modes

Figure 7.4 highlights that a stabilized state of elastic shakedown is attained, which justifies the implementation of the Dang Van fatigue criterion.

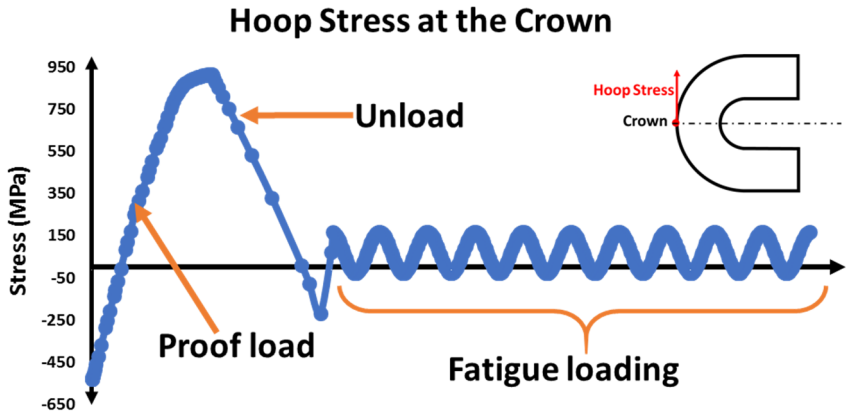

Figure 7.4 Evolution of the stress at the hoop direction at the crown

7.3 Fatigue Analysis

As before, the fatigue analysis has been performed by implementing the Dang Van criterion at nodes susceptible to fatigue failure. The fatigue failure location is not known a priori, therefore the fatigue criterion has to be applied at all nodes on the surface of the chain links. In order to carry out this operation in reduced computational time, BFGS optimization method was used for implementing the Dang Van fatigue criterion. Note that this method was found to perform best in terms of computational time when applying the criterion (for further details, see Chapter 3). A damage indicator has been computed [Eq. (6.11)] at every node for locating the fatigue hot spots (i.e the locations where fatigue cracks are predicted to initiate).

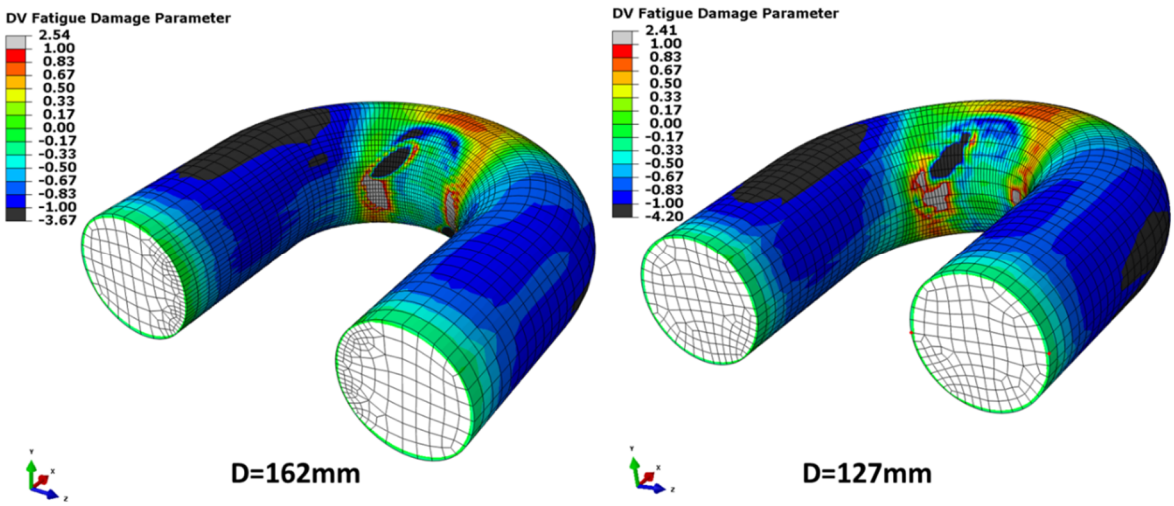

Figure 7.5 Contour plot of the Dang Van fatigue damage parameter for both diameters, D=162mm and D=127mm

Figure 7.5 displays the contour plot of the Dang Van Fatigue damage parameter (defined by Eq. (6.11)). If the damage parameter takes a value bigger than unity, fatigue cracks are predicted to initiate. For both diameters, D=162mm and D=217mm, fatigue failure is predicted at the boundary of the contact zone between chain links. There is not a significant difference between the damage parameter predicted for both diameters. A zoom in at the contact surface between chain links is illustrated in Figure 7.6 which confirms that fatigue cracks are predicted to initiate at a region starting at the boundary of the contact surface between chain links in

twisted conditions. In addition, another critical location is located midway between the intrados and extrados of the link's axis, however fatigue cracks are not predicted to initiate.

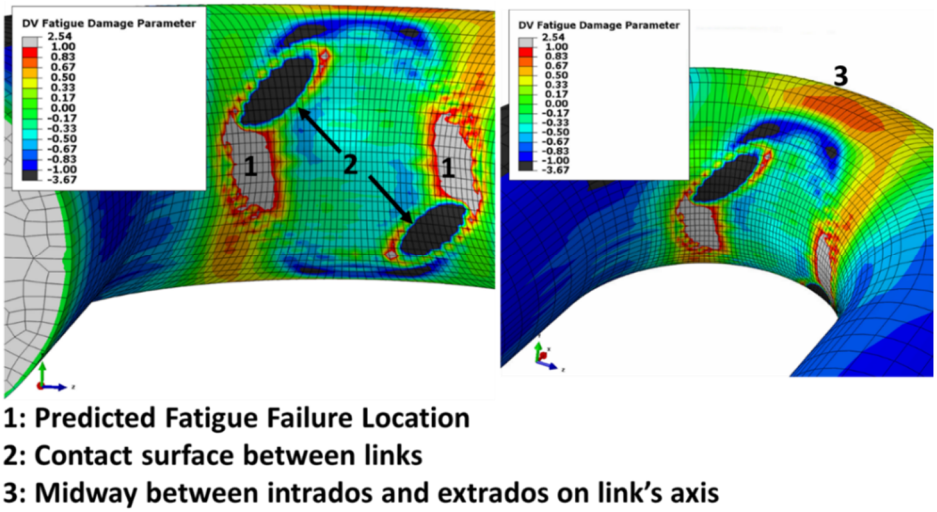

Figure 7.6 Zoom in of the contact surface between links (D=162mm)

Figure 7.7 displays the stress tensor at different locations surrounding the contact zone and where fatigue cracks are expected to appear (denoted as Point 1 in Figure 7.6). At all points considered the stress tensor is multiaxial, which justifies the use of a multiaxial fatigue criterion.

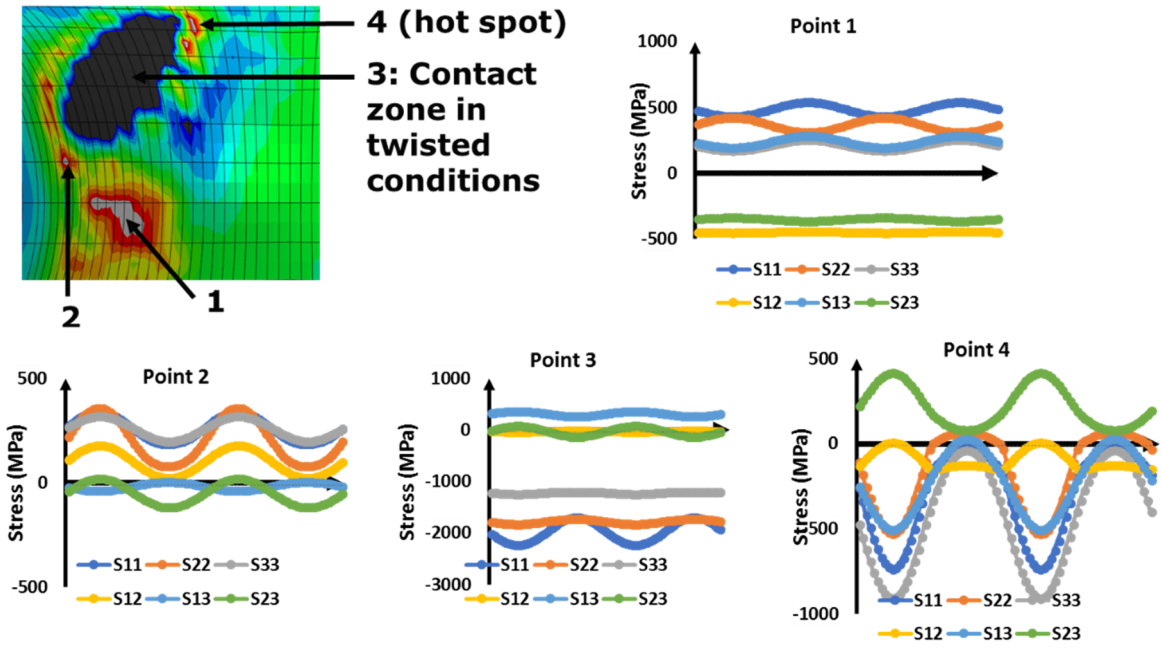

Figure 7.7 Stabilized stress tensor at different locations

Figure 7.8 present the paths on the Dang Van diagram of the points defined in Figure 7.7. Fatigue cracks are predicted to initiate at Points 1, 2 and 4. Moreover, as already said in the previous chapter, the Dang Van locus should be modified in both the high tensile and high compressive hydrostatic stress regions.

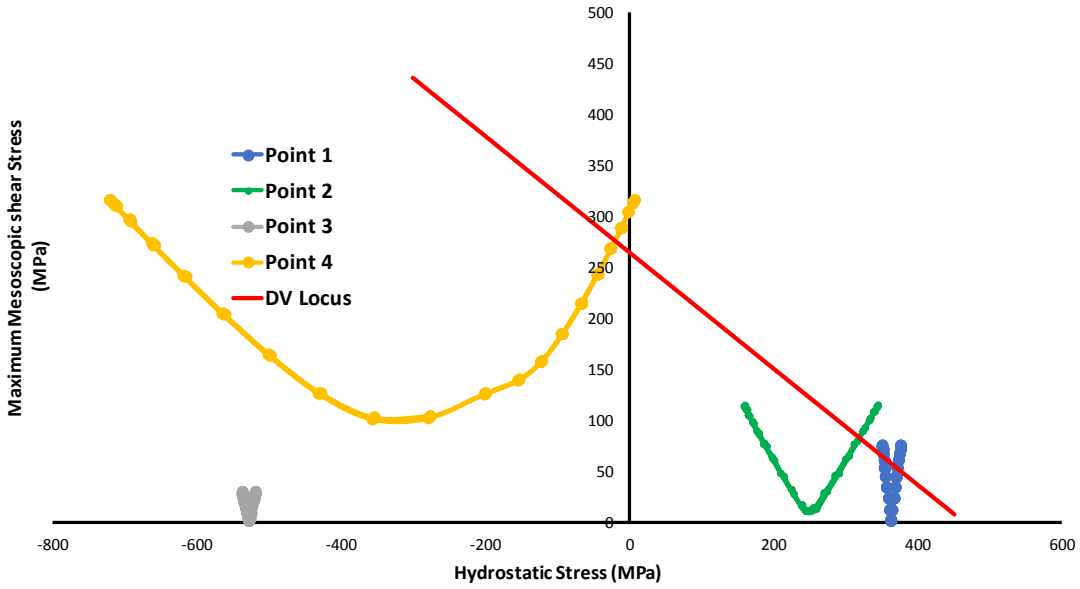

Figure 7.8 Paths in the Dang Van diagram of Points 1,2,3 and 4

7.4 Fatigue Analysis: Case Study of chain link recovered from the North Sea

Previously, it has been concluded that if the chain link works in twisted conditions, fatigue cracks are expected to initiate near the contact region, distributed symmetrically with respect to the axis link (as shown in Figure 7.6) and symmetrically with respect to the mid plane of the links. These predictions are in agreement with several chain links recovered from the North Sea after more than 15 years in service. The recovered chain link displayed in Figure 7.9 presents a number of parallel cracks at the same location predicted by the application of Dang Van fatigue criterion (Figure 7.6). The mechanism responsible for the appearance of these cracks was unknown; moreover, these chain links were not monitored, and so their loading conditions can only be estimated. The photograph has been kindly provided by Equinor (former Statoil). The measured distance between the centre of the chain and the fatigue cracks shows

good agreement with the distance at which the cracks are predicted by the computational fatigue assessment.

This finding has motivated a more in-depth analysis (for a 114 mm diameter R4 chain) of the effect of twist on the fatigue behaviour of mooring chains. First, a sensitivity analysis has been carried out to identify individually the effect the mean load, load amplitude, and twist angle. The Dang Van fatigue criterion predicts crack initiation; however, once these cracks have initiated, they do not propagate until failure. The second part answers the question as to why once these cracks have initiated, they do not propagate (or propagate very slowly).

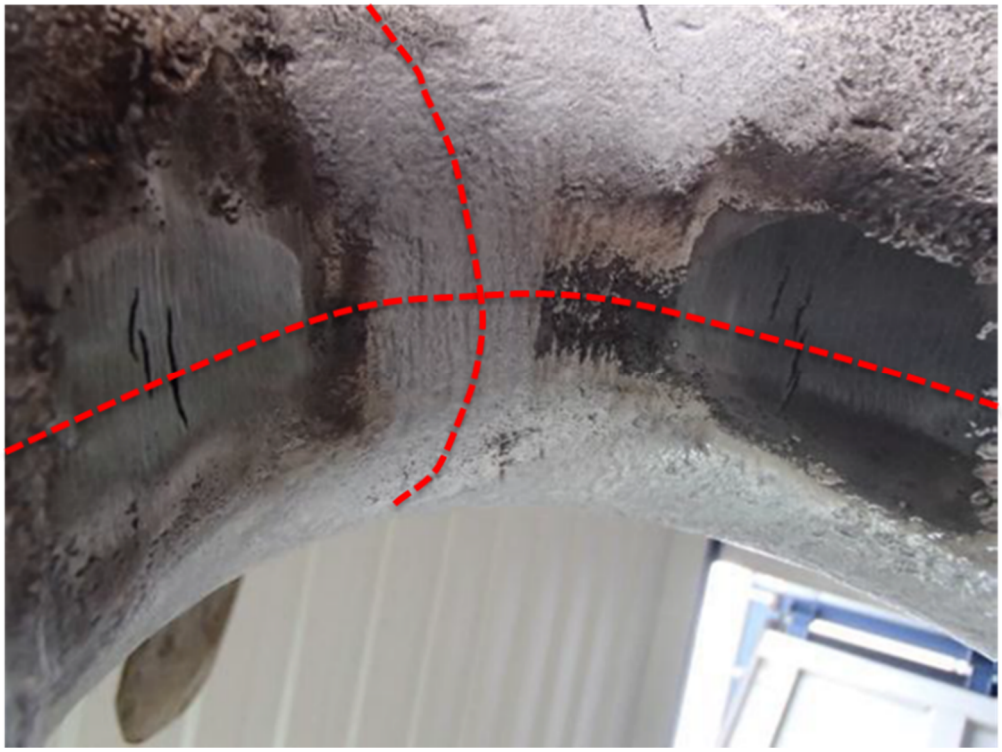

Figure 7.9 Fatigue cracks found at a recovered chain link. Courtesy of Equinor

7.5 Sensitivity analysis: Twist angle, mean load, and load amplitude

7.5.1 Twist Angle

For a given load condition (15% MBL mean load and 5%MBL load amplitude), three different twist angles have been studied, 5, 10 and 15 degrees. Figure 7.10 displays a contour plot of the Dang Van fatigue damage parameter corresponding to these cases. The contour plot shows that even though the maximum value of the damage parameter takes higher values for lower angles, in all cases, fatigue cracks are predicted to initiate. Furthermore, for all angles considered, the location of the fatigue cracks is the same, the only difference is the size of the zone where they are predicted.

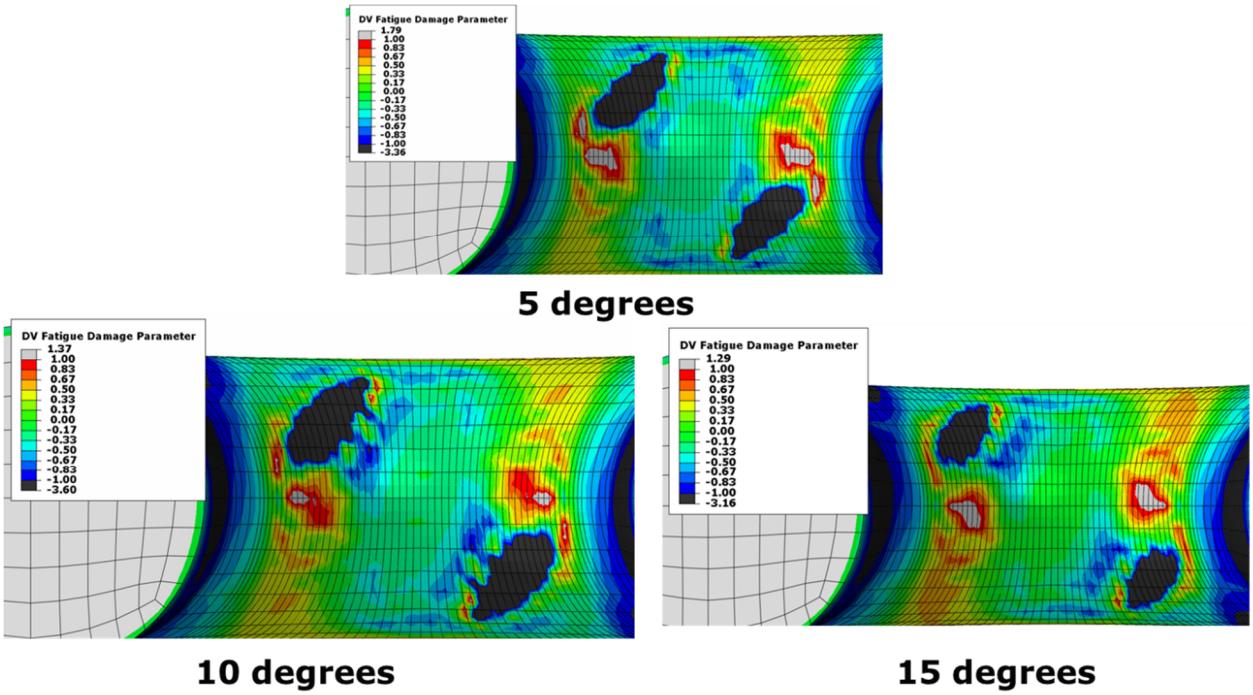

Figure 7.10 Effect of twist angle in the fatigue performance (D=114 mm, 15% MBL mean load and 5%MBL load amplitude)

7.5.2 Mean load

Generally, an increase in mean load has a negative effect on the fatigue lifetime. Figure 7.11 reports the contour plots of the Dang Van fatigue parameter for two different mean loads, 15 %MBL and 20% MBL respectively. No significant difference can be found between both mean loads. As expected, the contact zone is slightly bigger for the higher mean load.

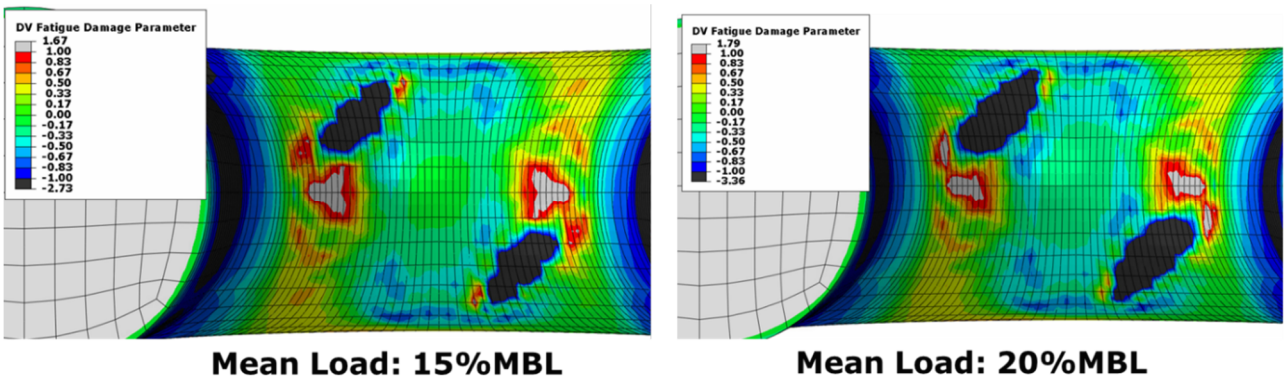

Figure 7.11 Dang Van fatigue damage parameter (D=114 mm, Twist angle= 10 degrees and 5%MBL load amplitude)

Load amplitude

From all the parameters studied in this sensitivity analysis, the load amplitude has been found to have greatest influence. Figure 7.12 shows contour plots of the Dang Van damage parameter for two different load amplitudes, 10 % MBL and 5 % MBL, respectively. For the higher load amplitude (10 % MBL), the maximum value of the damage parameter and the zone where fatigue cracks are predicted to initiate are significantly bigger than for the lower load amplitude (5 % MBL).

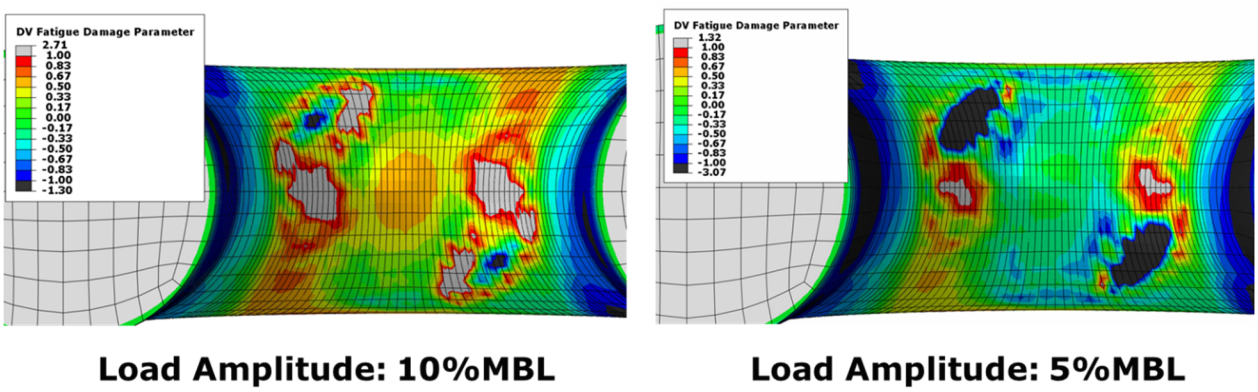

Figure 7.12 Dang Van fatigue damage parameter (D=114 mm, Twist angle= 10 degrees and 15%MBL mean load)

7.6 Propagation of fatigue cracks

The Dang Van fatigue criterion is based on crack initiation. In the High Cycle Fatigue regime, when fatigue cracks do not start from a macroscopic defect, more than 80% of the fatigue lifetime is spent on crack initiation [91]. This has been proven experimentally for mooring chain steel tested under sea water flow [33], [150].

The computational fatigue assessment implementing Dang Van fatigue criterion has been able to explain why fatigue cracks can appear at the boundary of the contact zone when the chain is working in twisted conditions. The next question that is worth to be asking is why these cracks do not propagate. It is important to remind that the mechanisms that drive crack initiation are different from crack propagation; in the first stage shear stress amplitude plays a primary role, whereas in the second stage, maximum normal stress has a great influence. The first stage is more sensitive to surface conditions, whereas the second stage is not.

Figure 7.13 highlights that the damage parameter is greater than unity only at the surface, becoming lower than unity a couple of millimeters away from the surface.

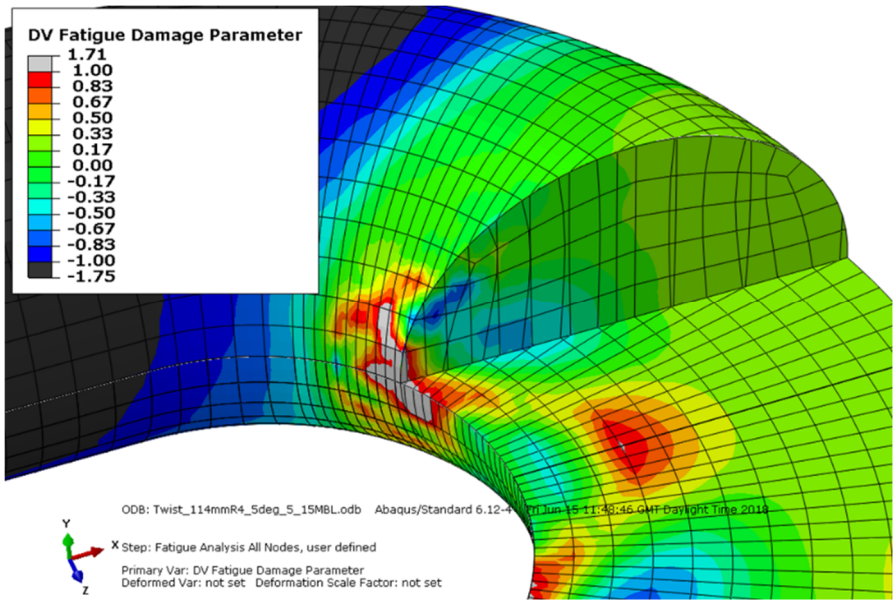

Figure 7.13 Contour plot of the Dang Van damage parameter (D=114, Twist angle= 5 degrees, 15%MBL mean load and 10%MBL load amplitude)

To perform a complete fracture mechanics study about the cracks that initiate when the chain is working in twisted conditions is beyond the scope of this research. Instead, some basic qualitative study has been done. The maximum and mean values of the stress component perpendicular to the propagation direction during the load cycle have been studied.

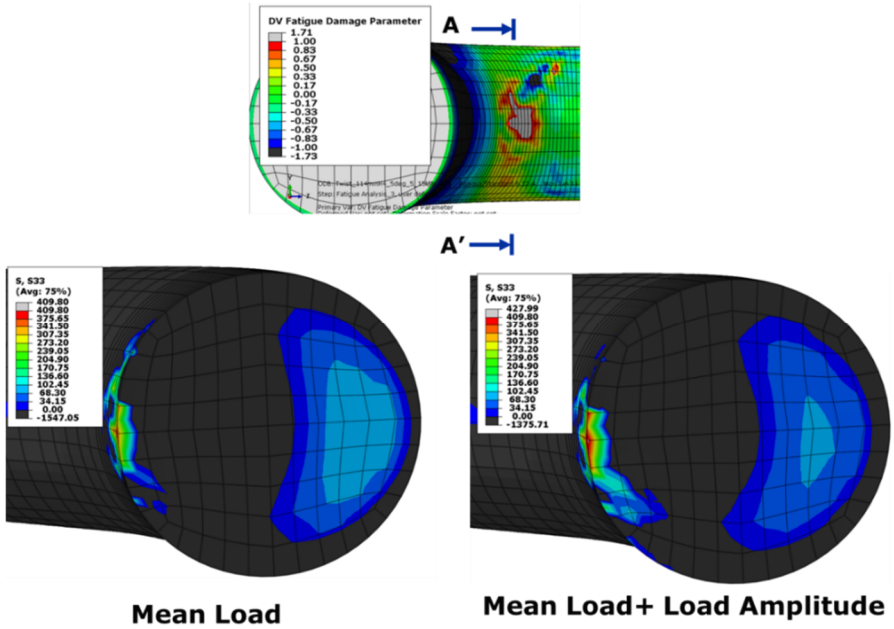

Figure 7.14 Contour plot of the stress component perpendicular to the propagation direction at section A-A' (D=114, Twist angle= 5 degrees, 15%MBL mean load and 10%MBL load amplitude)

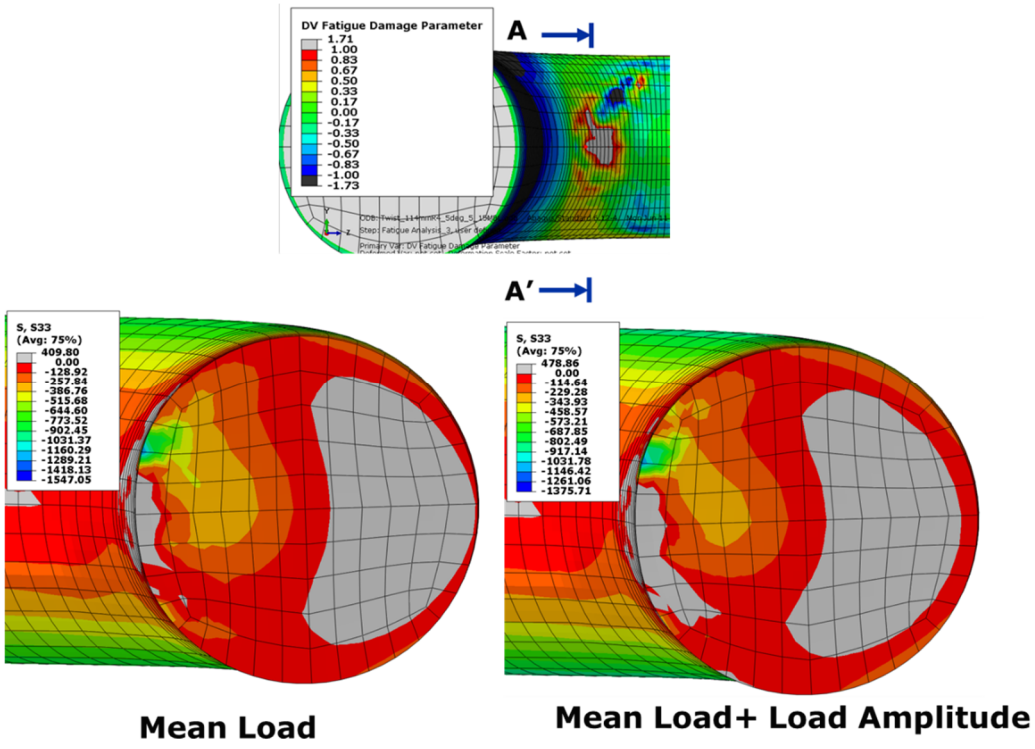

Figure 7.15 Contour plot of the stress component perpendicular to the propagation direction at Section A-A' (D=114, Twist angle= 5 degrees, 15%MBL mean load and 10%MBL load amplitude)

Figure 7.14 and Figure 7.15 show contour plots of the stress component perpendicular to the propagation direction at the section where fatigue cracks are predicted to initiate (Section A-A'). Both figures display the same magnitude but with different color codes. The stress values are the superposition of residual stresses (accounting for heat treatment and proof loading) and stresses from service loading. Figure 7.14 highlights that the stress component perpendicular to the propagation direction at section A-A' becomes compressive about 10 mm away from the surface into the core. Figure 7.15 indicates that there is a fast transition from the location where the stresses are zero (at 10mm approximately) to compressive stresses. In less than 15 mm, the stress varies from 0 to -300 MPa.

A high compressive stress acting perpendicular to a crack will delay or even stop completely crack propagation. The stress distributions displayed in Figure 7.14 and Figure 7.15 give a qualitative answer as to why, once initiated, fatigue cracks do not propagate further. Moreover, this is in agreement with observations; the fatigue cracks measured in recovered chains were

found to be shallow, of about 6 mm depth. Compressive residual stresses remaining after heat treatment are primarily responsible for this stress distribution which delays significantly crack propagation.

7.7 Chapter Summary

This chapter has demonstrated how the computational fatigue assessment method developed during the present doctoral research can be applied to loading configurations not currently covered in the Standards. A computational fatigue assessment of chains working in twisted condition has been presented. The predicted fatigue failure locations have been identified by applying the Dang Van fatigue criterion at all surface nodes. These locations are at the boundary of the contact surface between chain links. The predicted fatigue failure locations have exhibited good agreement with chain links recovered from the field after more than 15 years in service. The chain operator was aware of these cracks; however, their origin was unknown.

First, two chain sizes (127mm and 162mm) have been analyzed, both of them twisted at an angle of 5 degrees and an external loading defined as percentage of MBL. Surprisingly both chains had very similar fatigue performance. Nevertheless, this can be explained by analyzing residual stresses. Heat treatment leaves behind more compressive residual stresses distributed homogenously along the surface for bigger chains (As already shown in Chapter 5). These residual stresses are superposed with residual stresses from proof loading. As a result, the big chain (D=162 mm) presents more compressive residual stresses at the failure location than the smaller one (D=127 mm).

Second, for the diameter of the chain recovered from field, a sensitivity analysis has been carried out to determine the variable which has most influence. Load amplitude was found to have greatest impact on the fatigue performance of chains working in twisted conditions. Twist

angle and mean load play an important role. However, for the values studied, a variation in these values did not change significantly the fatigue behaviour. A more detailed sensitivity study should be carried out to assess the effect of each variable.

Finally, all the links recovered from the field showed fatigue cracks at similar locations; however, these cracks did not propagate until final failure. By studying the stress distribution at the section containing the cracks, it has been shown that stresses become highly compressive several of millimeters away from the surface into the core. This distribution is partly due to the residual stresses that remain after heat treatment and explains qualitatively why the propagation of these cracks has been significantly delayed or even stopped.

Chapter 8 Conclusions and Recommendations

The aim of this thesis is to propose a robust and comprehensive fatigue design method for lifetime prediction of mooring chains. The design method includes the combine effect of mean load and residual stresses. Residual stresses have been predicted accounting for all the relevant manufacturing stages, and not only the last one. The originality of the thesis lies essentially in adapting and interpreting classical notions, models and techniques in order to obtain a reliable fatigue prediction for mooring chains. This thesis proposes a computational fatigue assessment methodology of mooring chains applying the Dang Van fatigue criterion. The generality of the proposed method permits an analysis of different loading conditions, such as tension loading, twist and OPB. The first two have been studied in this thesis. The computational fatigue assessment is composed of two steps:

(i) A mechanical analysis based on the knowledge of the geometry, the constitutive law, the boundary conditions, the manufacturing process and the service loading, which will provide the cyclic response of the structure in terms of strain and stress.

(ii) A fatigue analysis based on the study of the stress-strain response computed before in each geometric point of the structure and the assessment of the local elastic or plastic shakedown state or a ratcheting state and the application of an appropriate lifetime criterion.

This thesis also studies different numerical methods that enable to implement Dang Van fatigue criterion and critical plane methods in reduced computational time. This is of special relevance for complex structural members whose fatigue failure location is not known beforehand. In such cases, the fatigue criterion must be applied at all the nodes of the surface.

8.1 Conclusions

8.1.1 Numerical Methods for fast fatigue analysis

Optimization is a common operation when applying Dang Van fatigue criterion or critical plane methods. Different numerical methods have been revisited at each of the stages of fatigue analysis that involve optimization. The aim has been to apply multiaxial fatigue criteria (i.e. Dang Van fatigue criterion, critical plane methods) in reduced computational time. A novel strategy for locating the critical plane has been proposed. Preference has been given to methods that have proven their robustness and performance in other applications. Comparison studies have been carried out to determine which of the methods is more efficient, and a series of improvements were proposed to enhance precision and speed up computation. For applying Dang Van fatigue criterion, BFGS optimization method implemented along Weak Wolfe Conditions (For example HANSO MATLAB Code [140], available in [129]) has been found to be the most performant method for deriving the change of scale expression [Eq. (4.1)]. This numerical method (BFGS) outperformed the other methods for computing shear stress amplitude with the minmax expression [Eq. (4.17)]. The effectiveness of BFGS has been illustrated by applying (on a standard desktop computer) the Dang Van fatigue criterion at all the surface nodes of a mooring chain link (10384 nodes) in less than 170 s run time. The novel strategy for finding the orientation of the critical plane consist of performing a pre-evaluation at planes distributed homogenously along the surface, and then, refine the critical plane search by means of Simplex optimization.

8.1.2 Residual Stress Prediction

Residual stress distribution after manufacturing was predicted by means of thermo-mechanical finite element models. Previous computational models presented in the literature [27], [172], [173] for predicting residual stresses in mooring chains neglected the effect of heat treatment in the final residual stresses field. Two models for predicting the residual stress field after the

manufacturing process have been presented, each of them with increasing complexity. The first one only accounts for proof loading (it is similar to [27], [172], [173]) whereas the second studies heat treatment and proof load. The predictions of both models were compared; and it was found that it is important to account for heat treatment when residual stresses are predicted, especially if the chain link is subjected to OPB fatigue loading.

8.1.3 Computational Fatigue Assessment of Mooring Chains

A computational fatigue assessment method is applied for studying the fatigue behavior of mooring chain under different loading modes, tension loading and twist. The computational fatigue assessment method comprises a mechanical analysis followed by a fatigue analysis. The mechanical analysis is performed in two steps: residual stress prediction and service loading. From this analysis, the shakedown cycle is extracted at the critical points, ie: the asymptotically stabilized stress-strain cycles. As the mooring chain under both service loadings is under elastic shakedown, the Dang Van fatigue criterion is applied for the fatigue analysis.

Tension Loading

Mean load is not currently accounted in standards, (DNV-OS-E301[8] and API-RP-2SK[9]). However, full scale fatigue testing of mooring chains [10] has demonstrated that it should be taken into account. The influence of the mean load in the fatigue performance of chains under tension was assessed by means of the previously described computational fatigue assessment method. The accuracy of the proposed method was proven by comparing the predicted fatigue lifetimes with experimental results from full-scale fatigue testing of mooring chain in seawater. The numerical results match both the experimental observations with respect to the localization of the damage zone and the lifetime. A drawback of the applied methodology is that it is computational expensive and time consuming, which does not make it very appropriate for routine use in industry. To overcome this, a simplified assessment method based on the Dang

Van fatigue criterion is proposed. This method has successfully been implemented in an Excel Spreadsheet (Appendix B).

Twist

Twist may occur during the installation of a chain or during service due to the torque generated in the nearby elements of the mooring (for example wire cables). Fatigue of mooring chains working in twisted conditions is not addressed in current standards. Nevertheless, DNV-OS-E301 [3] recommends avoidance of twist and limits the twist angle to 5 degrees. The computational fatigue assessment method was applied to mooring chains working in twisted conditions. Note that the assessment method (which applies the Dang Van fatigue criterion) is based on fatigue crack initiation. The predicted fatigue failure locations showed good agreement with fatigue cracks found on chain links recovered from the field after more than 15 years in service. The chain operator was aware of these cracks; however, their origin was unknown. These cracks did not propagate until final failure. A qualitative explanation was presented as to why the propagation of these cracks was significantly delayed or even stopped. This evidence that the mechanisms that drive fatigue crack initiation (mainly shear stress amplitude while normal stress has a secondary role although important) are different from fatigue crack propagation (maximum stress perpendicular to the direction of propagation)

8.2 Limitations and future work

The limitations of the research presented in this thesis might be considered as directions for future work and are the following.

The residual stress predictions of mooring chains after manufacturing have not been validated against experimental measurements. Measurement of residual stresses is an ongoing research topic; different measurement techniques are available. Techniques that rely on diffraction of a beam (X-Ray diffraction or neutron diffraction) are considered to be more accurate than

methods that measure strain (deep hole drilling or contour method) [187]. However, diffraction techniques depend on surface roughness, which in the case of mooring chains is not a controlled manufacturing parameter and depends on transport, storage, etc. In this research, the main reason for not performing residual stress measurements in mooring chain links has been due to a limited research budget. However, the numerical model predicting residual stresses after heat treatment (which is the manufacturing stage where modeling presents more complexity) was qualitatively validated against measurements available in the literature. Nevertheless, it is worth pointing out that one of the advantages of the Dang Van fatigue criterion is that it enables residual stresses to be accounted a posteriori; that is to correct the fatigue prediction if a more accurate estimation or measurement of residual stresses is available.

Residual stress relaxation or redistribution due to corrosion has been neglected. This phenomenon could be studied numerically by removing layers of material (this would represent the loss of section due to general corrosion or corrosion pits) and analyzing the change in the residual stresses field. When performing these studies, values of the initial residual stresses should be measured or obtained numerically by accounting for all the relevant manufacturing operations (i.e heat treatment and proof loading). In addition, only chain links with idealized geometry were considered. It is recommended to carry out a study for determining the local effect of corrosion pits in the mechanical response of chain links under service loading.

Appendix A: Smooth Approximation of functions using a log-exponential aggregation function

Finding the centre of the minimum enclosing circle (MEC) is a particular case of a more general problem, the Minimum Enclosing Ball problem (MEB). This problem has been widely studied in the literature, especially for high dimensions. The mathematical formulation of the minmax method for deriving the centre of the smallest enclosing ball for a given dimension (n) has been presented previously. The mean shear stress can be defined as:

$$\mathbf{C} = \min_{\mathbf{C}} \max_{\mathbf{P}_i} ||\mathbf{C} - \mathbf{P}_i||, \mathbf{C} = \min_{\mathbf{C}} f(\mathbf{C})$$

As already pointed out by Zhou et al. [134], the smoothness of ***f(C)*** is not guaranteed. Zhou et al. studied the MEB problem; however, their conclusion remains valid for the MEC problem. They proposed to use a smooth approximation of ***f(C)***. For any given p>0, they defined the smoothing log-exponential aggregation function of f as:

$$f(\mathbf{C}; p) = p \cdot \ln \sum_{i=1}^{m} \exp\left(\frac{g_i(\mathbf{C}; p)}{p}\right)$$

where

- $g_i(\mathbf{C}; p) = r_i + \sqrt{||\mathbf{C_i} - \mathbf{P_i}||^2 + p^2}$

- m: The number of points that define the circumscribed path

For the MEC problem the value of r_i will always be zero.

The definition of the gradient is the following:

$$\nabla f(\mathbf{C}) = \sum_{i=1}^{m} \frac{\lambda_i(\mathbf{C}; p)}{h_i(\mathbf{C}; p)}(\mathbf{C} - \mathbf{P_i})$$

where

- $h_i(\mathbf{C}; p) = \sqrt{||\mathbf{C} - \mathbf{P_i}|| + p^2}$

- $\lambda_i(\mathbf{C}; p) = \dfrac{\exp\left(\frac{g_i(\mathbf{C};p)}{p}\right)}{\tau(\mathbf{C}; p)} \qquad \tau(\mathbf{C}; \mathbf{p}) = \sum_{i=1}^{m} \exp\left(\dfrac{g_i(\mathbf{C}; p)}{p}\right)$

Good results were obtained with p=0.5. More information regarding this method can be found in [134]

Appendix B: Excel Spreadsheet for simplified fatigue assessment of mooring chains under tension loading

This appendix presents the implementation of the simplified fatigue assessment method proposed in Section 6.5.4 and Section 6.5.5 in an Excel Spreadsheet. Note that this simplified method, once calibrated (FEA are still needed for its calibration), enables the application of the Dang Van fatigue criterion to mooring chains under tension without the need of FEA or any other numerical tool such as MATLAB. This is very convenient for routine use in an industry environment.

The spreadsheet has been designed so that a small report is generated, the following pages display the spreadsheet as printed.

Simplified Fatigue Assessment of mooring chains applying Dang Van Fatigue Criterion.

Chain Grade: R5
Chain Diameter: 127mm

Imanol Martinez Perez

The University of Edinburgh

In this first tab the user has to introduce the values of mean load and load amplitude as a function of the MBL. Moreover, the user can optionally change de value of residual stresses (for example if residual stress measurements are available). The workflow at the left-hand side indicates the current step of the calculation.

Input Data

The following Values have to be filled: Grade, Mean load and Load Amplitude. Both of them as function of the respective MBL (Minimum Breaking Load). The Cells are colored in light blue

Diameter (mm)	Grade	MBL (kN)	Proof Load (KN)	Mean Load (%MBL)	Load Amplitude (%MBL)
127	R5	17466	12171	10.3	12.82

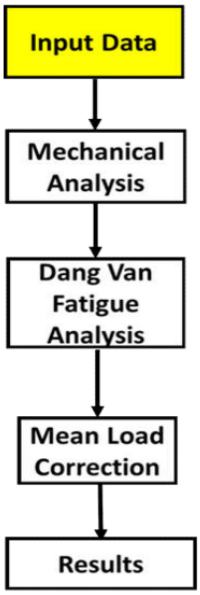

Residual Stresses

Residual stresses play an important role in the fatigue performance of mooring chains. In the case of mooring chains there are two main sources of residual stresses, Heat Treatment and Proof Loading. Both sources should be taken into account. Residual stress can be derived from FEA predictions or experimental measurements. Dang Van Fatigue criterion enables to decouple residual stresses from cyclic stresses. In this Spreadsheet residual stresses predicted with FEA have been implemented. Details regarding the models can be found in (2). For a 162mm chain, at Kt and the Crown, predicted residual stresses take the following values.

Location	S11(MPa)	S22(MPa)	S33(MPa)	Hydrostatic stress (MPa)
The Crown	0.47	41.39	-496.38	-151.50
Kt	-703.46	-129.24	-14.86	-282.52

Where:
S11, S22 and S33 are the stresses in x, y and z directions respectively. These directions are shown in the following figure. They axis convention remains the same for all the spreadsheet.

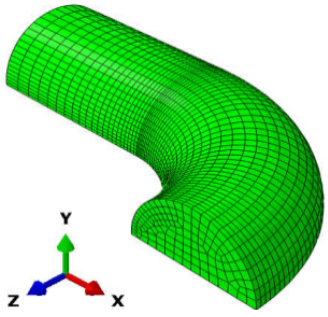

In this second tab, the cyclic stress tensor for a mean load of 20% MBL is derived. The fatigue analysis is carried out for a mean load of 20% MBL, in the following tab the fatigue prediction will be corrected to account for the current value of the mean load (in the example shown, 12. 82 % MBL).

Mechanical Analysis

The Elastic Cyclic stress tensor is derived. It is computed for a Mean Load of 20%MBL. In this section Residual stresses are not accounted. If Cyclic stress tensor atteints the Yield Strenght (Around 910 MPa) the cyclic stress tensor should be computed though elasto-plastic analysis, therefore this Spreasheet should not be used for deriving them

Mean Load (%MBL)	Load Amplitude (%MBL)
20	12.82

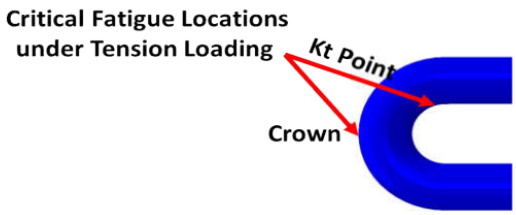

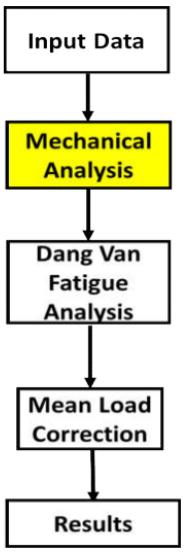

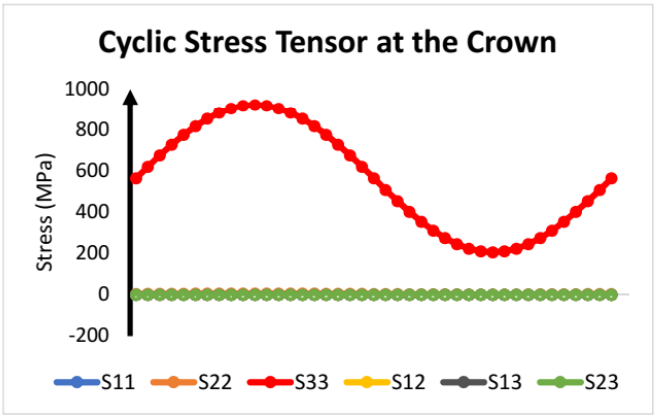

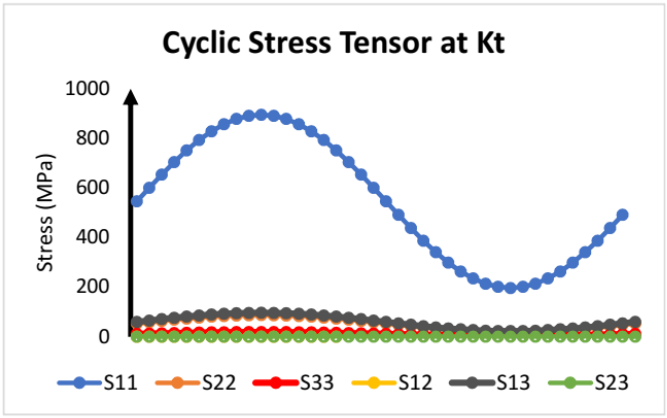

The fatigue analysis is presented in the third tab. Note that is performed for a value of 20% MBL mean load. The fatigue prediction will be corrected in the following tab in order to account for the current value of the mean load. The effect of residual stresses is shown in the Dang Van diagram.

Fatigue Analysis

In this section the fatigue analysis using the Dang Van fatigue criterion (3) is reported. For both locations, the Dang Van load paths(It is a plot of maximum shear stress vs Hydrostatic Stress) are represented for the Crown and the Kt point (Also known as inner bend). For each location, two load paths have been represented, one accounts for residual stresses, while the other one does not. The Dang Van plots are represented for a mean load of 20%MBL. In the following tab, they are corrected for the actual value of the mean load

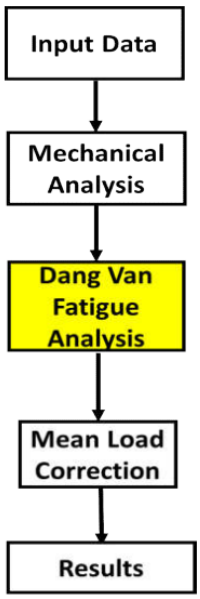

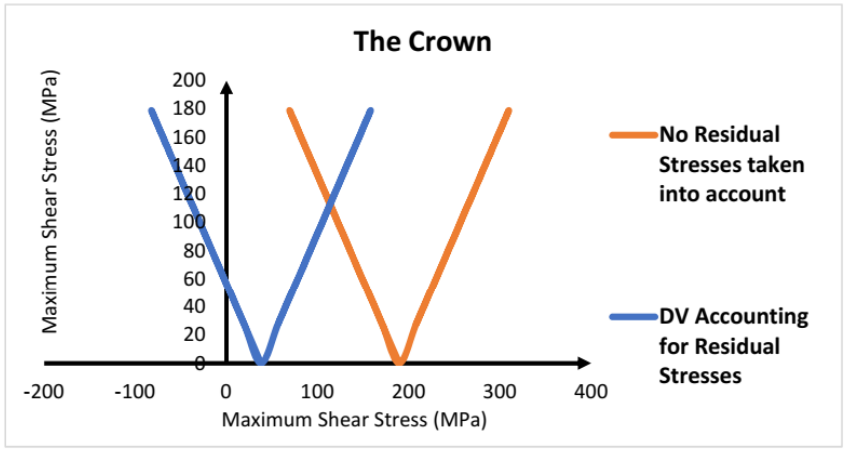

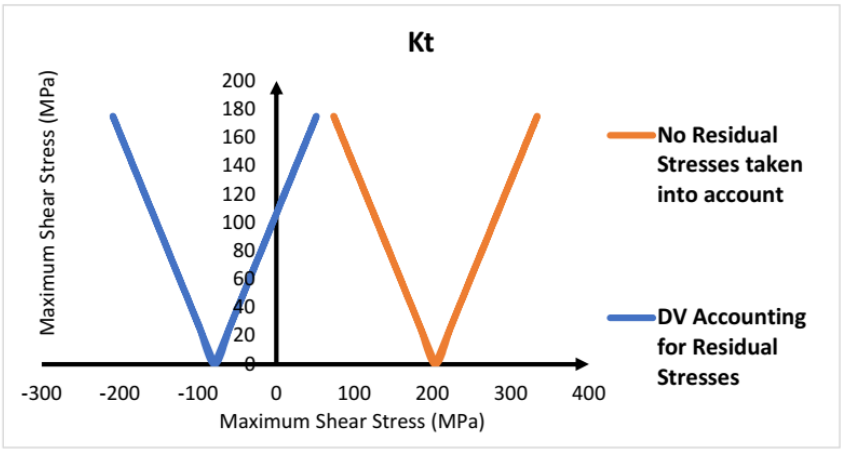

In this tab the effect of the mean load is taken into account and the fatigue prediction derived in the precedent tab (for a mean load of 20% MBL) is corrected.

Mean Load Correction

Mean Load has an influence in the fatigue lifetime of mooring chains under tension. The DV diagrams showed in the previous section where computed for a 20%MBL Mean Load.

Mean Load (%MBL)
10.3

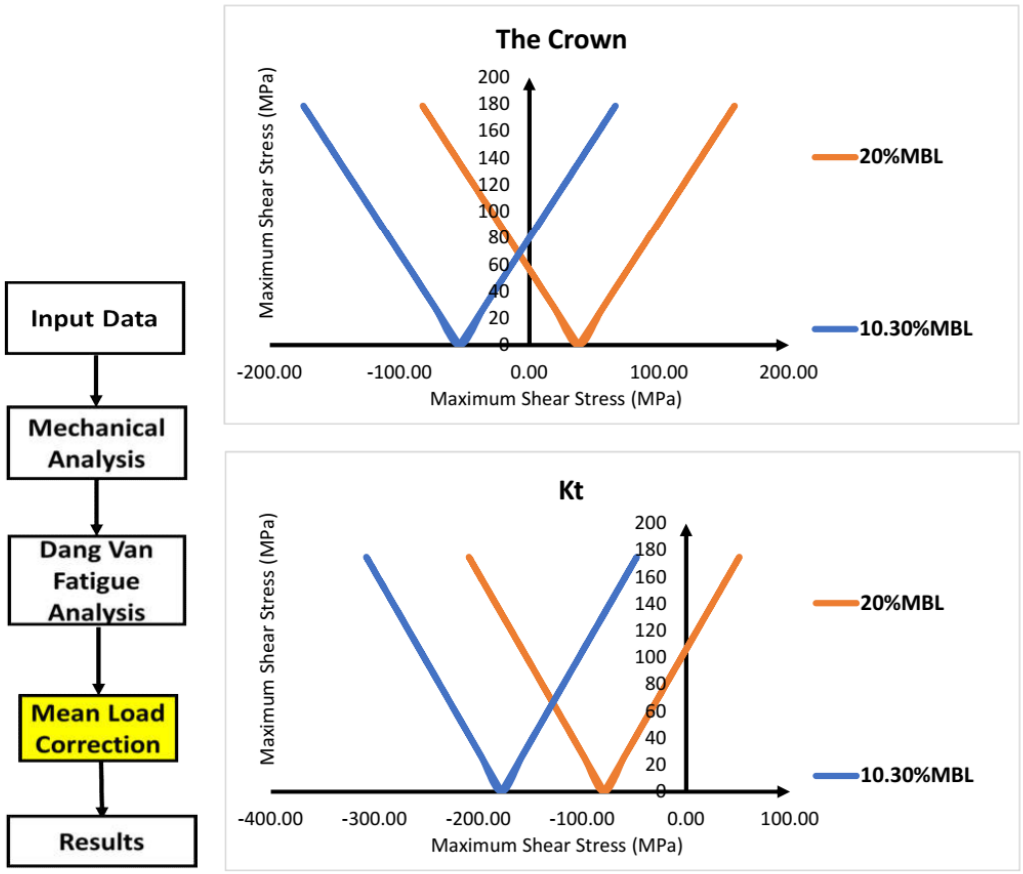

In the second-to-last tab of the spreadsheet the fatigue predictions are shown. Note that in tension loading mooring chains have two fatigue breaking points, Kt and the Crown, and so

the fatigue predictions are only performed at these locations. Moreover, as discussed in Section 6.4, for low mean loads the Dang Van locus should be corrected. The spreadsheet is designed to detect when the corrected Dang Van locus should be applied. Two different prints of the result tab are presented, the first for low mean load (modified Dang Van locus) and the second for high mean loads (conventional Dang Van locus)

Low mean load (Modified Dang Van locus)

Results

This section presents the fatigue lifetime prediction. Dang Van fatigue criterion needs to be calibrated with material properties, usually fatigue limit in alternated tension and alternated torsion. These fatigue properties should account for corrosion. In the literature, these fatigue properties accounting for corrosion are obtained from pre-corroded specimens tested in air, or specimens tested under sea water flow. These properties present an important scatter and influence considerably the predicted fatigue lifetime by Dang Van criterion, as discussed in OMAE2018-77552. Two curves (d1 and d2) have been considered, they account for the scatter of the fatigue properties. They have been obtained from (4) and (5). They bound the fatigue lifetime.

For high compressive mean stresses, Dang Van tends to over predict the Fatigue lifetime. Desimone et al (6) proposed to modify the Dang Van locus for compressive mean stresses. This modification is a conservative approach. It has been included in this analysis. If the mean value of hydrostatic stress is positive, the prediction derived from the original Dang Van locus and the modified locus proposed by Desimone et al coincide. In order to avoid to be over conservative, the modified locus proposed by Desimone et al has only been applied with fatigue properties from d1.

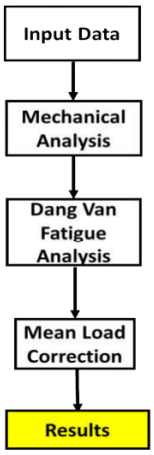

Diameter (mm)	Grade	Mean Load (%MBL)	Load Amplitude (%MBL)
127	R5	10.3	12.82

	Predicted Fatigue Life (d1)	Predicted Fatigue Life (d2)	Conservative DV Locus
Crown	1.18E+05	5.94E+04	8.05E+04
Kt	3.56E+05	1.80E+05	8.05E+04
Lifetime	**8.05E+04**	**N/A**	

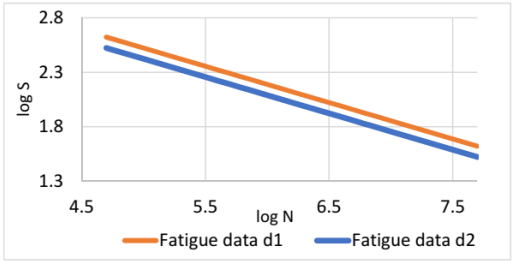

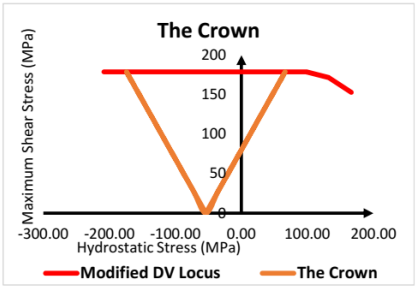

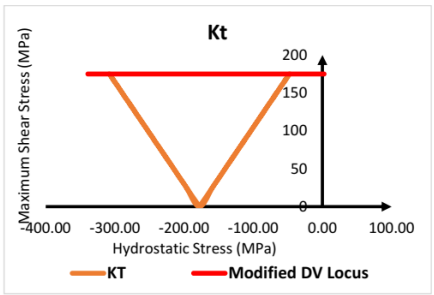

High mean load (Conventional Dang Van locus)

Results

This section presents the fatigue lifetime prediction. Dang Van fatigue criterion needs to be calibrated with material properties, usually fatigue limit in alternated tension and alternated torsion. These fatigue properties should account for corrosion. In the literature, these fatigue properties accounting for corrosion are obtained from pre-corroded specimens tested in air, or specimens tested under sea water flow. These properties present an important scatter and influence considerably the predicted fatigue lifetime by Dang Van criterion, as discussed in OMAE2018-77552. Two curves (d1 and d2) have been considered, they account for the scatter of the fatigue properties. They have been obtained from (4) and (5). They bound the fatigue lifetime.

For high compressive mean stresses, Dang Van tends to over predict the Fatigue lifetime. Desimone et al (6) proposed to modify the Dang Van locus for compressive mean stresses. This modification is a conservative approach. It has been included in this analysis. If the mean value of hydrostatic stress is positive, the prediction derived from the original Dang Van locus and the modified locus proposed by Desimone et al coincide. In order to avoid to be over conservative, the modified locus proposed by Desimone et al has only been applied with fatigue properties from d1.

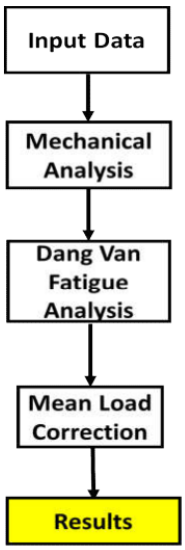

Diameter (mm)	Grade	Mean Load (%MBL)	Load Amplitude (%MBL)
127	R5	18.5	12.82

	Predicted Fatigue Life (d1)	Predicted Fatigue Life (d2)	Conservative DV Locus
Crown	6.83E+04	3.45E+04	6.83E+04
Kt	1.59E+05	8.02E+04	6.83E+04
Lifetime	**6.83E+04**	**3.45E+04**	

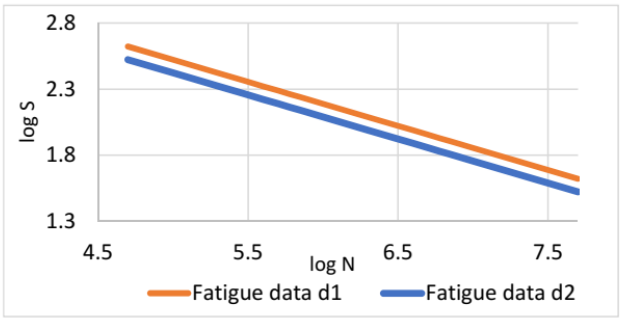

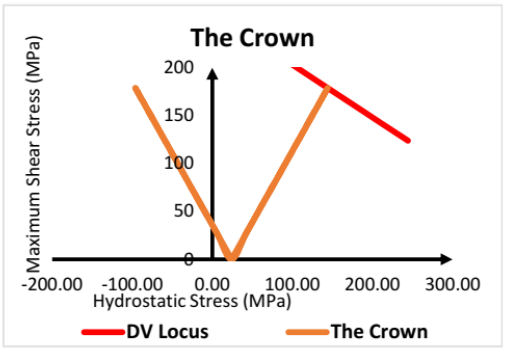

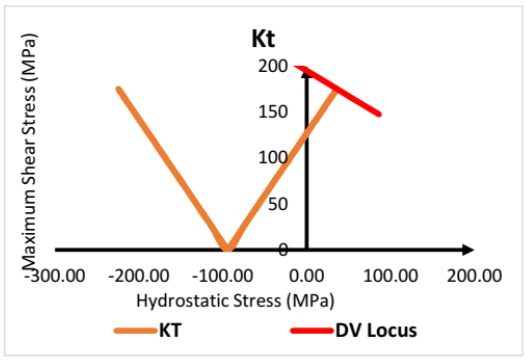

The last tab shows the references that are cited in the spreadsheet

References

1) J.Mathews and K D. Fink, Numerical Methods Using MATLAB , 3. ed. Prentice Hall, 1998.

2) I. Martinez Perez, P. Bastid, and V. Venugopal, "Prediction of Residual Stresses in Mooring Chains and its Impact on Fatigue Life," presented at the ASME. International Conference on Offshore Mechanics and Arctic Engineering, 2017, vol. Volume 3A: Structures, Safety and Reliability, p. V03AT02A034.

3) K. D. Van and I. V. Papadopoulos, Eds., High-Cycle Metal Fatigue. Vienna: Springer Vienna, 1999.

4) J. Fernández, W. Storesund, and J. Navas, "Fatigue Performance of Grade R4 and R5 Mooring Chains in Seawater," in ASME 2014 33rd International Conference on Ocean, Offshore and Arctic Engineering, 2014

5) CETIM, "Dang Van parameters determination on non corroded and corrosed ofshore chain steel," Jul. 2009.

6) H. Desimone, A. Bernasconi, and S. Beretta, "On the application of Dang Van criterion to rolling contact fatigue," Wear, vol. 260, no. 4–5, pp. 567–572, Feb. 2006.

References

[1] Kai-tung Ma, Arun Duggal, and Philip Smedley, "A historical Review on Integrity of Permenent Mooring Systems," presented at the OTC, Houston Texas, 2013.

[2] E. Fontaine *et al.*, "Industry Survey of Past Failures, Pre-emptive Replacements and Reported Degradations for Mooring Systems of Production Units," presented at the OTC, 2014.

[3] DNV, "Position Mooring-DNV-OS-E301_2010-10," Oct. 2010.

[4] M. G. Brown, T. D. Hall, D. G. Marr, M. English, R. O. Snell, and others, "Floating production mooring integrity JIP-key findings," in *Offshore Technology Conference*, 2005.

[5] A. Kvitrud, "Lessons Learned From Norwegian Mooring Line Failures 2010–2013," in *ASME 2014 33rd International Conference on Ocean, Offshore and Arctic Engineering*, 2014, p. V04AT02A005–V04AT02A005.

[6] D. Socie and G. Marquis, *Multiaxial Fatigue*. Society of Automotive Engineers, 2000.

[7] API, *API recommended practice for planning, designing, and constructing fixed offshore platforms*. American Petroleum Institute, Production Dept., 1977.

[8] DNV, "DNV-OS-E302 - Offshore Mooring Chain," Offshore Standard, 2013.

[9] American Petroleum Institute (API), *Design and Analysis of Stationkeeping Systems for Floating Structures*, 3rd Edition, October 2005. 2008.

[10] Ø. Gabrielsen, K. Larsen, and S.-A. Reinholdtsen, "Fatigue Testing of Used Mooring Chain," in *ASME 2017 36th International Conference on Ocean, Offshore and Arctic Engineering*, 2017, p. V001T01A072–V001T01A072.

[11] J. Fernández, W. Storesund, and J. Navas, "Fatigue Performance of Grade R4 and R5 Mooring Chains in Seawater," in *ASME 2014 33rd International Conference on Ocean, Offshore and Arctic Engineering*, 2014, p. V01AT01A035–V01AT01A035.

[12] H. M. Bolt, C. J. Billington, M. J. Humphries, and others, "Anchor Chain-New Data, New Design Lines and Practical Details," in *Offshore Technology Conference*, 1995.

[13] J. J. Stiff, D. W. Smith, N. F. Casey, and others, "Fatigue of mooring chain in air and water-Results and analysis," in *Offshore Technology Conference*, 1996.

[14] P. Jean, K. Goessens, D. L'Hostis, and others, "Failure of chains by bending on deepwater mooring systems," in *Offshore Technology Conference*, 2005.

[15] L. Rampi, F. Dewi, and P. Vargas, "Chain Out of Plane Bending (OPB) Joint Industry Project (JIP) Summary and Main Results," presented at the OTC, 2015.

[16] Bureau Veritas, "Fatigue of Top Chain of Mooring Lines due to In-plane and Out-of-plane Bendings," Guidance Note, Oct. 2014.

[17] T. Lassen, E. Storvoll, and A. Bech, "Fatigue Life Prediction of Mooring Chains subjected to Tension and Out of Plane Bending," in *ASME 2009 28th International Conference on Ocean, Offshore and Arctic Engineering*, 2009, pp. 229–239.

[18] L. Rampi, A. Bignonnet, C. Le Cunff, F. Bourgin, and P. Vargas, "Chain Out of Plane Bending (OPB) Fatigue Joint Industry Project (JIP) FEA Results and Multiaxiality Study Results," in *ASME 2016 35th International Conference on Ocean, Offshore and Arctic Engineering*, 2016, p. V001T01A002–V001T01A002.

[19] I. Ridge, P. Smedley, and R. Hobbs, “Effects of twist on chain strength and fatigue performance: small scale test results,” in *ASME 2011 30th International Conference on Ocean, Offshore and Arctic Engineering*, 2011, pp. 183–189.
[20] R. E. Hobbs and I. M. L Ridge, “Torque in Mooring Chain. Part 1: Background and Theory,” *J. Strain Anal. Eng. Des.*, vol. 40, no. 7, pp. 703–713, Apr. 2005.
[21] T. Hiroshima and T. Sawa, “Three-dimensional finite element analysis and strength evaluation of link chains in chain hoists subjected to impact loads,” *J. Strain Anal. Eng. Des.*, vol. 31, no. 1, pp. 43–51, 1996.
[22] C. R. Chaplin, G. Rebel, and I. M. L. Ridge, “Tension-Torsion Interactions in Multicomponent Mooring Lines,” 2000.
[23] I. M. L. Ridge, R. E. Hobbs, J. Fernandez, and others, “Predicting the torsional response of large mooring chains,” in *Offshore Technology Conference*, 2006.
[24] G. J. Shoup, S. M. Tipton, J. R. Sorem, and others, “The influence of proof loading on the fatigue life of anchor chain,” in *Offshore Technology Conference*, 1992.
[25] P. Pacheco, P. P. Kenedi, J. C. F. Jorge, H. S. Gama, M. A. Savi, and A. M. C. Paiva, “Modeling Residual Stresses in Offshore Chain Links using Finite Element Method,” in *COBEM-2003, 17th International Congress of Mechanical Engineering, São Paulo*, 2003.
[26] E. Abolfathi, G. F. Modlen, P. J. Webster, and G. Mills, “The effect of the manufacturing test load on the fatigue of hoist chains,” *Proc. Inst. Mech. Eng. Part B J. Eng. Manuf.*, vol. 209, no. 2, pp. 133–139, 1995.
[27] P. Bastid and S. D. Smith, “Numerical Analysis of Contact Stresses Between Mooring Chain Links and Potential Consequences for Fatigue Damage,” in *ASME 2013 32nd International Conference on Ocean, Offshore and Arctic Engineering*, 2013, p. V02BT02A037–V02BT02A037.
[28] M. G. Brown, A. P. Comley, M. Eriksen, I. Williams, P. Smedley, and S. Bhattacharjee, “Phase 2 Mooring Integrity JIP- Summary of findings,” presented at the OTC, Texas, 2010.
[29] G. E. Totten, M. A. H. Howes, and T. Inoue, Eds., *Handbook of residual stress and deformation of steel*. Materials Park, Ohio: ASM International, 2002.
[30] S. A. Al-Fozan and A. U. Malik, “Effect of seawater level on corrosion behavior of different alloys,” *Desalination*, vol. 228, no. 1–3, pp. 61–67, Aug. 2008.
[31] T. Magnin, “Recent Advances for Corrosion Fatigue Mechanisms.,” *ISIJ Int.*, vol. 35, no. 3, pp. 223–233, 1995.
[32] P. M. Ruben, “Study of the fatigue strength in the gigacycle regime of metallic alloys used in aeronautics and off-shore industries,” Arts et Métiers ParisTech, 2010.
[33] R. Pérez-Mora, T. Palin-Luc, C. Bathias, and P. C. Paris, “Very high cycle fatigue of a high strength steel under sea water corrosion: A strong corrosion and mechanical damage coupling,” *Int. J. Fatigue*, vol. 74, pp. 156–165, May 2015.
[34] T. Palin-Luc, R. Pérez-Mora, C. Bathias, G. Domínguez, P. C. Paris, and J. L. Arana, “Fatigue crack initiation and growth on a steel in the very high cycle regime with sea water corrosion,” *Eng. Fract. Mech.*, vol. 77, no. 11, pp. 1953–1962, Jul. 2010.
[35] A. Arredondo, J. Fernández, E. Silveira, and J. L. Arana, “Corrosion Fatigue Behavior of Mooring Chain Steel in Seawater,” in *ASME 2016 35th International Conference on Ocean, Offshore and Arctic Engineering*, 2016, p. V001T01A006–V001T01A006.
[36] British Standards Institution, *BS 7910:2013+A1:2015-Guide to methods for assessing the acceptability of flaws in metallic structures*, Third Edition. BSI Standards Limited, 2015.

[37] E. Fontaine, A. Potts, K. Ma, A. Arredondo, and R. E.Melchers, "SCHORCH JIP: Examination and Testing of Severely-Corroded Mooring Chains from West Africa," 2012.
[38] J. Rosen, K. Jayasinghe, and A. Potts, "SCORCH JIP: Findings from Investigatins into Mooring Chain and Wire Rope Corrosion in Warm Waters," presented at the OTC, 2015.
[39] J. Rosen *et al.*, "Chain FEARS JIP: Finite Element Analysis of Residual Strength of Degraded Chains," in *OTC-26264-MS*, OTC, 2015.
[40] G. H. Farrow, A. E. Potts, and D. G. Washington, "Investigations Into Fatigue Performance of Offshore Mooring Chains," in *ASME 2017 36th International Conference on Ocean, Offshore and Arctic Engineering*, 2017, p. V001T01A025–V001T01A025.
[41] HSE, "HSE Offshore: Safety Notice 3/2005 - Floating Production Storage and Offloading," 2005. [Online]. Available: http://www.hse.gov.uk/offshore/notices/sn_03_05.htm. [Accessed: 28-Oct-2015].
[42] A. Lotfollahi Yaghin and R. E. Melchers, "Long-term inter-link wear of model mooring chains," *Mar. Struct.*, vol. 44, pp. 61–84, Dec. 2015.
[43] K. Gotoh, K. Murakami, M. Nakagawa, and T. Utsunomiya, "Wear Performance of the Mooring Chain Used in Floating Wind Turbines," in *ASME 2017 36th International Conference on Ocean, Offshore and Arctic Engineering*, 2017, p. V004T03A032–V004T03A032.
[44] Y. Liu and T. Ishihara, "Fatigue Failure Accident of Wind Turbine Tower in Taikoyama Wind Farm," 2001.
[45] M. Fonte, B. Li, L. Reis, and M. Freitas, "Crankshaft failure analysis of a motor vehicle," *Eng. Fail. Anal.*, vol. 35, pp. 147–152, Dec. 2013.
[46] B. A. Cowles, "High cycle fatigue in aircraft gas turbines—an industry perspective," *Int. J. Fract.*, vol. 80, no. 2–3, pp. 147–163, 1996.
[47] A. Ktari, N. Haddar, and H. F. Ayedi, "Fatigue fracture expertise of train engine crankshafts," *Eng. Fail. Anal.*, vol. 18, no. 3, pp. 1085–1093, Apr. 2011.
[48] K. Iida, "A review of fatigue failures in LWR plants in Japan," *Nucl. Eng. Des.*, vol. 138, no. 3, pp. 297–312, 1992.
[49] P. Jean, K. Goessens, D. L'Hostis, and others, "Failure of chains by bending on deepwater mooring systems," in *Offshore Technology Conference*, 2005.
[50] *ASTM Standard Terminology Relating to Fatigue and Fracture Testing E1823-13*. .
[51] P. Forsyth, *The physical basis of metal fatigue*. New York: American Elsevier, 1969.
[52] F. C. Campbell, Ed., *Fatigue and fracture: understanding the basics*. Materials Park, Ohio: ASM International, 2012.
[53] J. Schijve, "Significance of fatigue cracks in micro-range and macro-range," in *ASTM Special Technical Publication N415*, 1966, pp. 415–459.
[54] S. De-Guang, Y. Wei-Xing, and W. De-Jun, "A new approach to the determination of fatigue crack initiation size," *Int. J. Fatigue*, vol. 20, no. 9, pp. 683–687, 1998.
[55] C. Bathias, "There is no infinite fatigue life in metallic materials," *Fatigue Fract. Eng. Mater. Struct.*, vol. 22, no. 7, pp. 559–566, 1999.
[56] H. J. Grover, "An Observation concerning the cycle ratio in cumulative damage," *ASME J. Eng. Ind.*, pp. 25–35, 1965.
[57] J. Lemaître and J.-L. Chaboche, *Mechanics of solid materials*. Cambridge: Cambridge University Press, 1990.
[58] L. Yang and A. Fatemi, "Cumulative Fatigue Damage Mechanisms and Quantifying Parameters: A Literature Review," *J. Test. Eval.*, vol. 6, pp. 89–100, Mar. 1998.

[59] A. Fatemi and L. Yang, “Cumulative fatigue damage and life prediction theories: a survey of the state of the art for homogeneous materials,” *Int. J. Fatigue*, vol. 20, pp. 9–34, 1998.
[60] API, *API recommended practice for planning, designing, and constructing fixed offshore platforms*. American Petroleum Institute, Production Dept., 1977.
[61] W. Cui, “A state-of-the-art review on fatigue life prediction methods for metal structures,” *J. Mar. Sci. Technol.*, vol. 7, no. 1, pp. 43–56, 2002.
[62] W. Schutz, “A History of Fatigue,” *Eng. Fract. Mech.*, vol. 54, pp. 263–300, 1996.
[63] S. Suresh, *Fatigue of materials*, 2nd ed. Cambridge ; New York: Cambridge University Press, 1998.
[64] I. V. Papadopoulos, P. Davoli, C. Gorla, M. Filippini, and A. Bernasconi, “A comparative study of multiaxial high-cycle fatigue criteria for metals,” *Int. J. Fatigue*, vol. 19, no. 3, pp. 219–235, 1997.
[65] Jan Papuga, “Mapping of Fatigue Damages – Program Shell of FE-Calculation,” Czech Technical University in Prague, Prague, 2005.
[66] A. Carpinteri, A. Spagnoli, and S. Vantadori, “A review of multiaxial fatigue criteria for random variable amplitude loads: A Review of Multiaxial Fatigue Criteria for Random Variable Amplitude Loads,” *Fatigue Fract. Eng. Mater. Struct.*, vol. 40, no. 7, pp. 1007–1036, Jul. 2017.
[67] H. J. Gough, “Engineering steels under combined cyclic and static stresses,” *Proc. Inst. Mech. Eng.*, vol. 160, no. 1, pp. 417–440, 1949.
[68] M. W. Brown and K. J. Miller, “A theory for fatigue failure under multiaxial stress-strain conditions,” *Proc. Inst. Mech. Eng.*, vol. 187, no. 1, pp. 745–755, 1973.
[69] Sines,G, “Failure of materials under combined repeated stresses with superimposed static stresses,” National Advisory Committee for Aeronautics, Washington DC, Tech Note 349, 1955.
[70] CROSSLAND, B, “Effect of large hydrostatic pressure on the torsional fatigue strength of an alloy steel,” presented at the Int. Conf. on Fatigue of Metals, London, 1956, pp. 138–149.
[71] W. N. Findley, J. J. Coleman, and B. C. Hanley, *THEORY FOR COMBINED BENDING AND TORSION FATIGUE WITH DATA FOR SAE 4340 STEEL. Technical Report No. 1 on BASIC RESEARCH ON FATIGUE FAILURES UNDER COMBINED STRESS*. 1956.
[72] T. Matake, “Matake, T.: An explanation on fatigue limit under combined stress. Bull. JSME 20, 257-263,” *Bull JSME*, vol. 20, 1977.
[73] D. L. McDiarmid, “A GENERAL CRITERION FOR HIGH CYCLE MULTIAXIAL FATIGUE FAILURE,” *Fatigue Fract. Eng. Mater. Struct.*, vol. 14, no. 4, pp. 429–453, 1991.
[74] D. L. McDiarmid, “A SHEAR STRESS BASED CRITICAL-PLANE CRITERION OF MULTIAXIAL FATIGUE FAILURE FOR DESIGN AND LIFE PREDICTION,” *Fatigue Fract. Eng. Mater. Struct.*, vol. 17, no. 12, pp. 1475–1484, 1994.
[75] F. C. Campbell, Ed., *Fatigue and fracture: understanding the basics*. Materials Park, Ohio: ASM International, 2012.
[76] K. D. Van and I. V. Papadopoulos, Eds., *High-Cycle Metal Fatigue*. Vienna: Springer Vienna, 1999.
[77] K. Dang Van, G.Cailletaud, J.F Flavenot, A.Le Douron, and H.P Lieurade, “Criterion for High Cycle Fatigue Failure under Multiaxial Loading,” *Biaxial Multiaxial Fatigue*, pp. 459–478, 1989.

[78] M. Ferjani, D. Averbuch, and A. Constantinescu, “A computational approach for the fatigue design of threaded connections,” *Int. J. Fatigue*, vol. 33, no. 4, pp. 610–623, Apr. 2011.
[79] P. Wackers, V. Arrieta, M. Alquezar-Getan, A. Constantinescu, and H. Maitournam, “A modeling approach to predict fretting fatigue on highly loaded blade roots,” *J. Eng. Gas Turbines Power*, vol. 132, no. 8, p. 082101, 2010.
[80] F. Auricchio, A. Constantinescu, M. Conti, and G. Scalet, “A computational approach for the lifetime prediction of cardiovascular balloon-expandable stents,” *Int. J. Fatigue*, vol. 75, pp. 69–79, Jun. 2015.
[81] F. Morel, N. Ranganathan, J. Petit, and A. Bignonnet, “A mesoscopic approach for fatigue life prediction under multiaxial loading,” *Eur. Struct. Integr. Soc.*, vol. 25, pp. 87–100, 1999.
[82] M. Jabbado, “Fatigue polycyclique des structures métalliques: durée de vie sous chargements variables.,” Ecole Polytechnique X, 2006.
[83] M. H. Maitournam, C. Krebs, and A. Galtier, “A multiscale fatigue life model for complex cyclic multiaxial loading,” *Int. J. Fatigue*, vol. 33, no. 2, pp. 232–240, Feb. 2011.
[84] I. V. Papadopoulos, “Long life fatigue under multiaxial loading,” *Int. J. Fatigue*, vol. 23, no. 10, pp. 839–849, 2001.
[85] M. W. Brown and K. J. Miller, “A theory for fatigue failure under multiaxial stress-strain conditions,” *Proc. Inst. Mech. Eng.*, vol. 187, no. 1, pp. 745–755, 1973.
[86] M. L. Roessle and A. Fatemi, “Strain-controlled fatigue properties of steels and some simple approximations,” *Int. J. Fatigue*, vol. 22, no. 6, pp. 495–511, 2000.
[87] G. Glinka, “Relations between the strain energy density distribution and elastic-plastic stress-strain field near cracks and notches and fatigue life calculation,” presented at the ASTM STP 942, 1022-1047, 1988.
[88] F. Ellyin, “Cyclic Strain Energy Density as a Criterion for Multiaxial Fatigue Failure,” presented at the Biaxial and Multiaxial Fatigue, 1989, pp. 571–583.
[89] W.-F. Pan, C.-Y. Hung, and L.-L. Chen, “Fatigue life estimation under multiaxial loadings,” *Int. J. Fatigue*, vol. 21, no. 1, pp. 3–10, 1999.
[90] F. Ellyin and D. Kujawski, “A multiaxial fatigue criterion including mean-stress effect,” in *Advances in Multiaxial Fatigue*, ASTM International, 1993.
[91] J. Schijve, *Fatigue of structures and materials*, 2. ed. Dordrecht: Springer, 2009.
[92] N. E. Dowling, “Mean stress effects in stress-life and strain-life fatigue,” *SAE Tech. Pap.*, no. 2004–01, p. 2227, 2004.
[93] L. Susmel, R. Tovo, and P. Lazzarin, “The mean stress effect on the high-cycle fatigue strength from a multiaxial fatigue point of view,” *Int. J. Fatigue*, vol. 27, no. 8, pp. 928–943, 2005.
[94] J. R. Barber, *Elasticity*, 3rd rev. ed. Dordrecht ; New York: Springer, 2010.
[95] “SDPT3 -- a MATLAB software for semidefinite-quadratic-linear programmin.” [Online]. Available: http://www.math.nus.edu.sg/~mattohkc/sdpt3.html. [Accessed: 17-Sep-2017].
[96] “dlib C++ Library - Optimization.” [Online]. Available: http://dlib.net/optimization.html. [Accessed: 17-Sep-2017].
[97] “SciPy.org — SciPy.org.” [Online]. Available: https://www.scipy.org/. [Accessed: 15-Sep-2017].
[98] B. Weber, B. Kenmeugne, J. C. Clement, and J. L. Robert, “Improvements of multiaxial fatigue criteria computation for a strong reduction of calculation duration,” *Comput. Mater. Sci.*, vol. 15, no. 4, pp. 381–399, 1999.

[99] L. Susmel, “A simple and efficient numerical algorithm to determine the orientation of the critical plane in multiaxial fatigue problems,” *Int. J. Fatigue*, vol. 32, no. 11, pp. 1875–1883, Nov. 2010.
[100] H. Svärd, “A branch and bound algorithm for evaluation of the Findley fatigue criterion,” *Int. J. Fatigue*, vol. 73, pp. 27–38, Apr. 2015.
[101] R. Rabb, C. Lönnqvist, and J. Kaas, “Multiaxial fatigue criteria applied to medium speed diesel engines,” in *ICMFF9*, 2010.
[102] M. Cerullo, “Application of Dang Van criterion to rolling contact fatigue in wind turbine roller bearings,” in *ICF13*, 2013.
[103] K. D. Van, H. M. Maitournan, and J. F. Flavenot, “Fatigue design of notched components by a multiscale approach based on shakedown,” *Secur. Reliab. Damaged Struct. Defective Mater.*, p. 325, 2009.
[104] O. Barrera, A. Makradi, M. Abbadi, M. Azaouzi, and S. Belouettar, “On high-cycle fatigue of 316L stents,” *Comput. Methods Biomech. Biomed. Engin.*, vol. 17, no. 3, pp. 239–250, Feb. 2014.
[105] H. Maitournam, *Matériaux et structures anélastiques*. Ecole Polytechnique Eds, 2017.
[106] J. Sandström, “Evaluation of Dang Van stress in Hertzian rolling contact,” *Fatigue Fract. Eng. Mater. Struct.*, vol. 35, no. 12, pp. 1088–1094, 2012.
[107] B. Li, J. L. T. Santos, and M. de Freitas, “A Unified Numerical Approach for Multiaxial Fatigue Limit Evaluation,” *Mech. Struct. Mach.*, vol. 28, no. 1, pp. 85–103, Aug. 2000.
[108] Deperrois, A, “Sur le calcul de limite d’endurance des aciers,” Thèse de Doctorat, Ecole Polytechnique, Paris, 1991.
[109] Jean Lemaitre, *Handbook of Materials Behavior Models*. Academic Press, 2001.
[110] Grubisic, V. and Simbürger, A., “Fatigue under combined out-of-phase multiaxial stresses,” presented at the International Conference on Fatigue, Testing and Design, London, 1976, p. 8.
[111] I. V. Papadopoulos, “Critical plane approaches in high-cycle fatigue: on the definition of the amplitude and mean value of the shear stress acting on the critical plane,” *Fatigue Fract. Eng. Mater. Struct.*, vol. 21, no. 3, pp. 269–285, 1998.
[112] A. Bernasconi and I. V. Papadopoulos, “Efficiency of algorithms for shear stress amplitude calculation in critical plane class fatigue criteria,” *Comput. Mater. Sci.*, vol. 34, no. 4, pp. 355–368, Dec. 2005.
[113] A. Bernasconi, “Efficient algorithms for calculation of shear stress amplitude and amplitude of the second invariant of the stress deviator in fatigue criteria applications,” *Int. J. Fatigue*, vol. 24, no. 6, pp. 649–657, 2002.
[114] L. Reis, B. Li, and M. De Freitas, “Biaxial fatigue for proportional and non-proportional loading paths,” *Fatigue Fract. Eng. Mater. Struct.*, vol. 27, no. 9, pp. 775–784, 2004.
[115] M. De Freitas, B. Li, and J. L. T. Santos, “A numerical approach for high-cycle fatigue life prediction with multiaxial loading,” in *Multiaxial Fatigue and Deformation: Testing and Prediction*, ASTM International, 2000.
[116] W. N. Findley, J. J. Coleman, and B. C. Hanley, *THEORY FOR COMBINED BENDING AND TORSION FATIGUE WITH DATA FOR SAE 4340 STEEL. Technical Report No. 1 on BASIC RESEARCH ON FATIGUE FAILURES UNDER COMBINED STRESS*. 1956.
[117] J.A Bannantine and D.F Socie, “A variable Amplitude Multiaxial Fatigue Life Methods,” presented at the Third international Conference on Biaxial/Multiaxial Fatigue, ttutgart, 1989.
[118] L. Susmel, R. Tovo, and D. F. Socie, “Estimating the orientation of Stage I crack paths through the direction of maximum variance of the resolved shear stress,” *Int. J. Fatigue*, vol. 58, pp. 94–101, Jan. 2014.

[119] S. Norberg and M. Olsson, “A fast, versatile fatigue post-processor and criteria evaluation,” *Int. J. Fatigue*, vol. 27, no. 10–12, pp. 1335–1341, Oct. 2005.
[120] J. A. Nelder and R. Mead, “A Simplex Method for Function Minimization,” *Comput J*, vol. 7, no. 4, pp. 308–313, Jan. 1965.
[121] W. H. Press, *Numerical recipes: the art of scientific computing*. Cambridge, UK; New York: Cambridge University Press, 2007.
[122] “Find minimum of unconstrained multivariable function using derivative-free method - MATLAB fminsearch - MathWorks United Kingdom.” [Online]. Available: https://uk.mathworks.com/help/optim/ug/fminsearch.html#bu9sp4b-1. [Accessed: 14-Jun-2017].
[123] J. C. Lagarias, J. A. Reeds, M. H. Wright, and P. E. Wright, “Convergence properties of the Nelder–Mead simplex method in low dimensions,” *SIAM J. Optim.*, vol. 9, no. 1, pp. 112–147, 1998.
[124] J. Nocedal and S. J. Wright, *Numerical optimization*, 2nd ed. New York: Springer, 2006.
[125] Eric Weisstein, *The CRC Concise Encyclopedia of Mathematics*, Second. CHAPMAN & HALL/CRC, 2003.
[126] A. S. Lewis and M. L. Overton, “Nonsmooth optimization via BFGS,” *Submitt. SIAM J Optim.*, pp. 1–35, 2009.
[127] D. C. Liu and J. Nocedal, “On the limited memory BFGS method for large scale optimization,” *Math. Program.*, vol. 45, no. 1, pp. 503–528, 1989.
[128] “FMINLBFGS: Fast Limited Memory Optimizer - File Exchange - MATLAB Central.” [Online]. Available: https://uk.mathworks.com/matlabcentral/fileexchange/23245-fminlbfgs--fast-limited-memory-optimizer. [Accessed: 17-Sep-2017].
[129] “HANSO.” [Online]. Available: http://www.cs.nyu.edu/overton/software/hanso/. [Accessed: 29-Aug-2017].
[130] “Dakota | Explore and predict with confidence.” [Online]. Available: https://dakota.sandia.gov/. [Accessed: 17-Sep-2017].
[131] M. de Berg, O. Cheong, M. van Kreveld, and M. Overmars, *Computational Geometry*. Berlin, Heidelberg: Springer Berlin Heidelberg, 2008.
[132] H. Hosseini Nasab, M. Tavana, and M. Yousefi, “A new heuristic algorithm for the planar minimum covering circle problem,” *Prod. Manuf. Res.*, vol. 2, no. 1, pp. 142–155, 2014.
[133] S. Xu, R. M. Freund, and J. Sun, “Solution Methodologies for the Smallest Enclosing Circle Problem,” *Comput. Optim. Appl.*, vol. 25, no. 1, pp. 283–292, Apr. 2003.
[134] G. Zhou, K.-C. Tohemail, and J. Sun, “Efficient algorithms for the smallest enclosing ball problem,” *Comput. Optim. Appl.*, vol. 30, no. 2, pp. 147–160, 2005.
[135] S. Pan and X. Li, “An efficient algorithm for the smallest enclosing ball problem in high dimensions,” *Appl. Math. Comput.*, vol. 172, no. 1, pp. 49–61, Jan. 2006.
[136] C.Lemaréchal, “Numerical experiments in nonsmooth optimization,” presented at the Progress in Nondifferentiable Optimization, Laxenburg, Austria, 1982, pp. 61–84.
[137] J. Guo and A. Lewis, “BFGS convergence to nonsmooth minimizers of convex functions,” *ArXiv Prepr. ArXiv170306690*, 2017.
[138] “Optimization Toolbox - MATLAB.” [Online]. Available: https://uk.mathworks.com/products/optimization.html. [Accessed: 18-Sep-2017].
[139] E. Welzl, “Smallest enclosing disks (balls and ellipsoids),” *New Results New Trends Comput. Sci.*, pp. 359–370, 1991.
[140] “HANSO: Hybrid Algorithm for Non-Smooth Optimization.” [Online]. Available: HANSO: Hybrid Algorithm for Non-Smooth Optimization.
[141] “Vicinay Cadenas, S.A.” [Online]. Available: http://www.vicinaycadenas.net/index/. [Accessed: 08-Jan-2017].

[142] Y. Wu, T. Wang, Ø. Eide, and K. Haverty, "Governing factors and locations of fatigue damage on mooring lines of floating structures," *Ocean Eng.*, vol. 96, pp. 109–124, Mar. 2015.
[143] E. Fontaine, A. Potts, K. Ma, A. Arredondo, and R. E.Melchers, "SCHORCH JIP: Examination and Testing of Severely-Corroded Mooring Chains from West Africa," presented at the OTC, 2012.
[144] G. J. Shoup, S. M. Tipton, J. R. Sorem, and others, "The influence of proof loading on the fatigue life of anchor chain," in *Offshore Technology Conference*, 1992.
[145] E. Abolfathi, G. F. Modlen, P. J. Webster, and G. Mills, "The effect of the manufacturing test load on the fatigue of hoist chains," *Proc. Inst. Mech. Eng. Part B J. Eng. Manuf.*, vol. 209, no. 2, pp. 133–139, 1995.
[146] P. Pacheco, P. P. Kenedi, J. C. F. Jorge, H. S. Gama, M. A. Savi, and A. M. C. Paiva, "Modeling Residual Stresses in Offshore Chain Links using Finite Element Method," in *COBEM-2003, 17th International Congress of Mechanical Engineering, São Paulo*, 2003.
[147] P. R. Woodard, S. Chandrasekar, and H. T. Y. Yang, "Analysis of temperature and microstructure in the quenching of steel cylinders," *Metall. Mater. Trans. B*, vol. 30, no. 4, p. 815, 1999.
[148] R. Schröder, "Influences on development of thermal and residual stresses in quenched steel cylinders of different dimensions," *Mater. Sci. Technol.*, vol. 1, no. 10, pp. 754–764, Oct. 1985.
[149] C. H. Gur and A. E. Tekkaya, "Numerical and experimental analysis of quench induced stresses and microstructures," *J. Mech. Behav. Mater.*, vol. 9, no. 4, pp. 237–256, 1998.
[150] T. Palin-Luc, R. Pérez-Mora, C. Bathias, G. Domínguez, P. C. Paris, and J. L. Arana, "Fatigue crack initiation and growth on a steel in the very high cycle regime with sea water corrosion," *Eng. Fract. Mech.*, vol. 77, no. 11, pp. 1953–1962, Jul. 2010.
[151] International Association of Classification Societies (IACS), "Requirements Concerning Materials and Welding, W22 Offshore Mooring Chain," 2011.
[152] B. Albisu *et al.*, "New Grades of High Strength Steel for Offshore Mooring Chains: R5S (1100MPa) and R6 (1200 MPa)," in *Offshore Technology Conference*, 2016.
[153] P. M. Vargas, T.-M. Hsu, and W. K. Lee, "Stress Concentration Factors for Stud-Less Mooring Chain Links in Fairleads," 2004, pp. 909–917.
[154] J. Lereim and others, "Summary of the 4-Year Research Project: Anchor Chain Cables Offshore," in *Offshore Technology Conference*, 1985.
[155] C. H. Gur and J. Pan, *Handbook of Thermal Process Modeling Steels*. CRC Press, 2008.
[156] D. P. Koistinen and R. E. Marburger, "A general equation prescribing the extent of the austenite-martensite transformation in pure iron-carbon alloys and plain carbon steels," *Acta Metall.*, vol. 7, no. 1, pp. 59–60, 1959.
[157] M. V. Li, D. V. Niebuhr, L. L. Meekisho, and D. G. Atteridge, "A computational model for the prediction of steel hardenability," *Metall. Mater. Trans. B*, vol. 29, no. 3, pp. 661–672, 1998.
[158] J. Chen, B. Young, and B. Uy, "Behavior of high strength structural steel at elevated temperatures," *J. Struct. Eng.*, vol. 132, no. 12, pp. 1948–1954, 2006.
[159] "Metallic Material Database (Kinzoku)." [Online]. Available: http://metallicmaterials.nims.go.jp/index_en.html. [Accessed: 08-Jan-2017].
[160] J. Rohde and A. Jeppsson, "Literature review of heat treatment simulations with respect to phase transformation, residual stresses and distortion," *Scand. J. Metall.*, vol. 29, no. 2, pp. 47–62, 2000.
[161] E. A. Ariza, M. A. Martorano, N. Batista de Lima, and A. P. Tschiptschin, "Numerical Simulation with Thorough Experimental Validation to Predict the Build-up of Residual

Stresses during Quenching of Carbon and Low-Alloy Steels," *ISIJ Int.*, vol. 54, no. 6, pp. 1396–1405, 2014.
[162] T. Inoue, S. Nagaki, T. Kishino, and M. Monkawa, "Description of transformation kinetics, heat conduction and elastic-plastic stress in the course of quenching and tempering of some steels," *Ing.-Arch.*, vol. 50, no. 5, pp. 315–327, 1981.
[163] CANER ŞİMŞİR, "3D Finite Element Simulations of Steel Quenching in order to determine microstructure and residual stresses," MIDDLE EAST TECHNICAL UNIVERSITY.
[164] C. H. Gür and A. E. Tekkaya, "Finite element simulation of quench hardening," *Steel Res. Int.*, vol. 67, no. 7, pp. 298–306, 1996.
[165] *Quenching Technology*. .
[166] R. Schröder, "Untersuchungen zur Spannungs- und Eigenspannungsausbildung beim Abschrecken von Stahlzylindern," University of Karlsruhe, 1985.
[167] A. Niesłony and M. Böhm, "Mean stress effect correction using constant stress ratio S–N curves," *Int. J. Fatigue*, vol. 52, pp. 49–56, Jul. 2013.
[168] N. E. Dowling, "Mean stress effects in stress-life and strain-life fatigue," *SAE Tech. Pap.*, no. 2004–01, p. 2227, 2004.
[169] A. Constantinescu and K. Dang Van, "A global computational approach in engineering problems: identification and fatigue," *Lect. Notes-AMAS*, 2004.
[170] J. Fernández, W. Storesund, and J. Navas, "Fatigue Performance of Grade R4 and R5 Mooring Chains in Seawater," in *ASME 2014 33rd International Conference on Ocean, Offshore and Arctic Engineering*, 2014, p. V01AT01A035–V01AT01A035.
[171] K. ENDO and Y. MIYAO, "Effects of Cycle Frequency on the Corrosion Fatigue Strength," *Bull. JSME*, vol. 1, no. 4, pp. 374–380, 1958.
[172] P. M. C. L. Pacheco, P. P. Kenedi, J. C. F. Jorge, and A. M. C. de Paiva, "Analysis of the Influence of Mechanical Properties on the Residual Stress in Offshore Chain Links Using the Finite Element Method," 2003, pp. 131–140.
[173] P. Pacheco, P. P. Kenedi, J. C. F. Jorge, H. S. Gama, M. A. Savi, and A. M. C. Paiva, "Modeling Residual Stresses in Offshore Chain Links using Finite Element Method," in *COBEM-2003, 17th International Congress of Mechanical Engineering, São Paulo*, 2003.
[174] I. Koutiri, D. Bellett, and F. Morel, "The effect of mean stress and stress biaxiality in high-cycle fatigue," *Fatigue Fract. Eng. Mater. Struct.*, vol. 41, no. 2, pp. 440–455, Feb. 2018.
[175] I. Koutiri, "Effet des fortes contraintes hydrostatiques sur la tenue en fatigue des matériaux métalliques," p. 244.
[176] H. Desimone, A. Bernasconi, and S. Beretta, "Are Multiaxial Fatigue Criteria Appropriate When Steels With Surface Defects are Subjected to Rolling Contact Fatigue," in *Bearing Steel Technology-Advances and State of the Art in Bearing Steel Quality Assurance: 7th Volume*, ASTM International, 2007.
[177] H. Desimone, A. Bernasconi, and S. Beretta, "On the application of Dang Van criterion to rolling contact fatigue," *Wear*, vol. 260, no. 4–5, pp. 567–572, Feb. 2006.
[178] Ciavarella M and Maittourman H, "On the Ekberg, Kabo and Andersson calculation of the Dang Van highcycle fatigue limit for rolling contact fatigue (Letter to the Editor)," *Fatigue Fract. Eng. Mater. Struct.*, vol. 27, pp. 523–526, 2004.
[179] M. Ciavarella, F. Monno, and G. Demelio, "On the Dang Van fatigue limit in rolling contact fatigue," *Int. J. Fatigue*, vol. 28, no. 8, pp. 852–863, Aug. 2006.
[180] S. Beretta and S. Foletti, "Propagation of small cracks under RCF: a challenge to Multiaxial Fatigue Criteria," in *CP2012*, 2012.

[181] P. S. van Lieshout, J. H. den Besten, and M. L. Kaminski, “Validation of the corrected Dang Van multiaxial fatigue criterion applied to turret bearings of FPSO offloading buoys,” *Ships Offshore Struct.*, vol. 12, no. 4, pp. 521–529, May 2017.
[182] John H.Mathews and Jurtis D.Fink, *Numerical Methods using Matlab*, Fourth Edition. Pearson, 2015.
[183] N. J. Higham, *Accuracy and stability of numerical algorithms*, 2nd ed. Philadelphia: Society for Industrial and Applied Mathematics, 2002.
[184] J. G. F. Francis, “The QR Transformation A Unitary Analogue to the LR Transformation—Part 1,” *Comput. J.*, vol. 4, no. 3, pp. 265–271, Jan. 1961.
[185] J. G. F. Francis, “The QR Transformation—Part 2,” *Comput. J.*, vol. 4, no. 4, pp. 332–345, Jan. 1962.
[186] A. S. Householder, “Unitary Triangularization of a Nonsymmetric Matrix,” *J. ACM*, vol. 5, no. 4, pp. 339–342, Oct. 1958.
[187] “Practical Residual Stress Measurement Methods CH 1 Overview of all methods,” .